Universitat Politècnica de València
Departamento de Máquinas y Motores Térmicos

COMBUSTION CONTROL OF DIESEL SPRAYS BY MEANS OF LASER INDUCED PLASMA IGNITION

Doctoral Thesis
Presented by:
Mattia Pinotti
Directed by:
Prof. José Vicente Pastor Soriano

Valencia, September 2019

Doctoral Thesis

COMBUSTION CONTROL OF DIESEL SPRAYS BY MEANS OF LASER INDUCED PLASMA IGNITION

Presented by: Mattia Pinotti

Directed by: Prof. José Vicente Pastor Soriano

Examining Board:

President: Prof. Jesús Vicente Benajes Calvo

Secretary: Prof. Juan José Hernández Adrover

Examiner: Prof. Andrés Melgar Bachiller

Reviewing Board:

Dr. Michele Bardi

Prof. Juan José Hernández Adrover

Dr. Jose Rodríguez Fernández

Valencia, September 2019

Abstract

In the recent years the engine research has been mainly focused on the pollutant emissions reduction and on increasing the efficiency. Many of the actual research efforts in the field of the Internal Combustion Engines are aimed to improve and develop new active strategies for emission reduction, particularly centered on new combustion concepts and a general improved combustion control. Their development requires the application of new experimental and theoretical tools, allowing both to be directly applied as an active pollutant control strategy and to permit to expand the basic knowledge of the governing processes' fundamentals. This is the concept where the main objective of this Thesis is framed: the development and optimization of a new, non-intrusive and modulable ignition system that will allow the control on the position and timing of the ignition spot. Such system will be applied to the ignition of direct injection diesel sprays in order to expand the knowledge of the ignition process, particularly considering how the local conditions at the ignition are affecting the subsequent combustion development.

In order to accomplish the proposed objective, the research work has been divided in two main blocks. The first one is focused on the development and optimization of the ignition system. Taking advantage of the possibilities granted by the laser plasma induction process and, once selected the best induction method for its application in an internal combustion engine environment, a process of optimization of the ignition system has been carried out. Such optimization process results to be of basic importance for this research development. In fact, the application of fully reliable ignition system is fundamental both in terms of its possible direct application for combustion modulation purposes and in terms of the new study possibilities that is able to deliver. At first, from an extensive literature survey upon the plasma laser induction process, the fundamental parameters to focus on for the application of the system to the ignition of direct injection fuel sprays have been obtained. Starting from these parameters, a first ignition system has been designed, and then its reliability in the plasma induction has been

experimentally tested under ambient and engine-like conditions, applying an original optimization methodology. As a main result of this first work block, a fully optimized and completely reliable laser induced plasma ignition system has been obtained, and an original system validation and optimization method has been developed.

The second work block corresponds to the application of the ignition system to a direct injection diesel spray under real engine conditions. This block aimed to accomplish two main goals: the determination of the system capabilities and limits for the spray ignition application and the development of a first experimental study regarding the influence of the local conditions at the ignition location on the subsequent development of diesel combustion. In order to do so, first the system ignition capability has been tested on a diesel spray, under an adequate set of thermodynamic conditions determined to maintain the maximum possible system feasibility. The results of this study, compared with the standard combustion diagnostics parameters for the autoignition event at the same conditions, proved its ignition capabilities. Then a parametric variation of the local timing and position of the induced plasma generation region has been carried out, in order to determine the effect of the local condition on the combustion development. By comparing the obtained results with standard autoignition parameters at the same conditions, interesting trends have been obtained, that underline the system ability to control and modulate the combustion event.

Resumen

En los últimos años, la investigación en motores se ha centrado principalmente en la reducción de emisiones contaminantes y en el aumento de la eficiencia. Muchos de los esfuerzos de investigación actuales en el campo de los Motores de Combustión Interna Alternativos están dirigidos a mejorar y desarrollar nuevas estrategias activas para la reducción de emisiones, en particular centradas en los nuevos conceptos de combustión y en la obtención de un mejor control de la combustión. Su desarrollo requiere la aplicación de nuevas herramientas experimentales y teóricas. Estas herramientas deberían permitir tanto el desarrollo y aplicación de nuevas estrategias activas de control de contaminantes como ampliar el conocimiento básico de los fundamentos de los principales procesos involucrados. En este contexto es donde se encuadra el objetivo principal de esta Tesis: el desarrollo y la optimización de un nuevo sistema de encendido no intrusivo y modulable, que permitirá el control sobre el tiempo y la ubicación del punto de encendido. Dicho sistema se aplicará para el encendido de chorros Diesel de inyección directa, para permitir ampliar los conocimientos sobre el mismo proceso de encendido. En particular, se pretende evidenciar cómo las condiciones locales al encendido pueden afectar al desarrollo de la combustión posterior.

Para lograr este objetivo, el trabajo de investigación se ha dividido en dos bloques principales. El primero se centra en el desarrollo y la optimización del sistema de encendido. Aprovechando las posibilidades que ofrece el proceso de inducción de plasma con láser y, una vez seleccionado el mejor método de inducción para su aplicación en un entorno especifico como el de un motor de combustión interna, se ha llevado a cabo un proceso de optimización y validación del sistema. Tal proceso resulta de importancia básica en el desarrollo de esta investigación, ya que la aplicación de un sistema de encendido totalmente fiable y consistente resulta ser fundamental, tanto en términos de su posible aplicación para propósitos de modulación de combustión como en términos de las posibilidades de estudios que pueda ofrecer. Al principio, a partir de un extenso estudio de la literatura sobre el proceso de inducción de plasma con láser, se han obtenido los parámetros

fundamentales a tener en cuenta para la aplicación del sistema al encendido de chorros de combustible de inyección directa. A partir de estos parámetros, se ha diseñado un primer sistema de encendido. Luego su fiabilidad en la inducción de plasma ha sido estudiada experimentalmente en condiciones ambientales y de motor, aplicando una metodología de optimización desarrollada en este mismo trabajo experimental. Como resultado principal de este primer bloque de trabajo, se ha podido obtener un sistema de encendido por plasma inducido con láser completamente optimizado y fiable, así como un método novedoso para su validación y optimización.

El segundo bloque de trabajo corresponde a la aplicación del sistema al encendido de un chorro Diesel de inyección directa en condiciones reales del motor. El objetivo de este bloque era lograr dos hitos principales: la determinación de las capacidades y los límites del sistema en su aplicación al encendido de chorros de inyección directa, y el desarrollo de un primer estudio experimental sobre la influencia de las condiciones locales de la zona de encendido sobre el desarrollo posterior de una combustión Diesel. Para lograrlo, primero se ha validado la capacidad de encendido del sistema bajo un conjunto adecuado de condiciones termodinámicas, previamente determinadas para mantener la máxima efectividad. Los resultados de este estudio, en comparación con los típicos parámetros de autoencendido en las mismas condiciones, han permitido demostrar la capacidad de encendido del sistema. Posteriormente, se ha llevado a cabo una variación paramétrica de tiempos y posiciones en las que inducir el plasma para forzar el encendido, con el fin de determinar el efecto de las condiciones locales sobre el desarrollo de la combustión Diesel. En este caso, al comparar los resultados obtenidos con los parámetros estándar de autoencendido, se han podido obtener tendencias interesantes, que subrayan la capacidad del sistema para controlar y modular el proceso de combustión.

Resum

En els últims anys, la investigació en motors s'ha centrat principalment en la reducció d'emissions contaminants i en l'augment de l'eficiència. Molts dels esforços d'investigació actuals en el camp dels Motors de Combustió Interna Alternatius estan dirigits a millorar i desenvolupar noves estratègies actives per a la reducció d'emissions, en particular centrades en els nous conceptes de combustió i en l'obtenció d'un millor control de la combustió. El seu desenvolupament requereix l'aplicació de noves eines experimentals i teòriques. Aquestes eines haurien de permetre tant el desenvolupament i aplicació de noves estratègies actives de control de contaminants com ampliar el coneixement bàsic dels fonaments dels principals processos involucrats. En aquest context és on s'enquadra l'objectiu principal d'aquesta Tesi: el desenvolupament i l'optimització d'un nou sistema d'encés no intrusiu i modulable, que permetrà el control sobre la posició de la ubicació del punt d'encesa. Aquest sistema s'aplicarà per a l'encesa de dolls Diesel d'injecció directa, per a permetre ampliar els coneixements sobre el mateix procés d'encesa. En particular, es pretén evidenciar com les condicions locals a l'encesa poden afectar el desenvolupament de la combustió posterior.

Per a aconseguir aquest objectiu, el treball de recerca s'ha dividit en dos blocs principals. El primer se centra en el desenvolupament i l'optimització del sistema d'encesa. Aprofitant les possibilitats que ofereix el procés d'inducció de plasma amb làser i, una vegada seleccionat el millor mètode d'inducció per a la seua aplicació en un entorn especifique com el d'un motor de combustió interna, s'ha dut a terme un procés d'optimització i validació del sistema. Tal procés resulta d'importància bàsica en el desenvolupament d'aquesta investigació, ja que l'aplicació d'un sistema d'encesa totalment fiable i consistent resulta ser fonamental, tant en termes de la seua possible aplicació per a propòsits de modulació de combustió com en termes de les possibilitats d'estudis que puga oferir. Al principi, a partir d'un extens estudi de la literatura sobre el procés d'inducció de plasma amb làser, s'han obtingut els paràmetres fonamentals a tindre en compte per a

l'aplicació del sistema a l'encesa de dolls de combustible d'injecció directa. A partir d'aquests paràmetres, s'ha dissenyat un primer sistema d'encesa. Després la seua fiabilitat en la inducció de plasma ha sigut estudiada experimentalment en condicions ambientals i de motor, aplicant una metodologia d'optimització desenvolupada en aquest mateix treball experimental. Com a resultat principal d'aquest primer bloc de treball, s'ha pogut obtindre un sistema d'encés per plasma induït amb làser completament optimitzat i fiable, així com un mètode nou per a la seua validació i optimització.

El segon bloc de treball correspon a l'aplicació del sistema a l'encesa d'un doll Dièsel d'injecció directa en condicions reals del motor. L'objectiu d'aquest bloc era aconseguir dues fites principals: la determinació de les capacitats i els límits del sistema en la seua aplicació a l'encesa de dolls d'injecció directa, i el desenvolupament d'un primer estudi experimental sobre la influència de les condicions locals de la zona d'encesa sobre el desenvolupament posterior d'una combustió Diesel. Per a aconseguir-ho, primer s'ha validat la capacitat d'encesa del sistema sota un conjunt adequat de condicions termodinàmiques, prèviament determinades per a mantindre la màxima efectivitat. Els resultats d'aquest estudi, en comparació amb els típics paràmetres d'autoencesa en les mateixes condicions, han permés demostrar la capacitat d'encesa del sistema. Posteriorment, s'ha dut a terme una variació paramètrica de temps i posicions en les quals induir el plasma per a forçar l'encesa, amb la finalitat de determinar l'efecte de les condicions locals sobre el desenvolupament de la combustió Diesel. En aquest cas, en comparar els resultats obtinguts amb els paràmetres estàndard d'autoencesa, s'han pogut obtindre tendències interessants, que subratllen la capacitat del sistema per a controlar i modular el procés de combustió.

To my Family, my Fuel

To Cecilia, my Spark

Acknowledgements

Firstly, I would like to thank the CMT – Motores Térmicos, and more specifically Prof. Francisco Payri and Prof. José María Desantes for accepting me into their research group and giving me this opportunity. Moreover, I would include also Prof. Jesus Benajes, director of the combustion group. My gratitude needs to be also extended to all members of the institute, who have assisted me in a major or minor way to the conclusion of this thesis and whose contribution perhaps is never recognized as should really be. From Juan Yustas to all the administration department (Amparo, Haby, Teresa, Elvira and Carmina), thank you very much.

With special affection, I would like to express my immense gratitude to my director, Prof. José Vicente Pastor. He has been a reference and a guide, both for scientific and personal issues all along the time I spent in the department. For sure, without his continuous help, advices, patience and guide, I would never been able to finish this document, and overcome all the difficulties I have been through this part of my life. He has always been available to me, gave me advices that go beyond the professional sphere of our work, helped me to grow up and face difficult problems. He has, and always will have, all my gratitude and respect, not only for his professional stands and trajectory but also, and most importantly, for his moral stands. Very similar words are all I have also for Prof. Antonio García, who has been my other reference point in this complicate journey. He has gave me all he could, without restrictions, limits and fundamentally, without having to. He has advised me, pushed me, spurred me when I needed it and he has always been there, on my side, like an old brother who cares for me. Also to him, I want to say, from the very deep of my heart, thank you: without him I would not been able to reach the end of this journey. He will always have my respect, my admiration for the person he is and, of course, my friendship.

Besides them, there is also Prof. José Maria García-Oliver who I might be always grateful to, and who also has been very important to me, both professionally and personally. To all this three great professors and human being, again, goes my most true gratitude and respect.

I also need to include in these acknowledgements the technical staff of the department, because in the end, without them is impossible to get the job done. Starting from the coordinator, Dr. Vicente Bermúdez, and going through every staff member. Between them, I have to highlight all the help provided by Daniel Lérida, who has been my laboratory master teacher; José Enrique del Rey, who always helped when I asked, no matter what the problem was, and who I also have to thank for the good times spent in the laboratory. I can not forget to mention "The Troner" José Gálvez and thank him for the help, the good times and the large talks.

The time I spent in the CMT – Motores Térmicos has been a lot of things to me. I passed through joys, I have had a lot of good time, but also difficulties and personal issues. I have been able to overcome some of them, and I will all of them, also thanks to the great people I have meet there and that will always be in my memory. Everyone who has been mentioned here has helped me in some way, and I am very grateful to have had the possibility to been there, and meet them. In all this, I could not forget to mention all the colleagues and friends I have met: Javier Monsalve-Serrano, Eduardo Belarte, Walter Vera-Tudela, David Villalta, Vicente Boronat, Daniel Vaquerizo, Alberto Viera, Daniel Estepa, Vincenzo Pagano and Marco Crialesi. I have to highlight the contribution of all my long-terms officemates (and friends) during these years: Carlos Micó, Tiemin Xuan, Leonardo Pachano, Felipe Lewinski, Alba Andreina and also of some of the most important short-therm colleagues and friends I had the fortune to meet there, such as Andres, Varun, Weinjun, Carles Oltra and Carlos Chacon. Every one

of them has contributed in some way to what I am now, to what I have been able to do.

To my family and close, but far, friends. Thanks for all the support given, for all the time spent listening to me, for all the advice, for all the love you always send me unconditionally. You know you have been, you are and always will be, the fuel to my life.

Last but not least, a very special mention goes to my girlfriend Cecilia Rosso, who through all this time has always been there, by my side, tolerating me, encouraging me in every step of the way, no matter how difficult it may look. Her overwhelming support, care and love, has always represented to me the spark to move on, the reason to fulfill my dreams and prospective, even when I thought it was impossible.

To all the friends I have, the one I have met during this journey, to all my guides, to my family and to Cecilia: thank you, I love you.

I would finally like to thank the Universitat Politécninca de Valéncia and the Spanish Ministry of Science and Technology, which supported this work through the grant BES-2015-072119.

Table of Contents

Index of Figures

Index of Tables

Nomenclature

Latin

AOI - Angle of Incidence

AHR - Apparent Heat Release

ARoHR - Apparent Rate of Heat Release

ASoE - After Start of Energizing

BTDC - Before Top Dead Center

CAD - Crank Angle Degree

CCD - Charged-Coupled Device

CFD - Computational Fluid Dynamics

CI - Compression Ignition

CMOS - Complementary Metal Oxide Semiconductor

CRT - Continuous Regeneration Trap

DI - Direct Injection

DPF - Diesel Particulate Filter

ECN - Engine Combustion Network

EGR - Exhaust Gas Recirculation

EoI - End of Injection

EoS - Equation of State

FPS – Frames per Second

FWHM - Full Width at Half Maximum

ICE - Internal Combustion Engine

IPC – Intake Port Closure

LAS - Light Absorption and Scattering

LIP - Laser Induced Plasma

LOL - Lift Off Length

MIE - Minimum Ignition Energy

Nd:YAG - Neodymium Yttrium Aluminum Garnet

NL - Natural Luminosity

OSLO® - Optics Software for Layout and Optimization

PIV - Particle Image Velocimetry

PM - Particulate Matter

PMT - Photomultiplier Tube

RMS – Root Mean Square

RoHR - Rate of Heat Release

SCR - Selective Reduction Catalyst

SoC - Start of Combustion

SoE - Start of Energizing

SoI - Start of Injection

SR - Success Rate

TDC - Top Dead Center

TDI - Turbocharged Direct Injection

VGT – Variable Geometry Turbocharger

UV - Ultraviolet

Greck

θ - Spray Cone Angle

λ - Wavelength

μ – Dynamic Viscosity

ρ - Density

Chapter 1

Introduction

Contents

1.1 Introduction

This introductory chapter has two main goals: on the one hand, it will provide a contextualization of the historical framework and the technological context on which this study has focused. A brief historical description of internal combustion engines (ICE) will be presented, with a particular focus on compression ignition engines, together with a discussion on its importance nowadays in various aspects of our society, from economical to environmental impacts and finally with the challenges that we must face in the near future.

On the other hand, the general structure of this document will be presented, detailing the content of each of the subsequent chapters and providing a global view on the study.

1.2 Context of the Study

The following paragraphs will introduce the context in which the study presented in this doctoral thesis is framed. At first, a general description of the global energy framework in the modern society will be presented, taking into account both its historical developments and present challenges. Later, this introductory chapter will be centered on the main focus of the research work, the compression ignition engine. Also here, its historical evolution will be presented alongside its major present and future open challenges.

1.2.1 The Energy Framework

One of the most important driving factors for the evolution of modern society and mankind in general has always been related with the production and management of energy. Especially in the last century of our history, the central paradigm of energy has been the production of abundant quantity of it. But only from the half of the last century to nowadays, the society has been more focused on the quality of the energy we are producing. The energy

availability and its distribution has allowed the fastest and highest growth in the history of mankind, permitting economic and technological progresses that were mostly unthinkable before. In the end, it has permitted to achieve the current life quality.

But now, considering on the quality and the type of energy that we use, Figure 1.1 shows a condensed statistics of the different energy consumption in the European Union, year by year, for 25 years, between 1990 and 2015. The graph shows the principal energy sources, and their impact on the total energy production evolution.

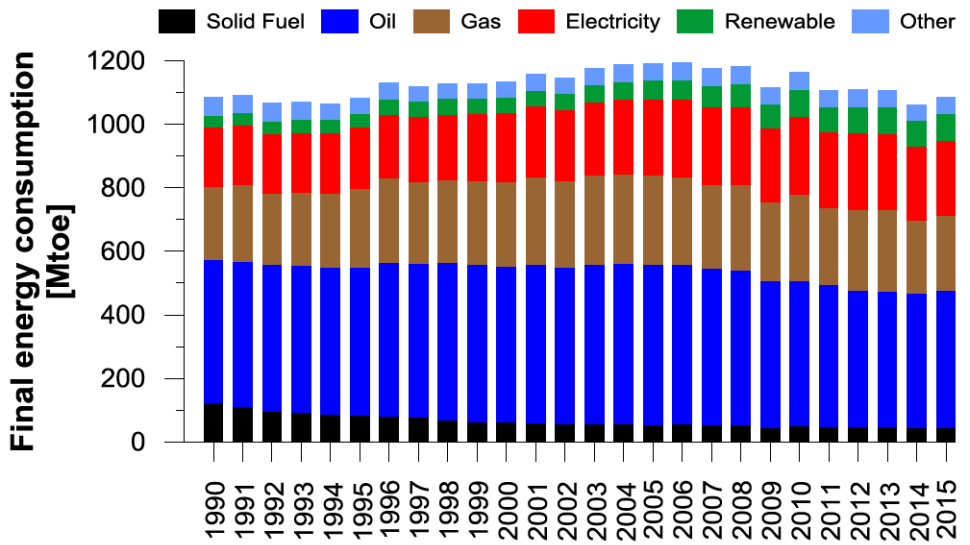

Figure 1.1. Evolution of final energy consumption by sources in Europe from 1990 up to 2015 [1].

At first, it is immediately appreciable how, along the considered 25-years period, the overall variation regarding the total consumed energy are very small, with a maximum deviation of 8%. Nevertheless, some trends could be observed in terms of energy sources evolution along this period. Solid fuels consumption has decreased around 40% from 1990, while electricity and renewable energy sources have experimented an opposite upward trend,

mainly centered around the year 2005 thanks to the promoted subsides of the European administration. Moreover, the demand for oil has also decreased, particularly in the last 5 years of the reported statistics. As a general point regarding this data, it is observable how, mainly maintaining energy demands and total production constants, the different employed energy sources have been redistributed all along this last time frame, towards the less environmental impactful ones.

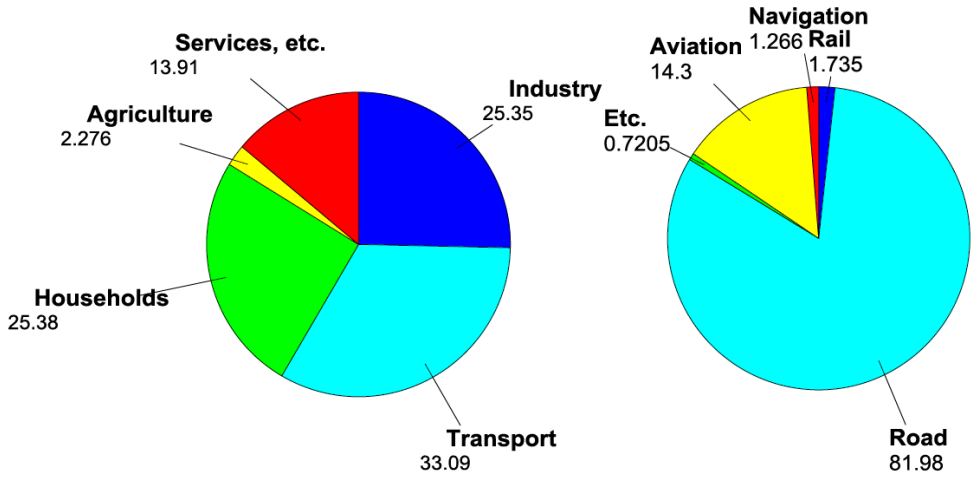

Figure 1.2. Energy consumption by sector in Europe in 2015 (left). Transport energy consumption in Europe by modes, in %, for 2015 (right) [1].

If we now consider the energy consumption distribution by sector in Europe during 2015, as reported in Figure 1.2 (left), it is appreciable how, form the total energy consumption for the considered year, 33% of that energy was consumed in the transport sector, being the sector with the highest share.

Still in Figure 1.2 (right), it is reported, for the same considered year, the distribution of energy consumption properly inside the most energy-demanding sector, the transport sector. It is clearly appreciable how the road transport mode agglomerates the major share, so mainly regarding the mobility of goods and people inside European countries. The second most

used mode results to be air transport, followed in order, but with considerable distance, by rail and navigation, representing in conjunction only the 3% of the energy consumption of the whole transport section. It can be so considered that the major part of the energy source consumed in the most energy-demanding sector comes from oil, as the compression ignition engine dominates the road transport market, especially in terms of goods transport and heavy-duty engines.

In any case, it is undeniable that engines, whether gasoline or diesel fueled, have an undisputed leadership position in road vehicles propulsion. But this will also lead to the question: *why is the compression ignition engine the best option for this type of application?*

1.2.2 The Compression Ignition Engine

The diesel engine has been around already for more than a century. It was 1892 when a French-German engineer, Rudolph Diesel, patented the design of an engine that worked forcing the fuel ignition by the heat of compressed air collected in a combustion chamber. The next year, 1893, Diesel presented the first working prototype of his engine, with which was able to reach a remarkable 26% fuel efficiency, easily doubling the current time standard set by steam engines. In particular, avoiding pumping energy losses and the application of a higher compression ratio offered a significant improvement in terms of efficiency when compared to spark ignited engines.

Since then, the compression ignition engine projected by Diesel has largely evolved and spread to very diverse applications, from passenger cars to trains, from boats to power plants, among others. Actually, the first diesel engines were large and heavy, limiting its applications only to some specific fields where these limitations were not central, particularly high-power applications such as power plants, boats, locomotives. It was only in 1936 and thanks to the work of Daimler-Benz, who first mounted it on a production passenger car, when the compression combustion engine really starts to spread all along the word in the transport's application field.

Time after, another major key point in the history of diesel engines evolution could be identified in the introduction from Mercedes-Benz of the first turbocharged diesel engine for a passenger car, making possible to obtain higher specific power whilst reducing its size. It was the year 1978. Ten years later, Fiat released the first direct-injection diesel engine, equipped on a Croma 2.0 TDI. Both turbocharging and direct injection technologies made the difference for the compression ignition engine evolution, overall in terms of power, performance and emissions, redefining it and opened new research fields unthinkable until those days. Moreover, these technologies have made it a commercial success.

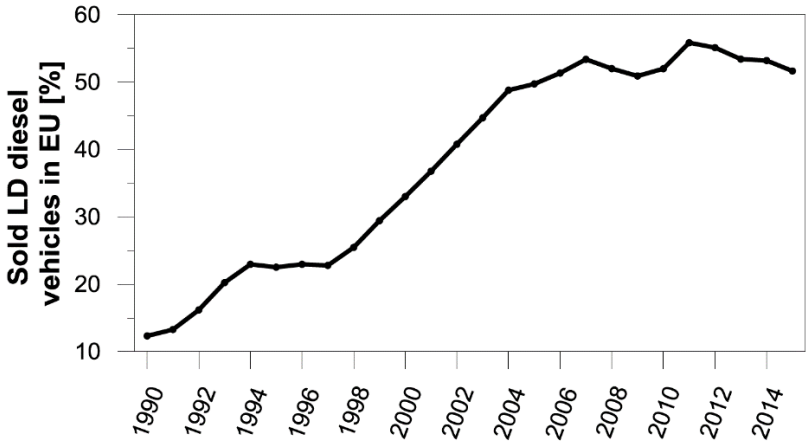

Figure 1.3. Light duty diesel vehicles market share evolution in Europe from 1990 to 2015.

Since the early 1990s to nowadays the diffusion of the diesel engine has grown rapidly, as appreciable from the data reported in Figure 1.3. They have reached a solid market share of the 50% in the European Union [2] and have become dominant in the heavy-duty sector, thanks to their lower specific fuel consumption and higher specific torque performance when compared to gasoline engines.

Moreover, diesel engines are more efficient, more reliable and durable than other ICEs. Summarizing such characteristics, diesel engines still

represent the most efficient propulsion form for road transport duties, whereas those are for passengers or goods transport. Generally speaking, the success of diesel engines could be identified in the unique combination of low fuel combustion, high reliability, durability and its competitive cost.

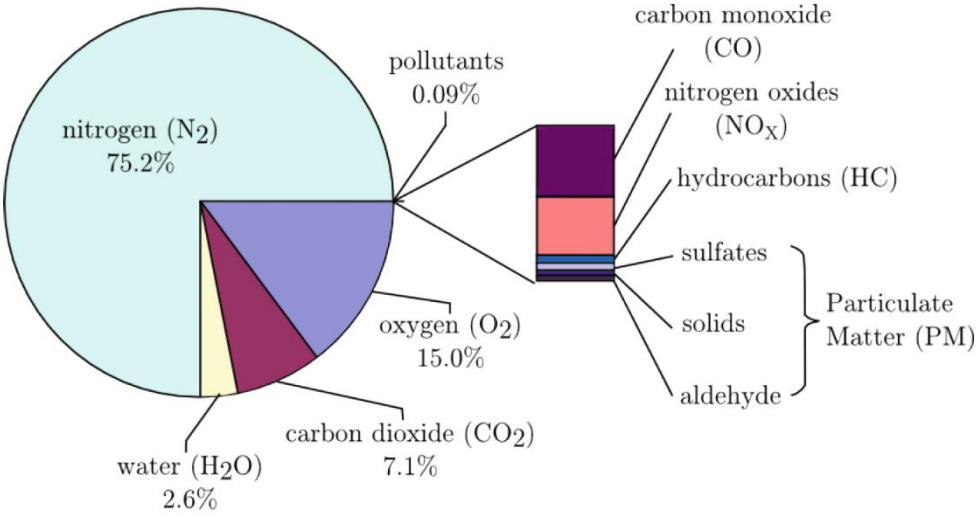

Figure 1.4. Exhaust gas composition for a real diesel combustion in percentage by weight [3].

However, despite its high efficiency, the compression ignition engines are considered as one of the main sources of environmental pollution. The ideal combustion of a hydrocarbon molecule generates Carbon Dioxide (CO_2), water (H_2O) and Nitrogen (N_2). Moreover, actual diesel combustion generates other pollutants, as reported in Figure 1.4 and here detailed as follows:

- *Nitrogen Oxides (NOx)*: mainly formed by *Nitric Oxide (NO)* and *Nitrogen Dioxide (NO_2)*, could also includes *Nitrous Oxide (N_2O)* in smaller portion. These emissions are considered mainly responsible for phenomena such as photochemical smog and acid rains, could also reduce the ozone concentration in the stratosphere and produce respiratory illness [4]. The majority of NOx emissions are due to reactions produced between oxygen and nitrogen at elevated

temperatures, and so related to the fuel characteristics and to the air/fuel mixing process.

- *Particulate Matter (PM)*: are solid and/or liquid particles classified and defined by their size. If smaller than 100 microns in size, they will remain suspended in air becoming dangerous for the human respiratory system. In particular, two grades of *PM* are regulated: *PM10* (sized between 10 and 2.5 microns) known as "coarse" particles, and *PM2.5* (sized less than 2.5 microns) known as "fine" particles. Really small particles are also referred as "ultra-fine" or "nano" particles. Actually, the ICE of the transport sector are considered responsible for the 11% of *PM10* emissions and 16% of *PM2.5* emissions to the atmosphere [5].

- *Carbon Monoxide (CO)*: it is an intermediate product of the hydrocarbon oxidation process. Most of such emissions are referred to the equivalence ratio miscontrol inside the combustion chamber: lean air/fuel ratios burn not fast enough while local very rich regions cannot completely burn due to the lack of oxygen. Carbon monoxide production is higher in gasoline engines in virtue of the richer equivalence ratio during engine operating conditions.

- *Hydrocarbons (HC)*: are the results of incomplete combustion, caused by local conditions of low temperature and rich or very lean fuel concentration inside the combustion chamber. This category also includes partially oxidized *HC* and unburned *HC*. As already underlined for carbon monoxide (*CO*), these emissions are less important in conventional diesel engines than in gasoline engines, particularly if compared with *NOx* and *PM* production.

In summary, considering what has been aforementioned regarding the generation of the four principal combustion pollutants, a compression ignition engine produces intrinsically high levels of *NOx* and *PM* while *CO* and *HC* do not represent a problem of this type of ICE.

The first pollutant regulation that has established limits for the four main pollutants engine emission has been legislated in United States in 1974, followed by Japan and Europe. The legislation of the EURO I pollutant emission standard started in the Europe Union in the 1992 and has been progressively updated since nowadays.

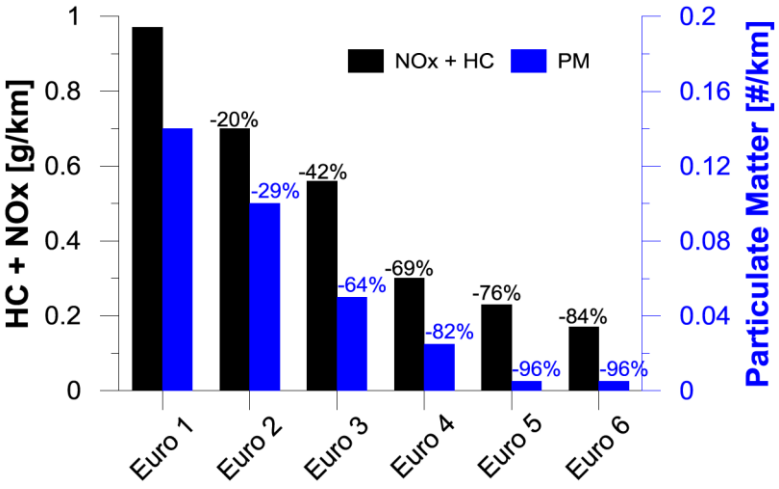

Figure 1.5. Evolution of the European emission standard regulation for NOx+HC and PM emissions for diesel vehicles [6].

Figure 1.5 reports the evolution of the EURO standard emissions regulation of *NOx+HC* and *PM* for light duty diesel engines. As is clearly appreciable from the graph, the European government has imposed a gradual but heavy reduction of the permitted diesel engines emission limits to extremely low levels, approaching in such way the growing social concern about environmental pollution and moving towards a less environmental impactful mobility. More in detail, the maximum level of *NOx* emission has been reduced by 84% and the *PM* by 96%.

In order to face these severe regulation limits, some major technological improvements have been brought to the diesel engines during the past decades. These technological developments can be divided into two major

groups, discriminated by the basic approach applied: active or passive solutions.

- *Active solutions*. These strategies, as indicated by its denomination, try to proactively act on the combustion/ignition processes in order to limit the pollutant generation right from the start, lowering them until the ideal limit to obtain a completely clean combustion. The focus is on the combustion control, and it is achievable via different approaches. Some of them try to modify and upgrade the control of the air management system. During the past years, the improvements on the turbocharging performance via the introduction of technologies such as variable geometry turbochargers (VGT), intercoolers and two-stage turbochargers have gone towards this direction. Moreover, still in the field of air management control, the introduction of Exhaust Gas Recirculation (EGR) strategies and its subsequent evolutions (EGR cooling, low pressure EGR) together with the variable valve systems has largely increased the flexibility of the overall engine air management processes. On the other hand, other approaches have focused on the upgrade of the fuel injection system, in order to improve the spray atomization, evaporation and timing control to obtain a better combustion with a higher degree of control. In this field, the progressive increase of the injection pressure, the reduction of the nozzle diameter, the increase of the orifice number and multi-injection strategies have allowed overall better performances and a higher flexibility of the injection systems.

- *Passive solutions*. These strategies, in opposition to the above exposed active ones, do not try to limit the pollutant generation of the combustion process but, instead, are focused on eliminating or reducing the pollutant concentration in the exhaust gases by means of after-treatment devices. During the past years, various after-treatment devices have been developed and placed along the exhaust

line of modern mass production engines. Each one of them could be classified according to the reduced pollutant. In this sense, the particulate emissions (*PM*) have been reduced by the application of particle filters (DPF) and continuous regeneration traps (CRT), while the *NOx* emissions have been lowered by the application of selective reduction catalysts (SCR) and/or passive catalysts (DeNOx) to the exhaust lines.

Measure	**NO_x**	**HC/CO**	**Soot**	**BSFC**	**Noise**
Retarded Start of Injection	+	−	−	−	+
Exhaust gas recirculation	+	−	−	−	+
Cooled EGR	+	−	+	+	0
Supercharging	−	+	+	+	0
Intercooling	+	−	+	+	0
Pilot Injection	0	+	−	0	+
Added post-injection	+	0	+	−	0
Injection pressure increase	0	+	+	+	0
Lower compression ratio	+	−	+	0	−

Table 1.1. Compendium of different measures for the diesel combustion optimization and their effect on major emissions. Symbols: + reduce; - increase; 0 no effect [3].

As a general consideration, a comparison of these two basic approaches to the pollutant reduction can evidence how the passive solutions presents some of the major drawbacks. In particular, they represent an increase in the fuel consumption, caused by the filter's regeneration and the increase in the total weight of the vehicle, joined with a raise in the total vehicle cost, mainly for the necessary installation of additional technology and greater maintenance services. The research institute of CMT –Motores Térmicos of Universitat Politècnica de València has presented several studies on this theme [7][8].

Moreover, the optimization of a diesel engine normally entails an intrinsic conflict between fuel consumption and emission reduction, common to both active and passive strategies. In fact, individual strategies are seldom able to reduce all pollutants in the same proportion, making additional strategies usually indispensable to achieve the global reduction objective. Thus, the engine tuning always requires a compromise between cost and complexity of the different applied measures and the obtainable results. Table 1.1 summarizes the effects of most currently common methods for emission reduction [3] over the different pollutant species mentioned before. It is appreciable how any measure its individually able to affects positively all the elements, so then normally a combination of them is needed to compensate detrimental effects. In particular, one of the main conflicts for the ICE optimization is represented by the simultaneous reduction of NOx and PM, commonly referred as "PM/NOx trade-off". Fulfill the actual standard emission limits always require a heavy application of passive solutions for the exhaust gas after-treatment, both in passenger cars and heavy duty engines. However, as already mentioned before, passive solutions are the one presenting the major drawbacks for their application, especially in terms of engine efficiency.

For this reason, many of the actual research efforts in the ICE field are aimed to improve and develop new active strategies for emission reduction, particularly centered on new combustion concepts and a general improved combustion control.

Considering what has been previously described, is seems so necessary to progress with such kind of research, both in terms of applied active strategies and in terms to expand the basic knowledge of the fundamental events governing the injection, ignition and combustion processes that will directly affect the pollutant production.

1.3 Structure of the document

The document is divided into six chapters including the present introduction:

- **Chapter 1: Introduction**: The first and current chapter, aimed to provide a contextualization of the approached problem and an overview of the whole document.

- **Chapter 2: The Diesel Combustion and the Laser Plasma Ignition processes**: The second chapter provides a general and qualitative description of the diesel spray structure and of the fundamental physical and chemical processes that govern the combustion event. With a particular focus on combustion control and the effects of the ignition process on the flame development, the implications of the application of a laser induced plasma ignition system to force/provoke the combustion of the diesel spray will also be presented. The technological viability of the non-intrusive ignition system will be discussed, focusing on its optimization for the obtention of the most reliable and stable ignition system possible in order to allow the study of the local conditions effects at the ignition location on the subsequent combustion development and general combustion modulation capability. In this chapter, the objectives of this doctoral thesis work will also be presented, as derived from the principal conclusions traced from the literature survey.

- **Chapter 3: Tools and Methodology**: The third chapter provides an exhaustive description of the experimental tools and theoretical methodologies applied to the development of the research work. The test facilities will be presented and described in detail. The optical techniques used for the study will be presented, both in terms of theoretical basis and in terms of experimental tools used to carry out the research. The numerical models used for the spray analysis will also be presented and described in detail.

- **Chapter 4: Laser Induced Plasma Ignition: System Optimization**: The fourth chapter will present the first experimental results obtained for the plasma induction system optimization and application to a direct injection diesel spray, obtained to fulfill the objectives of the proposed experimental study. In order to achieve a highly reliable ignition system for its subsequent application to a diesel spray, both optical system settings and thermodynamic combustion chamber conditions will be considered in a parametric study, aimed to find the highest laser plasma induction effectiveness.

- **Chapter 5: Laser Induced Plasma Ignition: application to Diesel sprays**: The fifth chapter will be focused on the application of the optimized laser induced plasma ignition system to a direct injected diesel spray under different real engine conditions. The effect of the variation of the local conditions at the spray ignition will be studied, in order to consider how it is affecting the combustion development. The limit of ignitability of the spray with the designed system will also be considered. In order to do so, at first a study on the reliability and ignition capability of the laser system will be carried on, followed by a parametric variation of the engine condition, aimed to determine whether engine working point will result more feasible for forcing the ignition. Once such results have been obtained, the autoignition baseline case at the selected work point will be determined, allowing to obtain a reference for the comparison of the subsequent parametric study on the plasma ignition point position and timing variation. Such results will finally allow to consider how the local conditions at the ignition location are affecting the combustion development of a diesel spray.

- **Chapter 6: Conclusions and Future Work**: The sixth and last chapter will summarize the obtained results all along the experimental research development, extracting the main conclusions of the work. Additionally, some suggestion for future research works in the same field will be presented.

1.4 Bibliography

[1] Pocketbook, European Commission - Transports. Statistical, "https://ec.europa.eu/transport/facts-fundings/statistics/pocketbook-2018_en," 2017. [Online].

[2] "http://www.acea.be," Europe, New passenger car registrations in Western, 2015. [Online].

[3] K. Mollenhauer and H. Tschoeke, Handbook of Diesel Engines, London, New York: *Springer Heidelberg Dordrecht*, 2010.

[4] Environmental Protection Agency, Nitrogen Oxides (NOx), why and how they are controlled, *Technical Report*, 1999.

[5] W. Wallace, M. Keane, D. Murray, W. Chisholm, A. Manyard and T. Ong, "Phospholipid lung surfactant and nanoparticle surface toxicity: Lessons from diesel soots and silicate dusts", *Journal of Nanoparticles Research*, vol. 9, no. 1, pp. 23-38, 2007.

[6] DieselNet: Diesel emissions online, "http://www.dieselnet.com.," [Online].

[7] F. Payri and J. M. Desantes, “Motores de combustión interna alternativos”, *Reverté*, 2011.

[8] A. García, P. Piqueras, J. Monsalve-Serrano and R. Lago, "Sizing a Conventinoal Diesel Oxidation Catalyst to be used for RCCI Combustion under real driving conditions", *Applied Thermal Engineering*, vol. 140, pp. 62-72, 2018.

Chapter 2

The Diesel combustion and Laser Plasma Ignition processes

Contents

2.1 Introduction

This second chapter has the main goal to present to the reader the fundamental concepts behind the development of this doctoral thesis, in order to be able to understand the justification of the study that has been carried out.

The chapter is structured as follows. At first, a conceptual and qualitative description of the main physical and chemical phenomena involved in the diesel combustion is carried out. The injection/combustion process will be detailed, the principal combustion phases presented and discusses as so for the autoignition process. Finally, the classical description of the diesel diffusion flame model will also be presented, with a particular focus on the processes that lead to the formation of the principal pollutant emissions.

Later, the different possible approaches and advantages brought by the application of a non-intrusive ignition system will be presented. Particular focus will be put on systems that allow time and position variation of the ignition spot. Such systems will allow to obtain a new tool for modulating the combustion development and for studying the effects of local conditions at ignition location on the combustion process. The advantages and possible drawbacks of such ignition system will be presented, joined with its applicability to internal combustion engines. Fundamental parameters for its application will be discussed in order to present the most important variables to take into account for its optimization and experimental application.

In the last part of the chapter, a brief resume of the reported contents is presented, along with a series of conclusions that justifies the objectives of the current work. In the end, the general methodology to achieve such objectives will be described.

2.2 The combustion process in a direct injection diesel engine

In the following section the main concepts of the physical-chemical phenomena related to the diesel diffusion combustion process will be described.

Traditionally, the temporal definition of the combustion processes of a diesel spray are best described by analyzing the rate heat release while the fuel is being injected into the combustion chamber. This will be presented at first. Then, the different phenomena that occurs at each stage of the combustion process will be qualitatively defined, such as, namely, the air/fuel mixture formation, autoignition process and diffusion flame propagation.

2.2.1 Combustion phases

The most typical way to describe and study the temporal evolution of a diesel combustion process is the analysis of the rate of heat release (RoHR) in comparison with the fuel injection rate. The RoHR is obtained as a function of the in-cylinder pressure trace, based on the application of the first law of thermodynamics to the cylinder closed volume [1][2], and represents the intensity of the chemical energy released by the fuel during the combustion process by time unit or CAD.

Figure 2.1 shows the time evolution of a real rate of heat release diagram compared to the fuel injection rate and in-cylinder pressure trace evolutions. Four phases are clearly distinguishable:

- The first one commences right after the injection has begun, also commonly defined as start of injection (SOI), and ends when the ignition of the air-fuel mixture takes place, referred as start of combustion (SOC). During this phase, the fuel is being introduced into the combustion chamber and there is no apparent heat released.

The fuel is mixing with the air while the processes of atomization, air entrainment and evaporation are taking place. Due to the high temperature of the air and the availability of oxygen, the fuel starts oxidizing and very low intensity pre-reactions appears prior to the breakdown of fuel molecules into shorter chain hydrocarbons and free radicals. Consequently, this will give place later to the spontaneous ignition of the mixture that defines the start of combustion (SOC). This first phase is known as the ignition delay and can be seen in Figure 2.1 from the points *a* to *b* as a flat line of value close to zero in the rate of heat release axis.

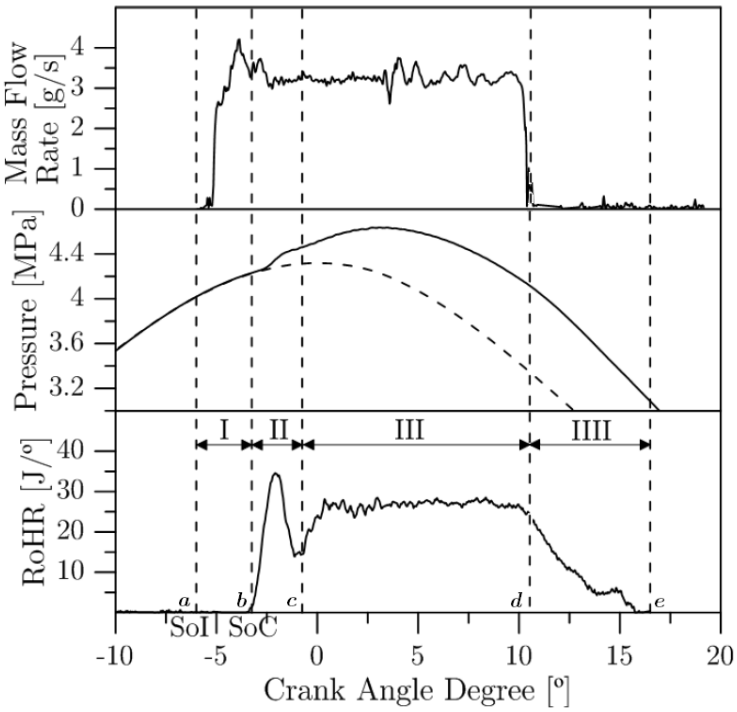

Figure 2.1. Fuel mass flow rate of injection (up), in-cylinder pressure (center) and rate of heat release (down) for a CI engine. Combustion Phases: I = Auto-ignition delay; II = Premixed Combustion; III = Diffusive Combustion; IIII = Late-cycle Diffusion Combustion.

- The second phase is a transient state, defined by a *premixed combustion* of the fuel-air mixture. It is included from the start of combustion (SOC), to the first relative minimum of the RoHR curve, here indicated in Figure 2.1 as *c*. As asserted before, during the ignition delay phase, the fuel had mixed with the entrained air and some low temperature pre-reactions had taken place, but the mixture has not burnt until SOC due to not being within the flammability limits of the fuel. Then, in this phase, combustion propagates quickly to all vaporized fuel mixed with air during the ignition delay time and generates a characteristic combustion with very high heat release in very short time, producing the typical peak of the RoHR trace as appreciable in Figure 2.1. This phase is also known as *premixed combustion* from the points *b* to *c*.

- The third phase begins when all the fuel mixed during the ignition delay phase burns completely. During this phase the heat is released at a much lower rate, controlled by the availability of new mixture formed for burning, hence by the rate at which air/fuel mixture process are taking place inside the combustion chamber. That is why this phase is commonly referred as *Mixing-controlled combustion* or *Diffusion combustion* [2][1]. While the injection event is still taking place, the rate of mixture formation is fundamentally controlled by the amount of in-cylinder spray momentum. Therefore, the length of the heat release depends on the injection length, defining this phase as limited by the end of premixed combustion till the end of injection process (EOI). In this phase the flame goes into an almost steady state, as the conditions results to be quasi-stationary until EOI (as opposed to the premixed combustion). In Figure 2.1, this is appreciable from the points *c* to *d*.

- The fourth and last phase takes place after the injection has ended and continues until the flame has completely disappeared. It is known as the *Late-cycle diffusion combustion phase*. Even once the injection process ended, there will still be heat released until the injected fuel

has not been completely oxidized. However, the contribution of mass and momentum to the combustion process ceases with the injection, so that this heat release is considerably lower due to much poorer mixing, causing the loss of the almost stationary flame structure of the diffusion combustion in favor of a an erratic flame behavior characterized by random flame structures (Figure 2.1, points *d* to *e*). It is appreciable how combustion loses intensity until it ends.

2.2.2 Air/Fuel mixture formation

During an injection process different physical phenomenon are initiated that finally will lead to the formation of a mixture between the injected fuel and the ambient air collected in the combustion chamber.

First of all, the injection takes place due to a pressure difference between the in-cylinder ambient pressure and the pressure at which fuel is being injected. Nowadays, typical pressure rations for modern engines are of 50-100 bars of in-cylinder pressure at injection (that variates with the boundary conditions of intake pressure and temperature, compression ratio etc.) with an injection pressure range varying from a minimum of 200 bar (needed for the injector needle to rise) to a maximum of 2500 bar [3], and its increasing with the further injector technology development. The high injection pressure and great pressure difference with the in-chamber ambient air causes the fuel to enter the combustion chamber as a liquid spray with a very high velocity and momentum associated. Thus, in contrast to the low air velocity within the chamber, converts the fuel spray in a turbulent spray.

Moreover, when the liquid fuel is injected into a high-pressure environment it starts breaking into very small drops by a process called atomization. In addition, as the fuel penetrates further away from the injector nozzle, it will start entraining more air, causing the he local mixture fraction to become leaner as the spray tip moves further. If the temperature of the environment is high enough the fuel will so start evaporating. These phenomena will take place wherever the local mixture fraction formed during

the injection results to be lower than the evaporation fraction of a given fuel under the associated boundary conditions. Each one of the aforementioned processes takes place through the whole injection event and will be explained in this section.

2.2.2.1 Atomization of the liquid fuel

The phase that takes place immediately after the fuel has been discharged into the injector nozzle is the atomization of the liquid fuel, which consists in the conversion of the liquid core (a continuum medium) of the fuel into fine droplets of different sizes. This process helps increase the area in contact between the fuel and air, and therefore helping the processes of air entrainment and evaporation that will follow. In literature, this first phase is also referred as *primary atomization*.

For a turbulent flow, such is a diesel spray, the atomization process does not start right at the nozzle exit, but instead takes place starting at a given axial distance from the injector nozzle. This distance is referred to as *intact length* and depends on various factors (physical properties of the fuel, injection pressure and ambient density among others). From this distance on, the break-up starts and so the liquid core of the spray is no longer intact (hence the name), but instead results to be a mixture of entrained air and droplets of the liquid fuel.

After a primary atomization, a secondary atomization phase takes place. As mentioned in [4], the atomization is basically a process in which a certain amount of liquid is converted into small drops. However, also many of the drops produced by the initial fragmentation of the injected liquid core may be further disintegrated into much smaller drops, during which will be so called a *"secondary"* atomization. Fuel droplets could be formed both by the initial ligament breaking up (*primary atomization*) or by the breaking of larger droplets into smaller ones (*secondary atomization*). The fluid ligaments are formed by the fuel mass exiting the nozzle, suffering a deceleration due to the surrounding air present into the combustion chamber. The secondary

atomization increases furthermore the air entrainment possibilities. However, it is important to note that simultaneously with the second atomization, also the coalescence phenomenon occurs. Drop to drop and ambient air interaction can lower the local flow velocities, causing coalescence to happen and so increasing the average drop diameter, leading to a worse global spray atomization [5].

Finally, in order to obtain a good atomization, various studies have reported how high injection pressure (spray velocity), small nozzle diameter, optimum fuel viscosity and high cylinder pressure (air density) are required [1][5][6].

2.2.2.2 Evaporation

This phase takes place after the atomization and air entrainment processes have been carried out. The liquid fuel has broken into very small droplets and while the spray keeps on entraining air, heat is being transferred from the high temperature ambient gas to the tiny drops of fuel. This energy exchange produces an increase in the fuel drop energy. Their relative velocities decrease as the droplets transfer their momentum to the air but the temperature of the liquid rises. This temperature raise causes a decrease in the vapour pressure of the droplets surface, so they start evaporating, becoming gaseous and considerably reducing its diameter.

It has been widely demonstrated by several researchers that, even though, the liquid core reaches the tip of the spray at the beginning of the injection event, after a while, it will stop advancing and it will stabilize at a certain axial distance from the injector tip. Such distance is known as *liquid length* [7][8][9]. From this distance on the drops disappears and the fuel becomes a complete gaseous state. This happens because the local air/fuel mixture composition becomes leaner further away from the nozzle, both radially and axially and in any place where the local mixture fraction results to be lower than evaporation fraction, the fuel will only exist in vapour phase.

Considering the aforementioned researchers results, the liquid length results to be influenced by different boundary conditions, such as the injector nozzle diameter [10], the ambient gas and fuel properties [11][12]. However, Siebers [7] found that the injection pressure does not reveal a significant influence on the development of a maximum liquid length, concluding so that the evaporation phenomenon under engine conditions results to be controlled by the mixing process. Using different words, the evaporation of the fuel droplets occurs as the surrounding environment transmits the necessary enthalpy by turbulent mixing.

Therefore, the fuel evaporation phenomenon results to be completed when it reaches the maximum liquid length, which usually results to be about 100 times the nozzle diameter. Moreover, a to conclude, according to what reported by Garcia [13], *the hypothesis of mixing control indicates that the evaporation process, despite only taking place in the diesel spray, does not establish important differences between it and the gaseous stream, it is a global phenomenon of air-fuel mixing.*

2.2.3 The autoignition process

Considering what reported in the previous sections, the fuel has evaporated and is well mixed with the air; however, the combustion will not take place immediately. The entrained air will cause the fuel temperature to rise and some low temperature pre-combustion reactions will start taking place in the zones with relatively rich local equivalence ratios. The presence of Oxygen, together with the appropriate temperature and pressure conditions, will lead to start a chemical reaction, called autoignition. This will give place to an initial premixed combustion, followed then by a continuous oxidation of the injected fuel with the remaining air.

During the autoignition stage, physical processes results strictly linked to chemical processes, since the heat release associated with the chemical reactions alters the local thermodynamic conditions of the spray. The autoignition phenomenon is understood as the beginning of the whole heat

release process. Its start is conventionally taken at the instant when a sensible increase in the in-cylinder pressure parameter is detected, due to combustion, or the moment when the RoHR starts to raise considerably.

With the application of advanced optical techniques, Espey and Dec [14][15] has presented results that confirms how the autoignition is not an isolated process in time. At contrary, it is a phenomenon that must be studied as a continuous process, both temporally and spatially. In this sense, the following paragraphs will describe the events sequence that occurs during the continuous autoignition process such as proposed by Higgins [16], which has divided it into three main stages:

- *Physical Induction Stage*: this phase as defined to extend from the beginning of the injection process until an instantaneous increase in the combustion chamber pressure is registered or, alternatively, until a first chemiluminescence emission is detected. In other terms, it extends until the very first heat release. During this temporal phase, the injected fuels enters the combustion chamber and suffers all the above-mentioned physical processes (atomization, evaporation and mixing). As the fuel evolves through the combustion chamber and the physical processes occurs, it is heating and evaporating, and so consuming energy, causing the heat release rate to go negative. At this point, the temperature of the mixture increases up to a level where the released heat becomes higher than the absorbed. From this point on, the reaction becomes unstable and starts propagating to the surroundings.

- *First-Stage Ignition period*: it begins at the instant when a chemical activity is detectable (in terms of chemiluminescence and/or pressure) lasts until a significant heat release is achieved due to the beginning of the premixed combustion phase. In this phase, the ignition reactions grow in the region between the liquid length and the tip of the spray, where the local equivalence ratio results to be rich, with approximate values variating between 2 and 4. During this first

ignition phases is commonly observed a low intensity radiation emission, which results to be, according to results reported by Kosaka [17], the chemiluminescent radiation from the CH and CH_2O (formaldehyde) chemical species appearing during this pre-reaction phase. Moreover, as the temperature increases due to the autoignition heat released, the chemical species dissociation reactions inhibit the further development of chains reactions. This clarifies the reduction in the rate of heat release observed before the start of the second ignition stage. Such phenomenon is also related to the appearance of cold flames, which are typical of autoignition processes of hydrocarbons in low temperature conditions.

- *Second-Stage Ignition/premixed burn period*: it corresponds to the aforementioned sudden increase in the rate of hear released. This occurs once the energy transferred to the mixture both by the hot air entrainment and the cool-flame reactions meet the threshold condition required to enter in the high-temperature ignition phase. Higgins et al. [16] reports that this transition should be cause by the trigger of hydrogen peroxide dissociation, which dominates the chemistry balances producing a significant heat release. At this stage, the chemical reaction propagates to the region of already vaporized mixture that has been accumulated during the ignition delay time but that has not already started an ignition by themselves. The significant local temperature increase lead to the appearance of incandescent soot, which requires both rich local mixtures and temperatures above the 1300 K. Its thermal radiation emission extends very fast, dominating the broadband luminosity now produced by the flame

2.2.4 The diesel diffusion flame model

Considering the complexity of the involved processes and its fundamental importance in the optimization of CI engines, the knowledge of the structure of a diesel diffusion flame in quasi-stationary conditions has

been studied by a multitude of authors through various years of scientific research.

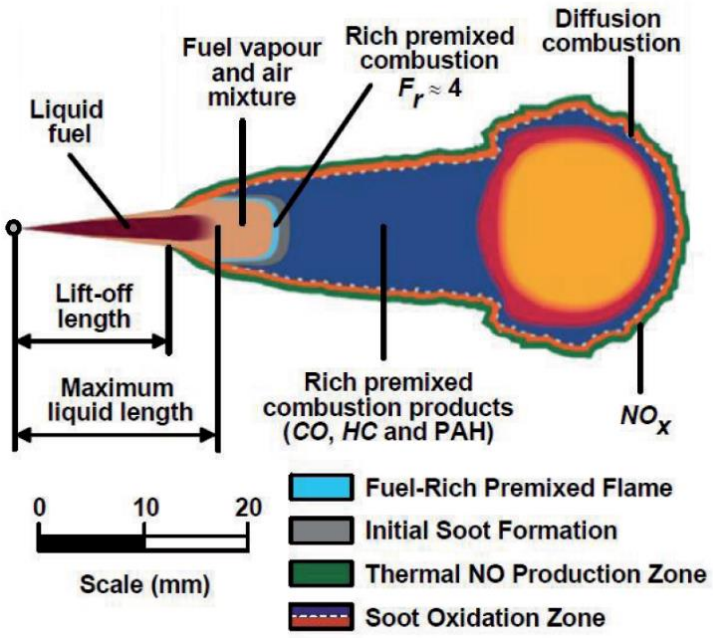

Figure 2.2. Scheme of the DI reactive diesel flame in quasi-steady state, for a diffusion combustion, according to the conceptual model proposed by Dec. [18].

This has led to several conceptual models that can be found in literature [18][19][20], each seeking to provide a clear and neat explanation of the structure of a reactive DI diesel jet. Currently, the most accepted and widespread version is probably the conceptual model proposed by Dec [18] in 1997 and later extended by Flynn et al. [21] in 1999, and which scheme is here reported in Figure 2.2.

It is important to highlight that the here reported model is valid only for a quasi-stationary flame in diffusive combustion, or, in other terms, referring to the abovementioned combustion phases, only in the temporal

interval between the beginning of diffusive combustion till the end of injection process.

Qualitatively, it can be distinguished the different important zones in the reported model scheme:

- *Zone 1*: it goes from the injector nozzle to the lift-off length. In this zone does not occurs any chemical reaction, hence is also referred as *inert zone*. The injected liquid fuel and the physical processes mentioned before in this chapter takes place in this zone: atomization, air entrainment and evaporation.

- *Zone 2*: it extends starting from the lift-off length, where in the spray reactive conditions takes place. In this area, Dec established the existence of a premixed reaction zone, where the oxygen included in zone 1 is burnt. As a consequence, the products of the premixed combustion, developing under rich equivalence ratio, are formed by partially oxidized hydrocarbons and are be considered to have the function of soot precursors.

- *Zone 3*: it is established from zone 1 and surrounding zone 2. In this zone, the flame reaches the characteristics diffusion flame structure and it is compound by two zones, internal and external. In the internal zone the partially oxidized products and soot formed in zone 2 are accumulated (mainly hydrocarbons). Instead, in the external zone, surrounding the internal one, the unburnt fuel reacts. Even though the soot formation process begins inside zone 2, is in zone 3 where the soot concentration growth results to be more important. In fact, as reported in the scheme of Figure 2.2, the maximum soot concentration is actually reached at the flame front. The main factor for the formation and growth of soot particles is the residence time. When the soot particles formed in the inside zone and zone 2 reaches the outer edge of the flame, it oxidizes completely thanks to the presence of OH radicals (generated in the diffusion flame) and to all

the available oxygen. For which concerns the nitrogen oxides production, Dec and Canaan [22] reported how they are formed on the outside of the flame, where the conditions are very favorable, especially in terms of temperature and oxygen availability. This models shows how the most favorable areas for soot oxidation are also ideal conditions for the formation of NO radicals.

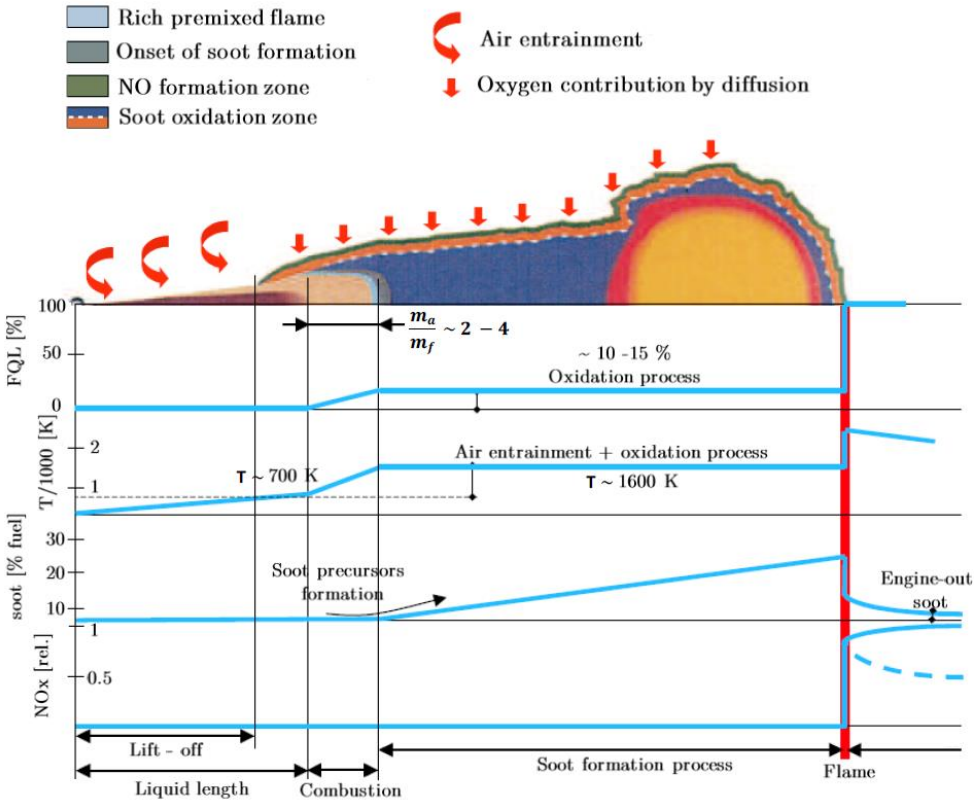

Figure 2.3. Schematic description of the spatial and temporal evolution of a fuel mass package injected during the stationary part of the diffusion combustion phase [23].

Now, the information reported in the flame model can be completed with a qualitative description of the processes that affects a fuel package during its spatial and temporal evolution, as it moves axially from the injector

nozzle through the zones of a quasi-steady diffusion flame. This information is supported by the scheme of Figure 2.3.

As mentioned in the previous paragraphs, thanks to the high injection pressure and in-cylinder temperature the injected fuel is atomized and mixed with the ambient air. The high temperature joined with the air entrainment process causes the fuel package to change state from liquid to vapour when reaches the maximum liquid length. Then, the evaporated fuel continues to mix up until the reaction zone, where reaches a local equivalent ratio between 2 and 4 and a local temperature around 700 K. The fuel mass package is then burned through the reaction zone, releasing between 10 to 15% of its total energy [24]. Hence, the temperature rises to around 1600 K and liberates partially oxidized products, particularly short chain unsaturated hydrocarbons (considered precursors of the soot formation) [25] and carbon monoxide. Here the local temperature and soot concentration results too low for the formation of NO species by the thermal route. Passed the premixed reaction zone, the fuel package enters the internal area of the diffusion flame where there is a complete absence of oxygen, which introduction is prevented by the premixed zone and the external reaction zone. In the meantime, the fuel continues to mix. With the absence of oxygen flow, it is difficult to produce a significant heat release in the internal flame. Then, at the inner part of the flame periphery, where the flame front is located, there is a substantial temperature increase. This, with the presence of the already generated soot precursor, causes the appearance of the first soot particles. These particles increase in size until they reach the flame front, where their size and concentration are maximum. Now, at the front flame surface, the partially oxidized products and the already formed soot, together with the diffused oxygen, burn out, releasing the most part of the energy (85-90%). At the flame front, the equivalence ratio results to be very close to the stoichiometric and so the produced temperature results to be very close to the adiabatic. At this temperature, the formed soot results to be almost completely oxidized but, on the contrary, the rate of nitrogen oxide formation increases considerably. At last, the obtained combustion products are diluted in the rest of the gases contained in the combustion chamber.

2.3 Fundamental characteristics of the laser plasma induction process

As seen in the previous section, ignition event in sprays can highly modulate the development of the combustion process and subsequent pollutants formation, as it directly affects all the flame and combustion development, either in spatial and or temporal magnitudes. Consequently, considering a way to interact with and modify such ignition process could be very interesting for active fuel combustion control. In particular, it could be appreciated how the implications of a versatile, controllable and non-intrusive ignition system could be really important. For this purpose, in the following sections, a review of theoretical fundaments of the laser plasma induction process will be presented and discussed.

The ignition of reactive mixtures by the application of a laser source could basically occur through four different mechanisms, whose relative importance is related to the wavelength of the laser beam employed:

- Thermal Ignition process.

This process occurs when a low-energy long-wavelength laser radiation impacts on a solid or gaseous medium, which is a good energy absorbent, that is rounded by a gaseous fuel mixture. The energy contained in the infrared portion of the laser beam spectrum is used to raise the translational, rotational and vibrational kinetic energy of the focused object, causing the breakage of its molecular bonds and allowing the chemical reaction to take place. The delay time is typically long.

As already detailed by other authors [26], the localized ignition of a mixture through this mechanism is very difficult to obtain. This is fundamentally due to the fact that the local heat deposition varies almost linearly with the intensity of the beam and that a focused beam has the tendency to produce a hot region of appreciable size rather than a well-defined Kernel. Therefore, the most common way used to take advantage of

such process is to heat small objects located inside the mixture, in order to cause self-ignition when these have transferred enough energy to the fuel, obtaining a spatially unlocated homogeneous ignition. These absorption vectors of the incident radiation can either be additives attached to the fuel, such as Al particles in suspension or chemical solutions more absorbent than the fuel itself, necessaries to locate and increase the absorption of heat; also gases such as SF_6, SiF_4, NH_3, CH_3F have been used as an inert resonant absorber necessary to sensitize the thermal ignition reaction. It could even be a part of the same engine, used as an absorbent medium instead of the mixture.

From an internal combustion engines' point of view, the requirement that a part of the system should be "sacrificed" to favor the heat absorption process for the ignition makes the application of this process not so appealable at a practical level. In terms of adding additives to the fuels, pollution concerns would again be proposed, while in terms of portions of the engine used as absorbent targets, problems comparable to the erosion of the electrodes in the spark plug would be experienced. On the other hand, this mechanism is optimal and widely used in the field of ignition of solid fuels (missiles applications) thanks to the great self-absorption ability of solids in the infrared field.

- Photochemical Ignition.

This ignition mechanism occurs when a high-energy photon dissociates a molecule, allowing its ionized constituents to react with the surrounding gases. The molecule will dissociate into highly reactive radical species that, once their production rate is higher than their recombination rate, can cause the beginning of a chemical reaction that will lead to the ignition and global combustion of the considered mixture. The principal differences with the previously described Thermal Ignition resides in the energy contained in the incident photons and the fact that in this case there is no need of a secondary absorbent medium as this role is carried out by the gas mixture itself. Furthermore, since the energy of a photon at visible and near infrared

wavelengths is less than the required for the dissociation of most gases, the photochemical ignition process is more effective in the ultraviolet region, since there a single photon already contains the sufficient amount of energy to exceed the ionization potential of some molecular species and directly cause a sustainable reaction. That's why in this case is the same incident radiation that is labeled as "ionizing".

Several studies have reported that, due to the high radical production's rate, the laser minimum energy needed to ignite some gas mixtures can be lower than 1 mJ [27][28]. This could make this mechanism very attractive for new ignition methods, since it allows igniting mixtures at lower pressures and closer to the flammability limit than other processes, since an adequate amount of reactive radicals in a sufficiently large volume it is generated from the dissociated molecules [29]. As a fact, for this process the laser energy density level is not a crucial factor, as it is for the Thermal Ignition. In addition, it seems reasonable to consider that the characteristic time needed for ignition should be shorter for this photochemical mechanism.

Considering as the "induction time" the time that elapses between the initial heating and the beginning of a rapid increase in temperature, the process of Thermal Ignition should be characterized by a long time of chemical induction (milliseconds) and a short time of excitation (microseconds). When the thermal energy is deposited in an ignition volume, only a part of it will be used to heat the surrounding gases, while other part will be lost. In a Thermal Ignition process, during the long period of induction the reactive radicals, necessary to sustain the consequent chain reactions, will be produced, while in the short period of excitation a strong exothermic reaction will take place leading to a typically stationary combustion reaction. Now, if in the same ignition volume are directly deposed the active radicals necessary to ignition and not only thermal energy, the energy loss and radical generation processes could be avoided, leading to a noticeably shorter total ignition time. That is why the photochemical process is able to ignite fuel mixtures under conditions where should normally be impossible otherwise.

Despite these advantages, this method presents some major drawbacks that make it almost unusable in most practical applications. As reported by various authors [30], the fundamental basic requirement of the method is that, in order to provoke the molecule dissociation event, the excitant laser wavelength should be as close as possible to the gas molecules' absorption wavelength. Being able to ensure such close match between wavelength is very complex, limiting possible applications only to certain type of mixtures and, more important, only with certain types of tunable laser systems, which nowadays still result to be very complex, expensive and difficult to set up in such limit conditions.

- Resonant Breakdown

This process consists in the non-resonant multiphotonic photodissociation of some of the molecules presents in the ignitable gaseous mixture, followed by a resonant photoionization of one or more atoms, previously generated by the photodissociation process, under continuous laser radiation bombing. This process sequence leads to the formation of the "free electrons", that are able to absorb even more energy through the inverse Bremsstrahlung effect, allowing the eventual occurrence of a breakdown event, reached through the electron cascade process, and finally generating plasma which in the end ignites the reactive mixture.

This process has been identified as cause of the plasma formation for the first time by Forch and Miziolek [31][32], who were able to obtain plasma with which ignite H_2/O_2 and H_2/N_2O mixtures at atmospheric pressures. Although only a limited number of studies on ignition mechanisms based on this phenomenon have been published, up to now the authors agree to indicate it as very attractive and viable process, due to the main advantage of the minimum ignition power needed, certainly very reduced if compared to a non-resonant breakdown, as long as the correct wavelength is applied to each specific gas mixture. Thanks to this match, most of the laser pulse energy is here used to heat up the generated plasma, representing a main difference with what happens in a non-resonant breakdown phenomenon.

However, technical limitations relatives to operate with systems able to generate always at the correct wavelength for each reactive mixture under ignition converts it in a very complex and expensive process.

- Non-resonant Breakdown (Laser induced spark ignition)

This mechanism takes place when a laser pulse of sufficient energy peak power is focused in an adequately small volume, where the components of the electrical field of the focused radiation reaches an energy level such to influence the gas molecules leading to its electrical breakdown. There are two different sub-mechanisms that dominate the beginning of the breakdown process, depending on the characteristics of both laser energy employed and gaseous media to ignite:

  - multiphotonic ionization

It involves the simultaneous absorption, by a molecule or an atom of the gas, of a number of photons such as to cause their ionization. The absorption of photons induces the expulsion of the valence electrons in the conduction band to a space where they can be considered free of atomic or molecular systems. There they acquire energy through the tempo-variant electromagnetic field produced by the focused laser radiation. In addition, the free electrons absorb also kinetic energy through the inverse-Bremsstrahlung process, thus being able to ionize more molecules and atoms contained in the same focal volume and, therefore, produce an even greater number of free electrons. This process goes on under exponential growth until the potential of the local electric field exceeds the threshold for the gas breakdown. Once these conditions are achieved locally, at that point happens a plasma discharge that can produce local temperatures in the order of 10^6 K and local pressures of 10^3 KPa.

This process results to be significant only for short wavelengths ($<$1 μm) or very low pressures ($<$ 1,33 KPa), where the collisional effects could be neglected. In fact, the energy of a photon at visible and

near infrared wavelengths is much smaller than the ionization potential of most gases. Especially for very short pulse durations (some picoseconds), the multiphotonic ionization represents the only process that can lead to a breakdown since, even considering any eventual collisional energy transfer, there is not enough time for collisions between electrons and molecules to happen.

- electronic cascade ionization

As reported by Weinrotter et al. [33], this is considered to be the dominant process in the plasma generation. In this process, the initial free electrons absorb photons from the laser beam through the inverse-Bremsstrahlung process. If the electrons gain a sufficient amount of energy, they can ionize other gas molecules by impact, leading to an electronic cascade and gas breakdown in the focal region. It is important to note that, although this process is identified as dominant in plasma production, it relies on two basic conditions:

- the "free electrons" formed should be inside the same focal volume region and be constantly irradiated by the incident laser radiation [34];

- the electrons should reach an energy level higher than the ionization potential energy of the gas. Only in this case the "cascade" effect could take place [34].

The generation of the initial free electrons is greatly facilitated by the presence of impurities in the gas mixture (dust, aerosols, soot particles), which absorb laser radiation causing a high local heating that leads to the release of electrons. Unlike what happens for the multi-photon ionization, in this case there is no dependence of the process from the radiation's wavelength.

Considering both sub-processes characteristics, it could be understandable how the multiphotonic ionization will be fundamental in the

first instants of a non-resonant breakdown process. That is because the photons' energy, in the infrared and visible wavelengths is much lower than the necessary for the gas ionization. In order to provide, through the laser beam, an emission of sufficient irradiance to generate the initial free electrons, pulsed laser equipment are typically used in the Q-switch mode.

With regard to the processes described, also the effect of losses (due to the diffusion of electrons outside the focal volume, by radiation or collision) has to be considered. Such energy losses make the critical energy for breakdown dependent on the size of the focusing volume, the global pressure in the location, the type of gas mixture where it should take place and the possible presence of impurities.

The spark produced by this process is a source of very reactive chemical "intermediaries" that are at a very high pressure and temperature (10^6K and 10^3atm reached at the end of the laser pulse) and have such a small time scale with respect to chemical kinetics of the combustion process that allows it to be considered as a punctual and instantaneous source of reagents (it can be estimated that the duration of a spark caused by the laser coincides with the duration of the laser pulse [35]). It emits light, heat and reaches such extreme local conditions that cause the development of a shock wave that expands rapidly in the surrounding environment and could became strong enough to ignite gaseous fuel mixtures, liquid fuel sprays or even extinguish a diffusive flame [36].

Concluding the analysis on the fundamental mechanisms at the base of a possible laser plasma ignition system, among all the possible mechanisms presented, the non-resonant breakdown represents the one that is most widely used to start a combustion. This is mainly because of its ease of implementation, since there are no constraints in the choice of the laser wavelength to be used, and it does not need a match between laser radiation and medium to ignite. The wavelength only influences the energy threshold to obtain breakdown and, once it is reached, the ignition depends only on the energy absorbed from the plasma. Therefore, the critical parameter is not the

wavelength of the incident radiation, but the irradiation of the laser condensed in a sufficiently small focal volume. Such process is generally referred as "laser-induced spark ignition"

2.3.1 Laser pulse duration and wavelength influences on the non-resonant breakdown induction

Different authors highlight how neither the duration of the laser pulse used, nor its wavelength influence the physical process of igniting a fuel mixture. In fact, this represents the main characteristic that has allowed the non-resonant breakdown mechanism to become the most used in this field of research. In practice, the mechanism allows to eliminate any limitations in the type of laser source necessary for its implementation, leaving a high flexibility that, at a practical level, replaces the disadvantage of needing a greater energy with respect to, for example, a resonant breakdown.

It has been shown in the work of Syage et al. [37] that variations in the duration of the laser pulse, but always under 15 ns, and the wavelengths of the laser source do not significantly affect the ignition process or the minimum energy required. More in detail, the authors describe an ignition study on mixtures of H_2/air and H_2/air/CO_2 using an Nd-YAG laser (Quantel QY471) set under different conditions: in Q-switched mode at 532 nm and 355 nm with pulses, respectively, of 12 ns and 9 ns; and in pulse mode-locked at 1064nm, 532nm, 355nm with pulses of respective duration of 50 ps, 35 ps and 25 ps.

When measuring the minimum energy required for ignition of the H_2/air mixture in all these configurations, the authors found that differences between pulse durations and wavelengths are negligible when compared to the uncertainties of the measurements and also various orders of magnitude smaller than the differences between the form of energy deposition under study and the typical of other ignition systems, such as electric discharge (according to results reported by Lewis and von Elbe [38]). For this reason,

the authors conclude that, for pulse durations under 15 ns, the laser source wavelength and the pulse duration do not affect the minimum ignition energy.

Looking for a physical explication of the observed events, it could be stated that:

- the independence with respect to the wavelength is intrinsic to the type of physical mechanism used to cause the ignition. As already noted in the physical explanation of the phenomenon of non-resonant breakdown, it does not depend on the wavelength of the incident radiation, because it is not needed to excite the chemical components with a laser radiation frequency close to its absorption spectrum to achieve breakdown.

- the independence with respect to the duration of the laser pulse could also have been imagined a priori of the reported results. In fact, physically it is the chemical kinetics of combustion which determines the relevant time scale for the phenomena governing ignition. However, the duration of a laser pulse (typically 10 μs) is orders of magnitude smaller, than the induction time of the reaction. This allows, then, reasonably to consider the laser ignition mechanism as instantaneous for what concerns the effects of the energy deposition. By contrast, the phenomenon of energy deposition by electric discharge is characterized by time periods comparable to the scale of combustion (typically about 100us), which is one of the major differences between the two ignition phenomena.

2.3.2 Energy breakdown threshold definition

Probably the most common definition has been given by Weyl et al. [34] and Chen et al. [39]. Both authors define the optical breakdown threshold level as the energy level above which the breakdown event is appreciable for more than 50% of the laser pulses fired at the focusing zone. This definition

results necessary when dealing with the extremely stochastic aspect of the phenomena of laser-induced breakdown. In fact, the authors report that, near the threshold value ($E_{thr} \pm 10\%$) the probability to obtain breakdown is always lower than 100%. This leads to significant fluctuations in the obtained spark energy, in the order of $\pm$ 20% near the threshold value. Therefore, it must be underlined how the strongly random aspect of the breakdown phenomena causes great difficulties in obtaining a low energy spark as, in order to have 100% confidence in the breakdown generation, its energy should always be greater than the real threshold value. That is also the reason why other authors [35] report how they have decided to fix the minimum energy level for laser ignition to a value higher than the real threshold for breakdown, and then extrapolating results at lower values for the ignition energy with a polynomial fit.

2.4 Considerations upon LIP applicability under engine-like condition

In the following paragraph, some consideration will be made about the possibility to apply this technique in a typical engine environment, taking into consideration the a priori advantages and drawbacks of its application.

2.4.1 Minimum ignition energy differences between Laser induced plasma and traditional spark plug

Considering again results obtained by Lewis et al. [38] it can be stated how the laser ignition technique requires a minimum power for ignition larger than the electric discharge, with a difference of almost 5 times in the energy of the spark near the stoichiometric conditions. Similar results have been reported by various authors in literature, such as Lim et al. , Phuoc et al. [41] and Kingdon et al. [42], in particular for the ignition of CH_4/air mixtures. The fact that a greater amount of energy is required for ignition for the laser spark with respect to electric spark, can be identified as a feature of the laser

ignition system itself, verified by different authors, that have also tried to give a physical explanation:

- Syage et al. reports an explanation based on the Homogeneous Hot-Gas Model. They start from the inevitable observation that the high energy density and the short duration of a laser induced plasma make it less effective for the ignition process if compared to the spark obtainable from an electric discharge. Then, based on the homogeneous hot-gas model they develop these considerations:

  I. The creation of a flame kernel requires that a sufficient amount of energy is condensed to heat up a minimum volume of the mixture until it reaches a threshold temperature level.

  II. A characteristic induction time τ [37] is associated to the ignition process. Therefore, it is also necessary to consider the dissipative phenomena that can play an important role in the initiation or eventual extinction of an incipient flame. In general, it could be stated that the generation of local conditions that allow to lengthen the residence time of the energy deposed into the flame's volume will favor the application of lower ignition energies. Such conditions could be commonly reached with the growth of the induction time τ and the decrease of the local temperature.

  III. The optimal heating rate to favor ignition will result from a balance between the benefits of a long induction time (then a lower temperature threshold) and the disadvantages due to heat lost by dissipation.

  IV. An optimal value of the deposed energy density can be identified: excessive values could cause blast wave losses and turbulences that would destroy the natural evolution of the flame.

  By considering all these factors, they explain the energy difference observed between electrical discharge and laser induction by the fact

that the electric discharge satisfies condition III, and it is favored by it, while the laser plasma induction suffers from the consequences of condition IV. In other words, the energy deposition by electrical discharge provide an optimal heat rate, taking more advantage from the benefits of a large induction time τ than what it loses for energy losses during the process. At the same time, the laser ignition process is affected by its short induction time and its high value of energy density deposed. In fact, the breakdown energy contained in the laser induced plasma is referenced as *overkill* [43] with respect to the minimum energy theoretically needed for the mixture ignition.

Conventionally, also the sparks generated by electric discharge imply an overkill with respect to the minimum energy required, but it is possible to provide more controlled impulses in time and power, being able to deposit an energy closer to the minimum value. As for the laser ignition mechanism, that form of control turns out to be more complicated, as will be better highlighted later in this document. The authors also propose some examples to resolve the overkill problem, such as depositions of fibers of high reactive materials in the focal zone that should absorb part of the deposed energy. In addition, always in [37], it is also argued that the distribution of energy in a region of space cylindrical, as provided by the electric discharge, with respect to the spherical region of a laser-induced plasma, allows a more favorable flame propagation in the first instants of flame development.

- Phuoc and White [41] consider that the highest minimum energy required for ignition with a laser source has to be ascribed fundamentally to the short pulse duration and small focal volume provided by this method, including some eventual considerations upon the flow field in the ignition zone. They argue that, in an electric discharge ignition, the duration of the spark is long, its energy density is low and the effects of the disturbance in the flow field due to the shock wave produced are reasonably negligible. That is why the flame

kernel expands into a practically steady gas and the ignition mechanisms are controlled by a diffusive process.

However, a spark created by focusing a laser pulse of ps/ns provides a different ignition mechanism. Such a spark can ignite the mixture directly, either thanks to the force of the shock wave that provokes or thanks to the hot gases that remain after its expansion. The rapid dissipation of energy and the small size of the spark increase the heat losses and limit the time in which the deposed energy can stay contained in the dimensions relevant to the support of the flame kernel. That is why the laser spark kernel quickly falls to ambient conditions without being able to heat the gases around it at a temperature higher than the ignition threshold for a time greater than the induction time of the process. They conclude the analysis proposing how this is the effective reason from which derives the need to increase the energy provided by the laser source in comparison to an electrical discharge.

In conclusions, even though different considerations and with the application of different models, it could be seen how various authors reach the common conclusion upon the systematical need of higher minimum energy for the laser ignition system than a traditional electrical one. The different explanations provided results to agree between them

2.4.2 Effect of local mixture and air flow conditions upon laser induced plasma effectivity

Results obtained by Phuoc et al. [41] upon CH_4/air mixtures highlights another interesting characteristic of the laser induced plasma ignition. It could be appreciated how the laser system ignites mixtures with a volumetric methane fraction higher than the upper flammability limit, while it fails to ignite mixtures with less than 6.5% in methane volume, which is higher than the lower flammability limit of 5%.

Similar results have been obtained by Bradley et al. [43], who reports how, with initial conditions of a steady mixture, the ignition limit of the laser system for lean conditions is found to be at values not only higher than the lower flammability limit, but also higher than the one observed applying, in the same conditions, an electrical discharge system [44]. They justify this low effectivity of the laser system in lean mixtures ignition as a direct consequence of the "third lobe" generation phenomenon in the special conformation of the induced plasma kernel.

The generation of this "third lobe" has been explained through gas-dynamics effects due to the rarefaction wave produced by the breakdown, as numerical studies from Morsy and Chung [29] and Spiglanin et al. [45] confirm. The appearance of the third lobe implies a fast increase of the superficial area at the plasma borders, with a consequent high rate of narrowing that could inhibit the propagation of the flame. For lean mixtures ratios, near the flammability limit, and for fuels heavier than oxygen, this rate of narrowing may be sufficient to completely prevent the development of the flame. They also report how the effect of the average flow velocity (u') in turbulence conditions is similar to the one in the conventional case of an electric discharge. In such case, various experiences have found that a raise in the average velocity u' implies a reduction of the interval available to ignition between the flammability limits [46]. Similar effects have been observed by Bradley et al. [43] using mixture of isooctane/air at 358 K and varying pressures between 0.05, and 0.25 MPa at different flow velocities u', with a laser energy prior to the focal point of 180 mJ. They report how an increment in the average velocity, independently of the pressure, implies a raise in the equivalence ratio that the system is able to ignite at the lower flammability limit.

In tests conducted with a laser energy of 90 mJ, the authors report that the value of equivalence ratio at the limit of flammability increases of 0.15 for very low speeds and remains practically unaffected when the speed reaches 7 ms^{-1}. This is another indicator of how the local gas-dynamic effects have a strong effect on the plasma kernel, effects that start to become negligible as

the flow velocity increases and so does the magnitudes of the turbulent phenomena. On the other hand, authors also report that, if the narrowing rate is not as high as to prevent ignition, the greater surface area due to the third-lobe phenomenon and the effects of turbulence on the flow field, increase the flame propagation ratio.

Likewise, the highly reactive species generated in the plasma, thanks to their effects on the subsequent reactions that take place in the flame, contribute to the increase of the propagation rate. This phenomenon has been clearly demonstrated in the experience of Lawes [47] where, measuring the intensity of CH* emission by spherical laminar flames at constant pressure, has been demonstrated that the intensity per unit area of the flame front result to be much more persistent when high energy sparks are used. Such sparks are similar to those that can be induced by a laser. Normally, for low energy sparks, it rapidly decays to a constant value. The combined influence of these three effects leads to an "overdrive" in flame propagation speeds, different by its characteristics from what could be seen in flames started by classical ignition conditions.

Consistent with the results previously reported, Beduneau et al. [35], in their parametrical studies on the MIE (minimum ignition energy) of a laser-induced spark, highlights how misfires are mainly attributable, under conditions of induction in a laminar flow, to instabilities of the same flow around the flame kernel caused by the elevated temperature gradient. This observation turns out to be consistent with other results from Spiglanin et al. [45], who report an observation about the discontinuity in the OH* position generated when the kernel disappears in the first phases of its expansion.

The authors attribute the cause of these discontinuities to the high expansion speed of the flame kernel itself (estimated to be 30 ms^{-1} for high energy cases), which causes it to become fragile with respect to heat losses induced from the surrounding flow, as highlighted before in 2.4.1. In addition, the flame kernel is subject to energy losses by dilution and conduction, so the

energy available in the induction zone must be able to compensate all these losses in order to carry a self-sustaining flame.

On the other hand, as already reported, imposing high energetic deposition rates, the appearance of the temperature gradient around the kernel provokes instabilities in the flow increasing even more the discussed energy losses. So, according to the authors, even for the typical high rates of energy deposition of a plasma induced laser, misfire can occur. Even though these high rates of energy deposition are necessary to compensate local losses, they can still lead to flame kernels that, growing in a laminar way, can not develop and disappear, suffering from the disturbance of the instabilities of the flow and so causing the consequent misfire. Also for the critical ignition conditions (rich and lean limits of the mixture) the flame kernel cannot propagate in the opposite direction to the local flow if too low deposition rates are maintained while at a sufficiently high rate it can do it only for few milliseconds.

By considering all these factors, Beduneau et al. highlight how the local equivalence ratio of the areas around the formation of the flame kernel proves to be equally important as the spark energy itself to determine the success of the ignition event, since the expansion of the kernel becomes much more difficult in rich or lean conditions and the kernel is very sensitive to flow instabilities.

To corroborate this type of analysis, the authors report some images of ignition by laser induced plasma, focused through a 100 mm focal lens, obtained through the Schlieren visualization technique and recorded at a frequency of 5 KHz with a high-speed digital camera, which are here reported in Figure 2.4. Each series shown refers to a single event and cases (*a*) and (*b*) are ignition failure. From the analysis of these images it can be appreciated how, for a lower energy deposition rate and a equivalence ratio that favors ignition (close to stoichiometric), the flame expands in a completely laminar way (Figure 2.4 (*d*)).

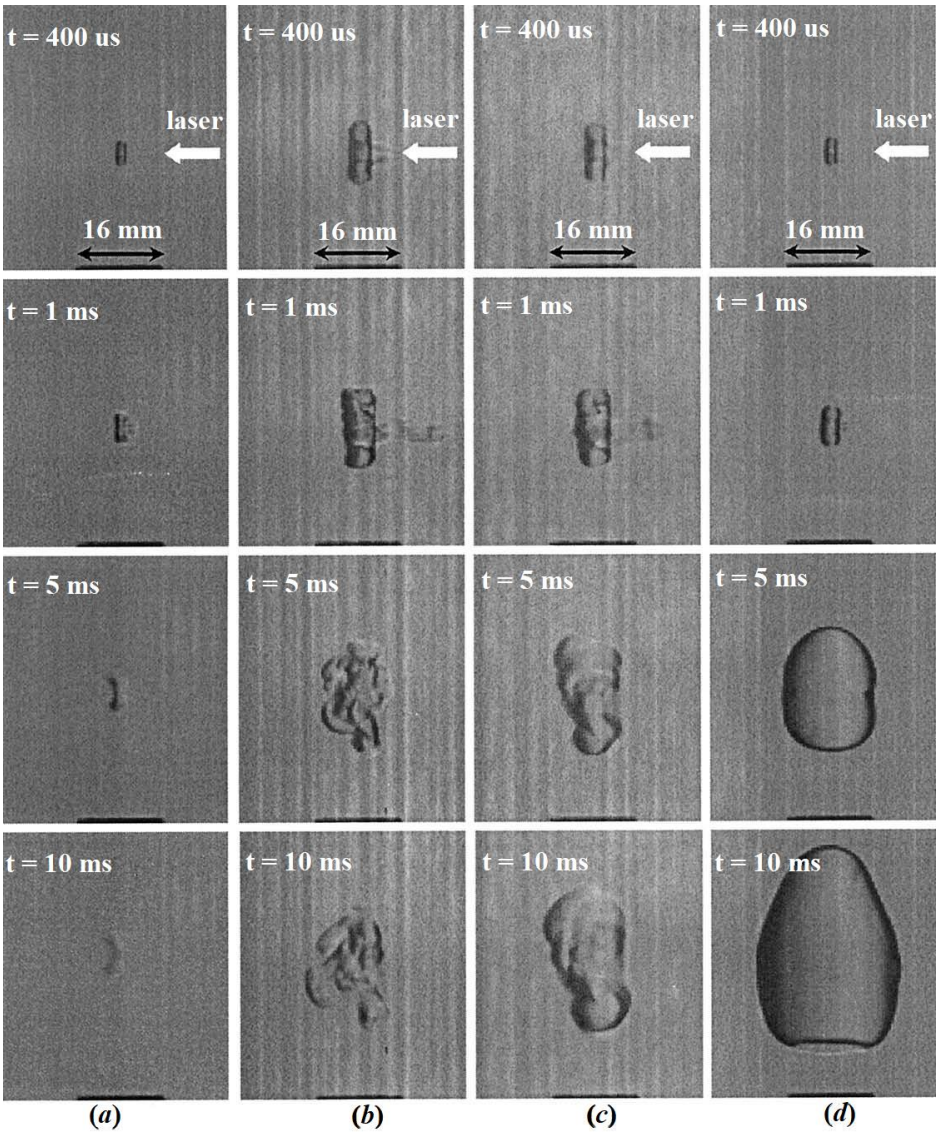

Figure 2.4. Schlieren images of laser-induced plasma ignition in pre-mixed flows of CH_4/Air at the speed of 66cms^{-1}. Adapted from Beduneau et al. [35]. The focal distance of the focusing lens is 100 mm, with the laser beam coming from the right side of the images respectively providing energies prior to the focal area of: 2.1 mJ (a), 79.5 mJ (b), 26.5 mJ (c), 2.6 mJ (d). The respective equivalence ratio are: 0.65 (a), 0.6 (b), 0.65 (c), 1.3 (d).

To explain such difference it is necessary to consider the ignition process taking place in each of the two cases. As mentioned by Spiglanin [45], the local equivalence ratio in the early stages of kernel formation is not significant with respect to its generation, since the high amount of energy deposited in the plasma in such a short period of time (≈8 ns) is able to completely oxidize the mixture. This can be precisely noted by looking at cases *a* and *d*, which basically have the same laser energy in different air/fuel ratio conditions. In these cases, it can be seen how the flame kernel dimension in the first milliseconds is comparable but it leads to two completely different expansions. On the contrary, cases (*a*) and (*c*) have the same equivalence ratio but different laser energies, and it can be clearly observed a smaller kernel for the lower energy case.

Considering all the recollected contributions from different authors regarding this topic, it can be concluded in first instance how the laser ignition technique results penalized in the ignition of lean mixtures with respect to a more traditional electric discharge technique. In the end, this is because the breakdown provided by the laser system causes important gas-dynamic effects that create a high rate of surface stretching between the plasma and the flame in development that, for lean mixtures, could stretch the kernel to its extinction. This effect is always less evident with the increase in the level of turbulence in the ignition zone, because these gas-dynamic effects become negligible compared to the magnitudes of the turbulent phenomena.

On the other hand, Bradley et al. comment that the aforementioned *overdrive* phenomenon, i.e. the fact that the species generated by the plasma contribute to increase the propagation rate, may represent a considerable advantage for combustion applications with lean mixture in the automotive field, particularly as a substitute for the load stratification strategy. All this should be valid under the condition to maintain operating regime not too close to the lower equivalence ratio limit and if the NO produced by the plasma is maintained at a low concentration, or can be then removed in other

ways (Dale et al. [48] report that the production of NO_x depends on the time scale of the spark).

In the same sense, Ma et al. [49] report an effective decrease of 4-6 ms in the time for ignition using a laser system, thanks to the aforementioned overdrive, which leads to a decrease in time required by a complete combustion, allowing the ignition advance to be lowered and thus increasing the overall efficiency of the engine. The effect of overdrive could also be exploited in the field of causing combustion in gas turbines, in which the laser can be sent directly to a region of optimal ignition probability, where the mixture is not excessively lean, in a more convenient way than a plasma-jet igniter or a surface discharge igniter that are typically employed nowadays.

However, the difficulties encountered in the ignition of lean mixtures cannot be underestimated. It must be taken into account when considering a direct implementation of the system in the automotive field, that one of the main benefits of this technique nowadays should be favoring ignition under lean conditions.

2.4.3 Considerations upon the optimal kernel radius for ignition

The possible existence of an optimal radius of the spark allowing to obtain the ignition of a fuel mixture in reliable way has been commented for the first time by Ronney [50], and it can also be found in the work of Phuoc et al. [41], where they compare the laser energy necessary for ignition and the energy threshold for breakdown in CH_4/air mixtures. In particular, the authors observed that the minimum ignition energy remains the same for mixtures of methane/air containing from 8% to 15% of methane, and indicate as a reason for this that, if the energy provided from the laser source is sufficient to guarantee breakdown it also guarantees the mixture ignition. This could only happen because, between those limits, the equivalence ratio does not contribute to vary the energy threshold for ignition. In this way, the

determination of the ignition threshold will only be referred to the single necessity of inducing plasma. This, once generated, ensures by itself the ignition of the mixture under exam. This would then also indicate that the size of the induced spark, for the energy level of breakdown, will be large enough to allow the combustion development.

However, too rich or too lean air methane mixture have not been ignited by a spark created at its corresponding energy level for breakdown. The authors explain this behavior arguing that the problem does not resides in the energy level concentration, but in the fact that the sparks created are too small to achieve ignition for too rich or lean mixtures. This would be so the reason why it would take more energy from the laser to ignite these mixtures: not to create a more energetic spark, but to obtain a bigger spark.

As an example, from their reported data, it is noticeable how, at a 9.5% methane concentration in volume (corresponding to an equivalence ratio of 1) the formation of the spark and the ignition both occurred at an intensity of laser of 39.2mJ while, for a mixture of 7.2% methane in volume (equivalence ratio = 0.74) a spark can be already formed at 32mJ but, in order to achieve ignition, the laser intensity needs to be increased up to 39mJ. For a mixture of 16% methane volume (equivalence ratio = 1.81), the formation of the spark occurs at 60mJ while it is possible to ignite the mixture only with an intensity of 100mJ. The authors have used a CCD camera system mounted perpendicular to the direction of the focused laser beam and a photomultiplier tube (PMT) with a 1:1 optics to records time-resolved images of the spark emission. The size of the spark has been determined in terms of FWHM of the intensity profile in the recorded emission. From these measurements they were able to confirm their hypotheses, assuring that the need to provide a greater laser energy than that required to obtain breakdown only lies in the need to increase the induced spark dimensions, in order to reach a minimum flame kernel size that allows to sustain the ignition without quenching in the first instants.

2.4.4 Minimum ignition energy variation under engine-like conditions

The dependency of the Minimum Ignition Energy on some typical parameter of an engine-like condition will be now analyzed, particularly considering its possible variation with pressure, in-chamber air flux and finally the focal length of the system focusing lens. Consider the possible variation of the MIE of the media under breakdown results fundamental at the time to consider the possibility to obtain an ignition system reliable in all the possible conditions under test. Knowing the variation of the minimum energy allows, in fact, to control more precisely the energy used for the plasma generation and avoid possible drawbacks effect such overkill.

2.4.4.1 Minimum ignition energy dependency on pressure variation

Bradley et al. [43] report a parametric study for the variation in the energy required for breakdown with respect to the pressure in the induction zone. These results presents the variation in the probability of obtaining a breakdown in air by varying the laser energy before the focal spot under different pressure conditions, at the same temperature of 300 K, and for a quiescent mixture. As experimental device to create breakdown, they used a pulsed Nd:YAG laser (Spectron SL800) set in Q-switched mode and operating at 1064 nm wavelength, with a beam diameter of 6 mm, pulse duration of 15 ns at a repetition rate of 10 Hz and with a peak shot energy of 200 mJ.

In such tests they identify the breakdown events through measurements of luminous intensity made with a photomultiplier. For each laser energy they fired 20 pulses in a row. They noted how the energy needed for breakdown decreases with the increase of the pressure. Considering the physical process of breakdown, the authors justify the phenomena explaining that the initial phase of multiphotonic ionization, which allows the generation of the free electrons that will be then excited up to high energy levels to start

the electronic cascade, is favored from an increase in pressure, since the frequency of interatomic collisions increases. It can also be seen how, as the pressure decreases, the sensitivity of the breakdown probability is increased.

Accordingly, for low pressures, the range of probability of obtaining breakdown becomes wider in addition to move to higher energy levels. This makes very difficult to obtain reliable plasma induction in a low-pressure environment, especially when considering the typical shot to shot power peak fluctuations of a laser system and the associated modal changes in the laser beam profile. The breakdown threshold at sub-atmospheric pressures is very high, and obtaining plasma is practically impossible if the intensity of the beam falls slightly because of the modal variations.

The same authors also present a study for the variation of the energy threshold necessary for 100% breakdown effectiveness in different mixtures. If the dependence from the pressure is expressed as an exponential function p^{α} Bradley et al. report to have obtained an α of -0.54 from their tests. The exponent of the energy threshold variation seems to be consistent with those reported by other authors, such as Chylek et al. [51] who found an α of -0.45 for a range of lower pressure variations, at a laser wavelength of 532 nm and a smaller focal point (corresponding to a lens of a shorter focal length). Phuoc and White [43] report an α value of -0.5, with the same laser equipment at 1064 nm, but with a different optical system from Bradley.

The results reported by Bradley are referred to breakdown in clean air, rich (equivalence ratio of 7) and lean (ratio of 0.4) iso-octane/air mixtures at a temperature of 358 K. In both cases, the study have been performed outside the flammability limit. No significant difference in the breakdown thresholds was found between rich and lean mixtures, with α values obtained respectively of -0.36 and -0.37. The maximum pressures reached have been of 0.5 MPa for the rich mixture and 0.25 MPa for the lean mixture, so as to avoid in both cases to cause ignition, thus not affecting the experimental measure. At a pressure of -0.5 MPa, the measured threshold energy for breakdown has been of 36 mJ for both air and Isooctane/Air mixture. In the

end, it could be stated how Bradely's study results to be in accord to what Hickling reports [52]: there are no significant differences between air and a mixture of air/fuel in terms of the energy needed to obtain a breakdown.

2.4.4.2 Minimum ignition energy dependency on local air flux and focal length

Beduneau et al. [35] report a systematic study on the effect of the focal length of the ignition system lens and the local flow rate in the combustion chamber upon the minimum energy needed for ignition. The authors define the cases of ignition success as those where a flame front in laminar propagation is visible in the recorded Schlieren images 10 ms after the energy deposition, as seen in images reported in Figure 2.4.

From the results analysis, the authors highlight how the minimum energy necessary to ignition increases with the focal length used in the laser focusing system, and so, with the focal volume. Therefore, it seems evident how the energy for unit volume deposited from the laser should be an important parameter for the later evolution of the flame kernel. The authors confirm their observations through the graph here reported in Figure 2.5, where the evolution of the minimum energy necessary to the ignition is shown only in function of the focal length of the focusing lens used in the system, using a normalization of the data based on the minimum measured MIE. With respect to this graph, they show the discrepancy between conditions of rich and lean mixtures, as an indication of the importance of the size of the focal volume in the development of the flame kernel.

These observations seem consistent with the sensitivity of the kernel with respect to its initial dimensions, which explain the increase of the MIE in the zones of rich equivalence ratios. This is also consistent with the results reported from Phuoc et al. [41] and Lee et al. [53] in tests carried out under quiet conditions, in which Phuoc presents values of MIE higher than those of Lee, using a laser of the same characteristics and wavelength but with a

75mm focal lens instead of the 50mm lens used by Lee. In addition, results of Bedueneau et al. are also corroborated from the results reported by Lim et al. [40] for a mixture of CH4/air.

Following with the data analysis, the authors highlight, as has also already been reported before from the observations made by Phuoc et al. [41], how they were be able to provoke ignition for mixtures that have an equivalence ratio up to 2, which is higher than the observed values using an electrical spark. This has been explained by referring to the physical differences between the ignition processes of the two techniques.

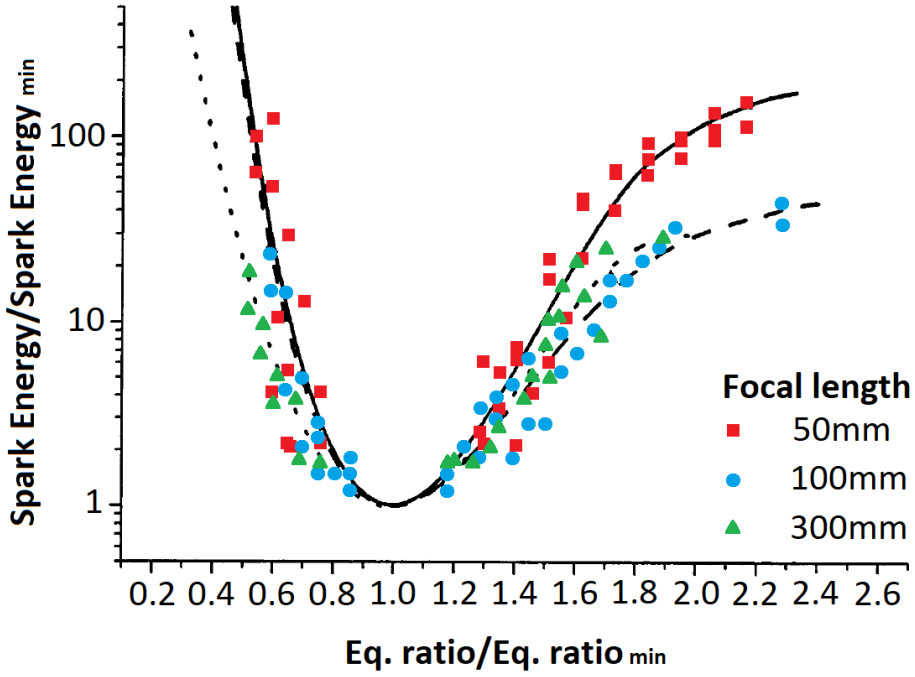

Figure 2.5. Results of minimum energy measurements for the laser ignition with the variation of the focal length. The showed results are normalized with the equivalence ratio requiring the minimum energy for ignition, and the spark energy at that equivalence ratio. Adapted from Beduneau et al. [35].

The evolution of the MIE with the equivalence ratio of the mixture, presents a different shape for the two techniques if the poor or rich equivalence ratio are considered. From Figure 2.5 can be seen, in the rich equivalence ratio zone for the laser ignition, how the MIE tend to a constant value while for lean mixtures it increases rapidly lowering the a/f ratio towards the flammability limit of the CH4/Air mixture (5% by volume). This behavior pattern for the lean zone is typical of electric spark ignition. In addition, it can be noted that the equivalence ratio corresponding to the minimum measured MIE varies and grows with the lens' focal length (going from 0.95 for a focal of 50 mm to 1.05 for a focal of 300 mm, in the case of a flow speed of 66 cms-1).

All the observations made by the authors remain consistent with the consideration of the irrelevant impact of the local a/f ratio on the development of the flame kernel in the first phases of its formation. In fact, whatever the equivalence ratio, at the kernel formation all the molecules are oxidized thanks to the high energy deposition in a very short period. Consequently, a high a/f ratio implies that the appropriate amount of radicals that allow the development of a self-sustaining flame should be easily formed. In this way, the characteristic behavior of the laser source in the rich ratios zone results to be explainable: the MIE reaches a stabilization since, after a threshold value for the equivalence ratio, an adequate amount of radicals is always formed.

For what concerns more specifically with the effect of air movement, the authors highlight how with the increase of the flow speed also increases the energy required for ignition. This should be direct consequence of the increased convection losses in the areas around the flame kernel. However, this trend is reversed if lean mixture conditions are considered, where the MIE falls with the increasing of the flow speed. The explanation to this phenomenon considers the existing differences between rich and poor equivalence ratio areas. As already highlighted more than once in this work, the formation and the first instants of the flame kernel development are not affected by the local a/f ratio of the mixture. Anyway in the kernel formation

area, in conditions of lean mixture, a lack of CH_4 (in this case) atoms also involves a lack of carbon atoms, even for a high energy deposition. So, with the increase in the flow velocity, there will be a corresponding increase of the CH_4 atoms available for ignition.

Therefore, this takes the authors to reasonably consider that the expansion phase of the flame kernel occurs in a condition of steady flow, contrarily to what happens in the phase of its formation, when there may be expansion speeds between 10 and 30 ms^{-1}, depending on the energy of the spark. The observation is also consistent with Spiglanin et al. [45] statement that the flow can be considered basically stagnant during the kernel formation. Finally, they also noticed that the impact of flow velocity near the stoichiometry mixture conditions is more important when using a small focal focusing lens, a result that fits well with the consideration that a smaller kernel is also more fragile.

In the end, the considerations reported from Beduneau et al. [35] regarding the effects of focal length and velocity of the flow on the MIE, confirm the conclusions of other authors, which have already been presented before in this chapter, that the first stage of the kernel formation is fundamental for the propagation of a self-sustaining flame.

2.5 Objectives of the study and Thesis approach

Considering the literature survey presented above, from the description of the diesel spray formation and combustion process, it could be outlined how the generation of pollutant and combustion products results to be strictly related to the characteristic timing and spatial evolution of the diffusion flame. In particular, the ignition delay time and the spatial development of the zones described by the combustion flame model has shown to have an important influence on the evolution of the diesel combustion itself.

In this sense, the possibility to control the location and timing of the ignition phases of such combustion process could lead to a modulation of the flame development and so, of the pollutant formation. In particular, the possibility to variate the local condition at which the ignition phases take place, could produce a strong influence on all the subsequent combustion development.

Nowadays, spark assisted ignition systems only admit the possibility to varying the timing of the ignition process, being the location of the provoked ignition fixed by the physical presence of a spark plug system. However, in the literature survey it has been shown how the application of a non-intrusive, modulable and controllable laser ignition system to an adequately equipped internal combustion engine is feasible, once the appropriate adjustment to the system are made. Such ignition system will allow to gain an additional degree of freedom for the control of a combustion system, allowing not only to time-phase the ignition at some selected conditions, but also, and more importantly, to space-phasing it wherever it should be more convenient. This approach allows new kind of studies regarding how the local conditions at ignition are affecting the combustion development and finally, permits to think on a new active control and modulation system for the combustion.

For such reasons, this doctoral thesis will pursue the following main objectives:

- Develop and optimize a versatile ignition system that will allow the controlled selection of the timing, position and energy deployed for the ignition of a direct injection diesel spray. Such new ignition technique could open various new considerations upon the ignition/combustion processes research. This kind of technique needs to be completely reliable and feasible, in order to permit its application in adequately equipped optical tests rig without introducing any new uncertainty factor, especially considering the spark generation repeatability and indeed its spray ignition

capability. In this sense, this first major objective will present a sub-objective:

  - The development of a robust methodology for the ignition technique set-up, optimization and validation. It must allow a precise quantification of its capabilities and limits to force fuel spray ignition both theoretical and technologically.

- Study the influence of the local conditions at ignition upon the combustion development of a direct injection diesel spray, performing a first analysis of advantages, problems and general possibilities given by the new developed ignition system. The application of such provoked ignition technique to a diesel spray, will permit a direct comparison of the generated combustion with the autoignition reference, obtainable at the same boundary conditions, allowing to determine if the diesel combustion control will result favorable, moreover than possible. In particular it is intended to study the variations in the developing flame front position, lift-off, rate of heat release and soot generation of the provoked combustions when compared to the classical autoignition reference.

In order to accomplish the reported objectives, an experimental study of the diesel spray combustion will be carried out in an optical engine test rig, adequately equipped with optical accesses to the combustion chamber, with the application of a laser induction plasma ignition system developed during the realization of this doctoral thesis. All the details regarding the experimental equipment, applied methodologies, results of the studies and conclusions drawn will be detailed in the following chapters of this document.

2.6 Bibliography

[1] J. B. Heywood, "Internal Combustion Engine Fundamentals", *McGraw-Hill, Inc*, 1988.

[2] F. Payri and J. M. Desantes, “Motores de Combustión Interna Alternativos”, *Reverté*, 2011.

[3] Q. Xu, M. Xu, D. Hung and S. Wu, "Diesel Spray Characterization at Ultra-High Injection pressure of DENSO 250 MPa Common Rail Fuel Injection Sysem", *SAE Technical Paper*, 2017.

[4] A. Lefebvre, Atomization and Sprays, *Hemisphere Publishing Corporation*, 1989.

[5] J. Arrègle, “Análisis de la estructura y dinámica interna de chorros Diesel”, *Doctoral Thesis*, Universitat Politècnica de València, 1997.

[6] H. Hiroyasu and T. Kadota, "Fuel droplet distribution in diesel combustion chamber", *SAE Technical Paper*, no. 740715, 1974.

[7] D. Siebers, "Liquid-phase fuel penetration in diesel sprays", *SAE Technica Paper*, no. 980809, 1998.

[8] J. Hodges, T. Baritaud and T. Heinze, "Planar liquid and gas fuel and droplet size visualization in a DI diesel engine", *SAE Technical Paper*, no. 910726, 1991.

[9] J. Julía, “Analisis de chorros Diesel mediante fluorescencia inducida por láser”, Barcelona: Editorial *Reverté*, S.A., 2006.

[10] K. R. Browne, I. M. Partrifge and G. Greeves, "Fuel property effects on fuel/air mixing in an experimental Diesel engine", *SAE Paper*, no. 860223, 1986.

[11] B. Higgins, C. Mueller and D. Siebers, "Measurements of fuel effects on liquid-phase penetration in DI sprays", *SAE Paper*, no. 1999-01-0519, 1999.

[12] C. Espey and J. Dec, "The effect of TDC temperature and density on the liquid-phase fuel penetration in a DI Diesel engine", *SAE Papers*, vol. 104, no. 952456, pp. 1400-1414, 1995.

[13] J. García, “El proceso de combustión turbulenta de chorros diésel de inyección directa”, *Doctoral Thesis*. Universitat Politècnica de València, 2004.

[14] J. Dec and C. Espey, "Ignition and early soot formation in a DI diesel engine using multiple 2-D imaging diagnostics", *SAE Paper*, no. 950456, 1995.

[15] J. Dec and C. Espey, "Chemiluminescence imaging of autoignition in a DI diesel engine", *SAE Paper*, no. 982685, 1998.

[16] B. Higgins, D. Siebers and A. Aradi, "Diesel-spray ignition and premixed-burn behaviour", *SAE Paper*, no. 2000-01-0940, 2000.

[17] H. Kosaka, V. Drewes, L. Catalfamo, A. Araldi, N. Iida and T. Kamimoto, "Two-dimensional imaging of formaldehyde formed during the ignition process of a diesel fuel spray", *SAE Paper*, no. 2000-01-0236, 2000.

[18] J. Dec, "A Conceptual Model of DI Diesel Combustion Based on Laser-Sheet Imaging", *SAE Technical Paper*, 1997.

[19] G. Bruneaux, "Combustion structure of free and wall-impinging diesel jets by simultaneous laser-induced fluorescence of formaldehyde, poly-aromatic hydrocarbons, and hydroxies", *International Journal of Engine Research*, vol. 9, no. 3, pp. 249-265, 2008.

[20] H. A. T. K. T. Kosaka, "Two-dimensional imaging of ignition and soot formation processes in a diesel flame", *International Journal of Engine Research*, vol. 6, no. 1, pp. 21-42, 2005.

[21] P. Flynn, R. Durrett, G. Hunter, A. Zur Loye, O. Akinyemi, J. Dec and C. Westbrook, "Diesel combustion: An integrated view combining laser diagnostics, chemical kinetics, and empirical validation", *SAE Technical Paper*, 1999.

[22] J. Dec and R. Canaan, "PLIF imaging of NO formation in a DI diesel engine", *SAE Paper*, no. 980147, 1998.

[23] A. García, “Estudios de los efectos de la post inyección sobre el proceso de combustión y la formación de hollín en motores diésel”, *Doctoral Thesis*. Universitat Politècnica de València, 2011.

[24] P. Flynn, R. Durret, G. Hunter, A. Loye, O. Akinyemi, J. Dec and C. Westbrook, "Diesel Combustion: An Integrated View Combining Laser Diagnostics, Chemical Kinetics and Empirical Validation", *SAE Paper*, no. 1999-01-0509, 1999.

[25] L. Pickett and D. Siebers, "Soot formation in diesel jets near the lift-off length", *International Journal of Engine Research*, vol. 7, no. 2, pp. 103-130, 2006.

[26] P. Ronney, "Laser versus conventional ignition of flames" *Optical Engineering*, no. 33(2), p. 510, 1994.

[27] M. Chou and T. Zukowski, "Ignitionof H2/O2/NH3, H2/AIR/NH3 and CH4/O2/NH3 mixtures by excimer-laser photolysis of NH3.", *Combustion and Flame*, no. 87, p. 191–202, 1991.

[28] M. Lavid and J. Stevens, "Photochemical ignition of premixed hydrogen/oxidizer mixtures with excimer lasers", *Combustion and Flame*, no. 60, p. 195–202, 1985.

[29] M. Morsy and S. Chung, "Numerical simulation of front lobe formation in laser-induced spark ignition of CH4/air mixtures", in *29th Symposium (International) on combustion*, 2002.

[30] T. Phuoc, "Laser-induced spark ignition fundamental and applications", *Optics and Lasers in Engineering*, no. 44, pp. 97-351, 2006.

[31] B. Forch and A. Miziolek, "Oxygen-atom two-photon resonance effects in multiphoton photochemical ignition of premixed H2/O2 flows", *Optics Letters*, no. 11, p. 129–31, 1986.

[32] B. Forch and A. Miziolek, "Laser-based ignition of H2/O2 and D2/O2 premixed gases through resonant multiphoton excitation of H and D atoms near 243 nm", *Combustion and Flame*, no. 85, p. 254–62, 1991.

[33] M. Weinrotter, H. Kopecek, E. Wintner, M. Lackner and F. Winter, "Application of laser ignition to hydrogen–air mixtures at high pressures", *International Journal of Hydrogen Energy*, vol. 30, p. 319–26, 2005.

[34] G. Weyl, L. Radziemsky and D. Cremers, "Phsics of laser-induced breakdown: an update", in *Laser-inducted plasma applications*, M. Dekker, Ed., New York, 1989, p. 1.

[35] J. Beduneau, B. Kim, L. Zimmer and Y. Ikeda, "Measurements of minimum ignition energy in premixed laminar methane/air flow by using laser induced spark", *Combustion and Flame*, no. 132, pp. 653-665, 2003.

[36] T. Phuoc, C. White and D. McNeill, "Laser spark ignition of a jet diffusion flame", *Optics and Lasers in Engeneering*, no. 38, p. 217–232, 2002.

[37] J. Syage, E. Fournier and R. Rianda, "Dynamics of flame propagtion using laser-induced spark initiation: Ignition Energy measurements", *Journal of Applied Phisics*, no. 64, p. 1499, 1988.

[38] B. Lewis and G. von Elbe, "Combustion: Flames Explosions of Gases", *New York: Academic Press*, 1951.

[39] Y. Chen, J. Lewis and C. Parigger, "Spatial and temporal profiles of pulsed laser-induced air plasma emissions", *J. Quant. Spectrosc. Radiat. Transfer*, no. 67, pp. 91-103, 2000.

[40] E. Lim, A. McLLroy, P. Ronney and J. Syage, "Transport Phenomena in Combustion", London: *Taylor & Francis*, 1996, p. 176.

[41] T. Phuoc and F. White, "Laser induced spark ignition of CH4/air mixtures", *Combustion and Flame*, no. 119, pp. 203-216, 1999.

[42] R. Kingdon and F. Weinberg, "The Effect of plasma constitution on laser ignition energies", in *16th Symposuim (international) on Combustion*, Pittsburgh, 1977.

[43] D. Bradley, C. Sheppard, I. Suardjaja and R. Woolley, "Fundamentals of high-energy spark ignition with lasers", *Combustion and Flame*, no. 138, pp. 55-77, 11 May 2004.

[44] B. Yusoff, "Fundamentals of turbulent combustion related to gasoline engines", *The University of Leeds*, 1995.

[45] T. Spliganin, A. MCliroy, E. Fournier and R. Cohen, "Time-resolved imaging of flame kernels: laser spark ignition of H2/O2/Air mixtures", *Combustion and Flame*, no. 102, pp. 310-28, 1995.

[46] R. Abdel-Gayed, D. Bradley and M. McMahon, "Turbulent flame propagation in premixed gases: Theory and experiment", in *Symposium (International) on Combustion*, 1979.

[47] M. Lawes, "Effects of turbulence on combustion in engines", *Leeds: University of Leeds*, 1987.

[48] J. Dale, M. Checkel and P. Smy, "Application of High Energy Ignition Systems to Engines", *Prog. Energy Combust. Sci.*, no. 23, pp. 379-398, 1997.

[49] J. Ma, D. Alexander and D. Poulain, "Laser Spark Ignition and Combustion Characteristics of Methane-Air Mixtures", *Combustion and Flame*, no. 112, pp. 492-506, 1998.

[50] P. Ronney, "Laser versus conventional ignition of flames", *Opt Eng*, 1994.

[51] P. Chylek, A. Maurice, A. Jarzembsky, V. Srivastavam and R. G.Pinnick, *Appl. Opt.*, no. 15, 1990.

[52] R. Hickling and W. Smith, *SAE Trans*, vol. 84, no. 555, 1974.

[53] T.-W. Lee, V. Jain and S. Kozola, "Measurements of minimum ignition energy by using laser sparks for hydrocarbon fuels in air: propane, dodecane, and jet-A fuel", *Combustion and Flame*, vol. 125, no. 4, p. 1320–1328, 2001.

Chapter 3

Tools and Methodology

Contents

3.1 Introduction

In the previous chapters, the objectives and framework of the current thesis have been defined. Then, a description of the main experimental and theoretical tools is presented in this chapter. As it has been highlighted previously, optical techniques and laser systems have played a major role on the development of this thesis. Not only as experimental tools, but also as targets of the study. For this reason, all the experimental work was carried out in an optically accessible test rig. It is based on a two-stroke single cylinder engine, which made it possible to achieve a wide variety of thermodynamic conditions similar to those found within a diesel engine. Besides, some parts of the work have been complemented with theoretical calculations made with a one-dimensional model (1D-Model). As it is described in following chapters, these calculations were utilized both as part of the data processing algorithm and for previous determination of the experimental condition selection.

The experimental work was divided in two main groups: ignition system design and optimization and provoked ignition tests. In the first case, one of the most relevant parts of the work is the development and validation of the laser induced plasma ignition technique. In the second case, the obtained optical ignition system was used, in conjunction with different optical techniques, in order to identify the effect of the local conditions at the ignition location on the combustion development of a diesel spray. Thus, there is a close relation between these experimental tools and the different results presented. For this reason, it has been decided to present in this chapter only the elements that conform the ignition system, leaving the description of its design procedure and optimization to Chapter 4.

The current chapter starts with a description of the test rig. The information regarding hardware and working principle within the combustion chamber is presented. This section does not include the definition of the operating conditions chosen for the main experiment blocks, as this selection

has been a part of the laser ignition system optimization and testing process and it will be later reported in Chapter 4. Moreover, a detailed characterization of the air flow is presented. Next, the laser ignition system components are presented. The chapter ends with an exposition of the basis of the 1D-Model spray used for theoretical calculations.

3.2 Hot Spray Test Rig

3.2.1 Hardware description

The experimental work was performed in an optically accessible single cylinder engine, whose detailed description can be found in [1]. The facility is based on a 2-stroke single cylinder engine (Jenbach JW 50), with three liters displacement.

The engine was designed for research purposes as the large displacement limits the effect of endothermic (liquid vaporization) and exothermic (spray combustion) processes on the pressure trace. However, it is not able to develop enough work each cycle to keep running by itself. Therefore, it is paired with an asynchronous electric motor of 37 kW power, employed to start the system and allowing to keep the desired working conditions. The engine runs motored at low speed (500 rpm), in order to minimize the variation of in-cylinder conditions during a relatively long period (compared with typical DI diesel injection durations).

A scheme of the engine is here depicted in Figure 3.1. Both air intake and exhaust are handled by transfers on the cylinder liner. The cylinder head was specially designed to provide optical access to the combustion chamber. In order to avoid wall impingement effects when a single hole nozzle injector is used, it presents a cylindrical in shape. The effective compression ratio has been kept at 15.7. The chamber presents an upper port, where the injector is mounted, and four lateral accesses. A pressure transducer is installed in one of them, whereas the other three are equipped with oval-shaped quartz

windows (88 mm long, 37 mm large and 28 mm thick). The cylinder head and the block temperature are both controlled by a coolant recirculation system. Their temperature was set to 353 K, to guarantee good lubricity while the system is working.

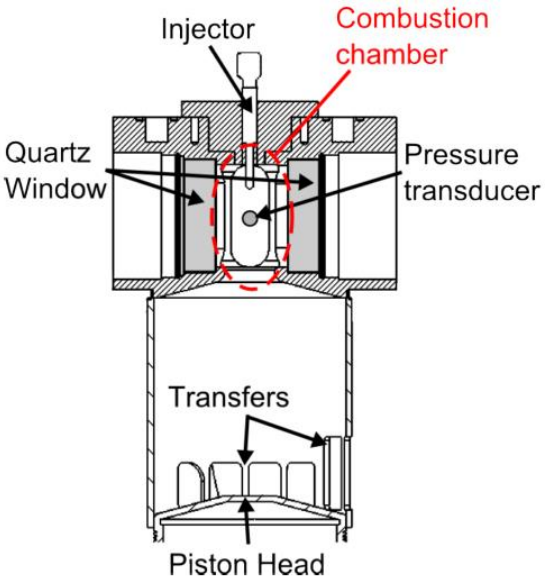

Figure 3.1. Scheme of the cylinder head and liner arrangement of the Test Rig.

According to the needs of the proposed study, the facility can be operated in two different working modes to achieve both inert and reactive operating conditions:

- *Reactive conditions*: A roots compressor takes atmospheric air and sends it into the cylinder, where the thermodynamic cycle takes place. The air goes through two conditioning units, which heat it and remove any liquid or particle before reaching the intake port. After combustion, the exhaust gases are expelled to the atmosphere again.

- *Inert conditions*: The working fluid is nitrogen, permitting to avoid any combustion reaction while keeping similar physical properties as the atmospheric air. For this purpose, the facility works under a closed loop scheme. When the exhaust gases (nitrogen + fuel) leave the cylinder, they flow through an intercooler and a cyclonic filter, to remove rests of fuel and oil out of the recirculated gas stream. This is made to ensure the proper operating conditions for a roots compressor, which is a part of the closed loop and it is used to assist the air management of the engine. Then, the nitrogen is impulsed into the cylinder through the same conditioning units as the ones used for the reactive configuration. The circuit is refilled through an electronic valve to achieve the desired intake pressure and eventual blow-by and/or leakages compensation.

In both configurations, the engine is usually operated under skip-fired mode, so that in-cylinder conditions are not influenced by the remaining residual gases from previous operated combustion cycles. An injection takes place every 30 cycles, which guarantees that ambient conditions are kept constant between consecutive repetitions also avoiding possible temperature transients.

For which concerns the facility itself, the test rig is mounted with respect to the optical tables as showed in Figure 3.2. In the scheme, the distances of the optical mounting tables with respect to the injector axis are shown in order to underline the practical limitations of the installation in terms of optical mounting possibilities. In fact, considering that the distance between the engines' head and the tables is the minimum possible by design of the test rig itself (particularly due to start-stop oscillation of the rig head and the needed accessibilities to the optical windows for replacement and substitutions), it is appreciable how the minimum possible focusing distance viable for the laser induction system design is of 300 mm. This will represent an important practical limitation for the optical system design and optimization for the plasma induction process and will be later discussed in detail in Chapter 4.

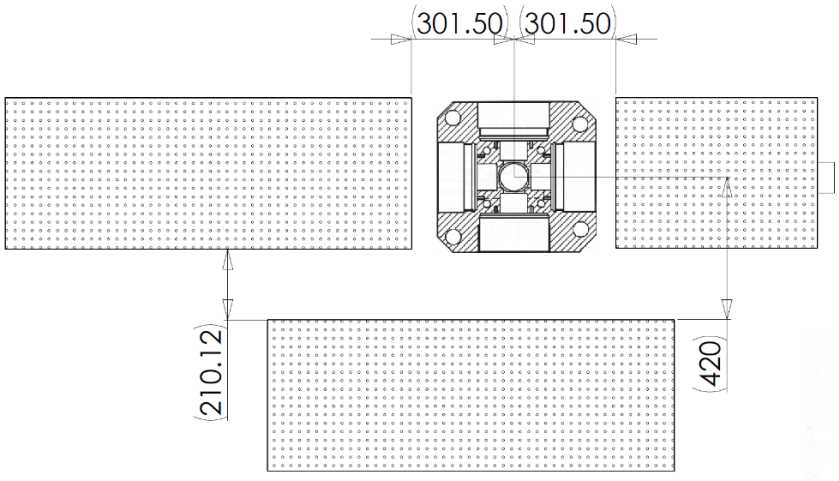

Figure 3.2. Plane reference of the optical test rig installation. The position of the mounting tables is shown referred to the axis of the injector located in the engines' head upper port.

3.2.2 Engine characterization

An accurate characterization of the engine test rig has been previously performed and detailed extensively in [2]. In this paragraph the general procedure followed and the most important results obtained from it will be reported, in order to provide ad adequately detailed description of the test installation employed in the research work.

The characterization was carried out selecting 35 points (couples of intake pressure and temperature), covering the entire range of operating conditions enabled by the engine, including the ones later used in this thesis tests, as represented in Figure 3.3. The thermodynamic conditions of motored cycles was calculated from the cylinder pressure using a first-law thermodynamic analysis, accounting for blow-by, heat transfer and mechanical stress (as derived from Calmec [3]).

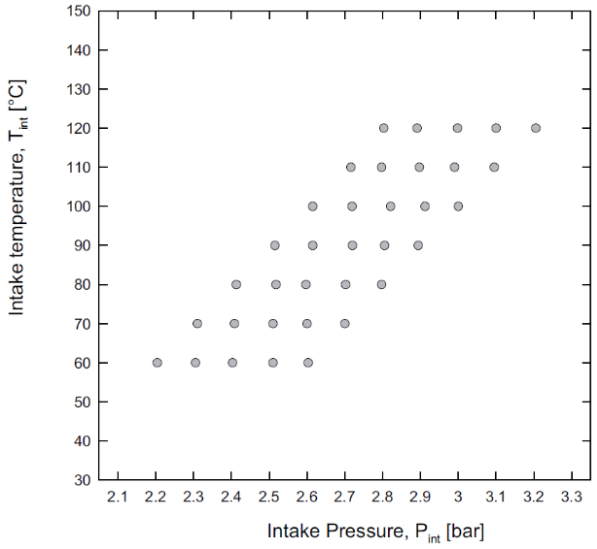

Figure 3.3. Intake thermodynamic conditions for engine characterization. Adapted from [2].

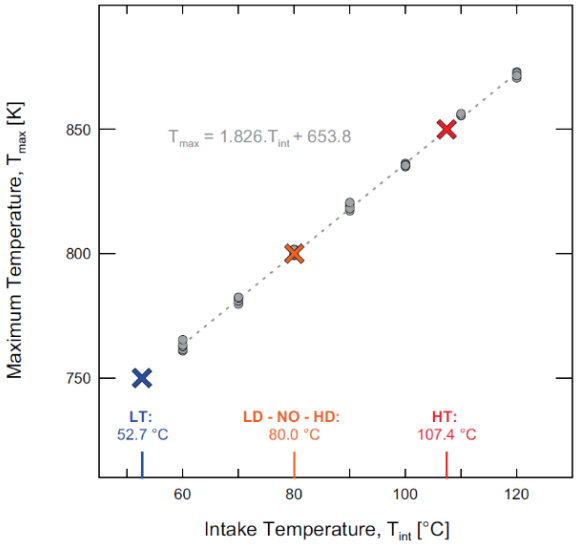

Figure 3.4. Maximum in-chamber temperature as a function of intake temperature. Circle symbols represent the results from conditions selected for calibration and showed in Figure 3.3. Adapted from [2].

With this process, the angular-resolved thermodynamic conditions of the 35 points have been obtained. Then, both maximum temperature and density have been derived for each considered condition. The angle of occurrence of both values varied very little between test points, resulting to be typically -3 CAD for temperature and -0.5 CAD for density (-1 CAD for P_{max}) [2]. As appreciable from what reported in Figure 3.4, T_{max} has shown to have a linear response to intake temperature (T_{int}), independently from intake pressure, and so from ambient density.

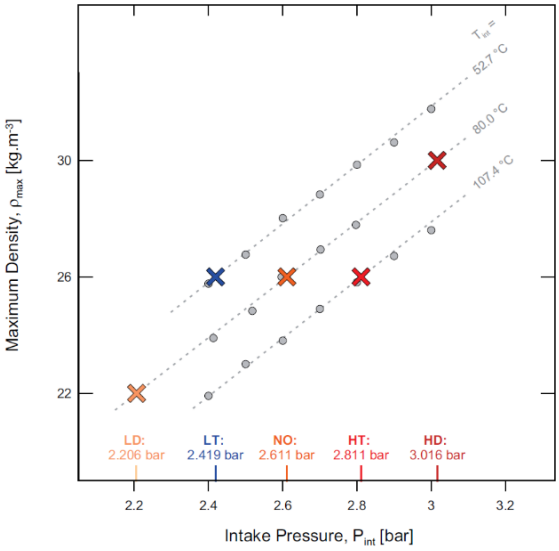

Figure 3.5. Maximum density as a function of intake pressure for the three intake temperature levels considered in the test matrix for the engine characterization. Adapted from [2].

This result is in agreement with equation (3.1) if the polytropic index n is maintained constant for all conditions. Eq (3.1) is derived from the ideal gas law in for a polytropic process, in which a would be the angle of IPC and b, the angle of maximum temperature (in this case, -3 CAD).

(3.1)

$$T_b = T_a \cdot \left(\frac{V_a}{V_b}\right)^{(n-1)}$$

Maximum density at the two simulated intake temperature conditions (52.7 and 107.4 C) was first derived for the intake pressure sweep and finally, as reported in Figure 3.5, the linearity between maximum density and intake pressure at each intake temperature condition has enabled to obtain the exact intake pressure by means of a last interpolation.

3.2.3 Thermodynamic conditions stability with fuel injection

The conservation of thermodynamic conditions during the injection event has been tested in previous work realized in the same experimental test rig [2], and will here briefly reported to complete the information regarding the experimental facility.

In order to consider the thermodynamic stability of the rig during the fuel injection event, at each tested injection, the pressure signal of the following 4 and 9 motored-cycles, respectively for inert and reacting conditions, was acquired and averaged. The temperature calculation was realized considering the following hypotheses:

- Pressure variations of either injection cycles or motored cycles with respect to that of calibration, for the portion prior to injection, were considered to be due to differences in the trapped mass. In this way, a density correction was applied, in order to match both pressure traces prior to injection. This correction seems reasonable considering that the intake temperature is very well-controlled for the rig, while the trapped mass and scavenging processes are quite more uncertain for a 2-stroke engine.

- The ambient density, as previously corrected, was maintained constant during fuel injection, assuming that the mass of fuel injected (between 8 and 20 mg) is insignificant respect to the trapped mass (between 4 and 7 g) and that the rate of blow-by leak is not modified by a potential pressure variation. Under these assumptions, any

pressure variation between injection cycles and motored cycles were so considered to be temperature dependent.

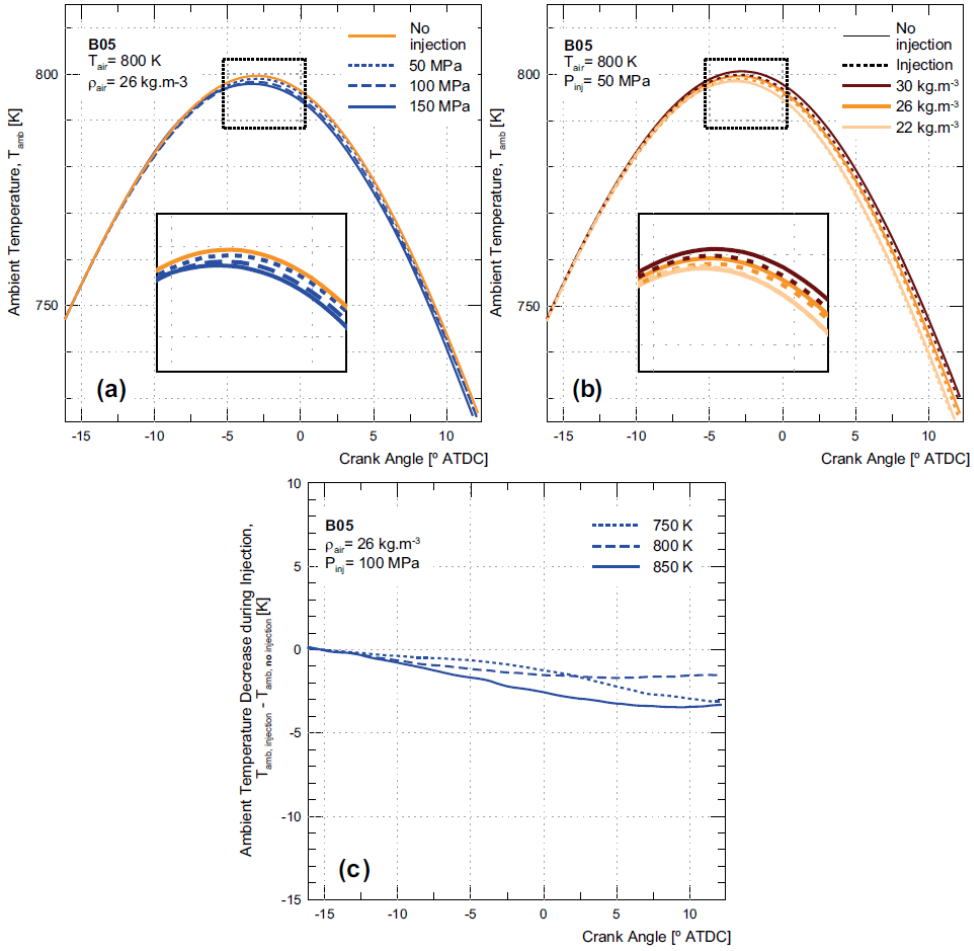

Figure 3.6. In-cylinder temperature variation with injection, under inert conditions. The effect of (a) injection pressure, (b) maximum ambient density and (c) maximum ambient temperature are reported. Adapted from [2].

Figure 3.6 reports the obtained results with respect the effect of (a) injection pressure, (b) air density (ρ_{max}) and (c) air temperature (T_{max}) on the

in-chamber temperature steadiness during injection under inert conditions. From plot (a) it can be appreciated how cooling gets more important as the rate of fuel injection increases but, in percentage terms, it still remains very low (<5 *K*). Plot (b) shows the density effect at constant temperature, and even in this case, the temperature variation has shown to be very small. In plot (c), the temperature variation between the motored cycles average and the cycles with injection has been represented, making possible the direct comparison between the different levels of ambient temperature for the three represented maximum chamber temperature conditions. From both plots (b) and (c) it can be inferred that cooling is more important as either temperature or density levels are increased. Such observation results rather surprising for density, since the higher trapped mass should be less sensitive to a constant amount of fuel injected. Therefore, due to the low differences measured, it is rather hazardous to push further the interpretation of these results that far.

Indeed, the major contribution obtained from the here reported results of [2], under inert conditions, should be summarized by the fact that, as shown, the ambient cooling remains very low, not to say insignificant at any of the tested conditions. In that sense, such results underlines a feasible average stability of the experimental installation during injection under inert conditions.

The exact same analysis was conducted for the reacting environment, and the obtained results are here reported in Figure 3.7 It could be clearly appreciated how the effect of combustion's heat release is much more important than fuel vaporization. In the same way as represented in Figure 3.6, effects of (a) injection pressure, (b) air density (ρ_{max}) and (c) air temperature (T_{max}) on the in-cylinder air temperature steadiness are reported. In (a), and (b), the temperature increase was about 70-80 K compared to the maximum temperature of the motored cycle (800 K). Reasonably, the major differences are observed in (a) when the mass rate of injection and the total mass injected are the greatest. In addition to the average, the cycle-to-cycle dispersion of 100 injections was also calculated and here represented at 100 MPa by means of the interval [T_{air}-σ; T_{air}+σ]. Plot (b) shows how ambient

temperature increases by decreasing air density, i.e. by decreasing the trapped mass in the cylinder. Moreover, plot (c) enables the comparison on a temperature increase basis between three different maximum in-chamber temperature conditions. The showed results of ignition delay are consistent, but the rate of temperature increase has shown to be quite independent from the temperature starting level.

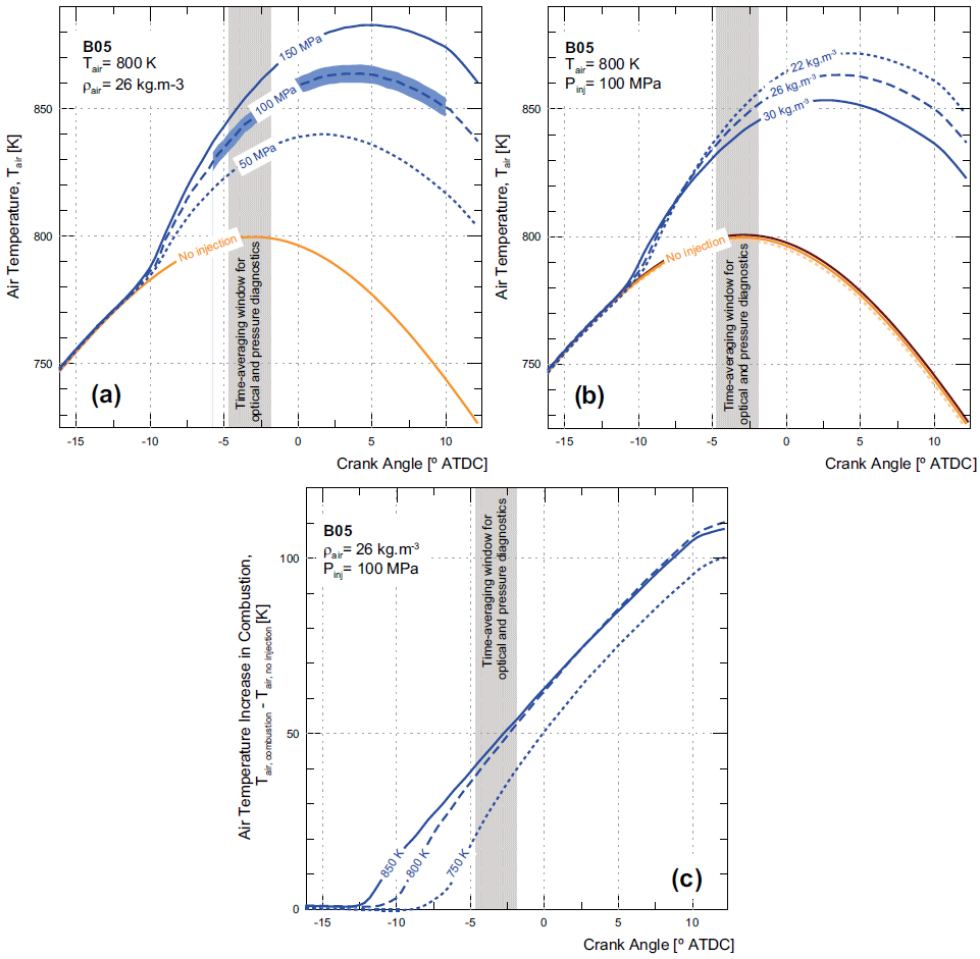

Figure 3.7. In-cylinder temperature variation with injection, under reactive conditions. The effect of (a) injection pressure, (b) maximum ambient density and (c) maximum ambient temperature are reported. Adapted from [2].

To summarize, despite the large volume, the in-cylinder temperature increase produced by combustion (~100 K) has shown to be significant and, as already stated for the inert conditions' analysis, there should be no concerns with respect possible instabilities of the installation during the injection event. In this sense, the selection of a single hole injector providing large injection rates should not represent a problem in terms of consistency of the data recollected upon the in-chamber thermodynamic parameters variations considered for this study.

3.2.4 Ignition delay and rate of heat release

In order to obtain detailed information of the in-chamber pressure trace, acquisition of the pressure signal was carried out by a pressure transducer (Kistler 6125B) and recorded at a sampling frequency of 100 kHz via a Yokogawa DL716E. Such 10 μs resolution was required in order to allow accurate measurements of ignition delay, as will later show in Chapter 5 of this document. To this end, ignition delay has been obtained for each considered test point by subtracting to the registered combustion cycles an average of the following and corresponding motored cycles.

Ignition delay was defined as the first instant where the pressure signal level exceeds three times the standard deviation of the time-average performed on the first 500 μs (for information, hydraulic delay was about 350 μs). The reason for the application of such threshold criteria was to detect the ignition delay as it has been defined by Ikegami and Kamimoto [4], namely the time at which heat release recovers from the fuel vaporization heat consumption.

For what concerns the determination of the average ignition delay, it was obtained considering the average combustion cycle as the average result of 100 combustion cycles and the motored cycles as resulted from 200 cycles, proceeding from the third and fourth cycles after combustion. The first two cycles following the injection were removed because of scavenging issues. The average of both combustion and motored cycles were calculated through a

robust average algorithm, applying the iteratively reweighted least-squares (Matlab robustfit function) [5] [6] to remove the influence of outliers, such as potential failure in the recording or randomly uncontrolled conditions.

With the information of instantaneous mass in the cylinder, the pressure increase was converted to heat release applying the first law of thermodynamics (Cf. Eq. (3.2)). As made for the ignition delay, the heat release was calculated for all cycles, but the average-RoHR was the result of calculations from the robust average of both combustion and motored cycles. The result of the autoignition registered cases shows the typical premixed burn that slowly decreases and tends asymptotically to a purely diffusive mode in the last instants, namely a point at which burning rate equals the injection rate. As stated in the previous chapter, the significance of the premixed burn varied strongly depending on ambient and ignition conditions, i.e. on the fuel amount mixed prior to ignition. These aspects will be approached in more details in Chapter 5.

(3.2)
$$RoHR = m \cdot c_{v,air} \cdot \frac{d\Delta T}{dt} + \Delta P \cdot \frac{dV}{dt}$$

With

$$c_{v,air} = -10.4199 \cdot \sqrt{T} + 2522.88 - 67227.1 \cdot \frac{1}{\sqrt{T}} + 917124.4 \cdot \frac{1}{T} - 4174853.6 \cdot \frac{1}{T^{1.5}} \left[\frac{J}{KgK}\right]$$

3.2.5 In-Cylinder Airflow

The test rig described in this section has been previously exploited for a wide variety of different studies, as extensively reported in literature [2] [7]-[9]. In particular, previous works [10] have taken into account the determination of the rig's cycle-to-cycle variability, as considered to have an important impact on the experimental tests realization, particularly when the application of optical techniques is involved.

In this thesis, the application of Schlieren visualization for the determination of the spray penetration has been carried out, and effects of the cycle-to-cycle variability and in-cylinder gas motion interaction with the spray has shown to be non-negligible, affecting the collected results. So, in order take into account such effects, the quantification of such magnitudes variation realized in [10] is here reported for completeness and will be later considered in the results analysis of Chapter 5.

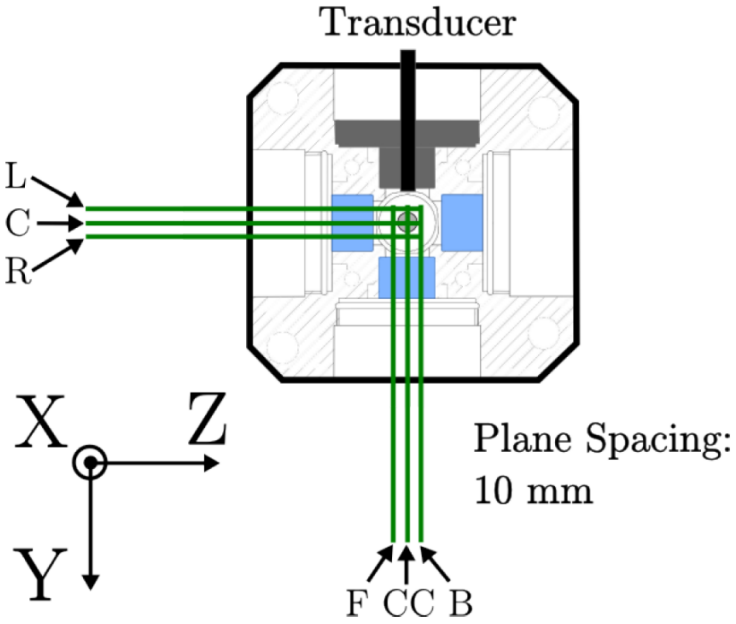

Figure 3.8. Scheme of the distribution of the PIV measuring planes. Adapted from [10].

Aiming to better understand such fluctuations in the spray behavior, the internal airflow movement has been characterized by means of Particle Image Velocimetry (PIV) [10]. This technique is based on measuring the displacement of a cloud of particles between two consecutive images. For this purpose, a pulsed laser is usually employed to create an intense light sheet that illuminates the particles (same system that has been later adapted for

the plasma induction tests). The scattered light is registered by a CCD camera. A detailed description of this technique can be found in [11].

In order to show the obtained results, a brief description of the applied methodology is here reported. Six different planes within the combustion chamber were measured. In Figure 3.8, a scheme of the distribution of the region of interest is shown. As it can be observed, two perpendicular planes crossing the injector axis were chosen (labelled as C and CC respectively), together with the corresponding parallel planes separated 10 mm at both sides of the combustion chamber and labelled as L (left), R (right), F (front) and B (back), respectively. Therefore, it was possible to determine both the flow pattern and possible asymmetry. The measurements were performed between -10 and 15 CAD, with 1 CAD increments and for each plane and CAD, 75 cycles were recorded. In the following paragraph are reported the details of the obtained results.

3.2.5.1 Average Flow Field

In Figure 3.9, the resultant velocity fields corresponding to the plane CC are shown as obtained from the study reported in [10], by averaging the velocity magnitude from 75 repetitions. The colormap corresponds to the velocity magnitude (i.e. the modulus of the 2D projection of the velocity vector on the measurement plane), while the black lines represent the flow streamlines.

As it can be observed, at -10 CAD the airflow is entering the combustion chamber at almost 30 m/s, whilst at the upper part of the combustion chamber the speed is reduced to 5 m/s approximately. As CAD increases, velocity values globally decrease but it can be observed that the high-speed region is moving closer to the nozzle and towards the left part of the combustion chamber. As expected, near TDC there is a drastic slowdown. However, a clockwise vortex appears on the right part of the combustion chamber, whose rotational velocity has resulted to be of the same order of magnitude as the airflow in the rest of the combustion chamber. This vortex

moves towards the left part of the combustion chamber and disappears as the piston moves down and the outlet flow speed increases.

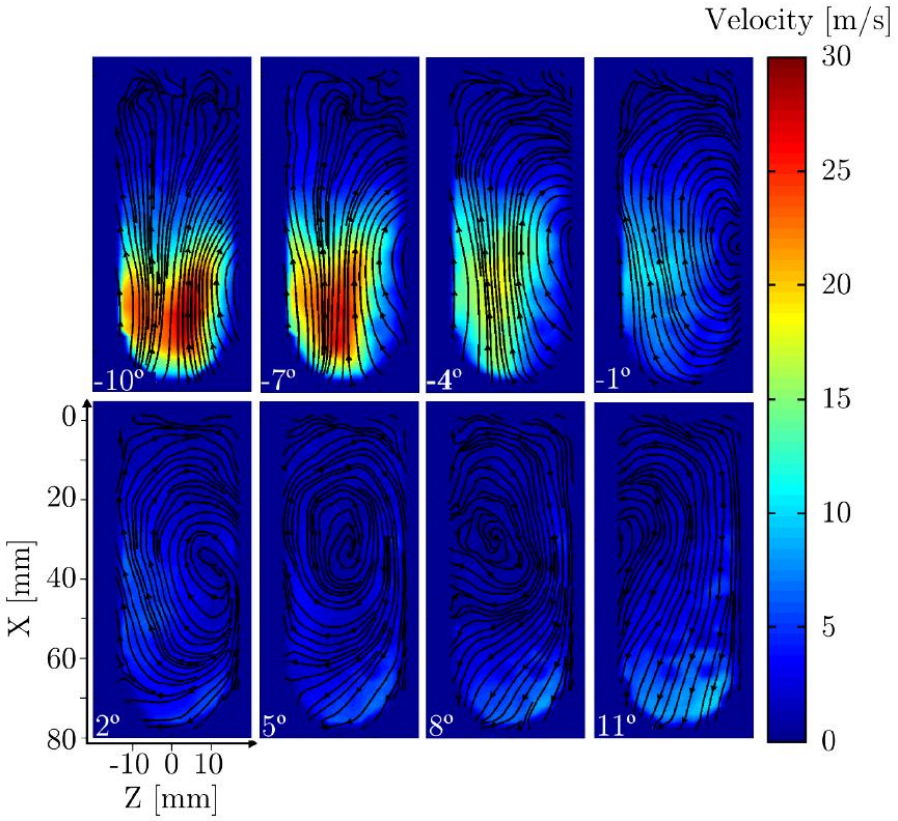

Figure 3.9. Evolution of the average airflow velocity at the CC plane. Adapted from [10].

The evolution shown in Figure 3.9 is considered to be representative of the average behavior within the whole combustion chamber. However, differences both in magnitude and distributions has been observed between the different measuring planes.

For this reason, it is also here reported, in Figure 3.10, a comparison between the different measured planes, where only the flow fields at -5, 0 and 5 CAD have been included.

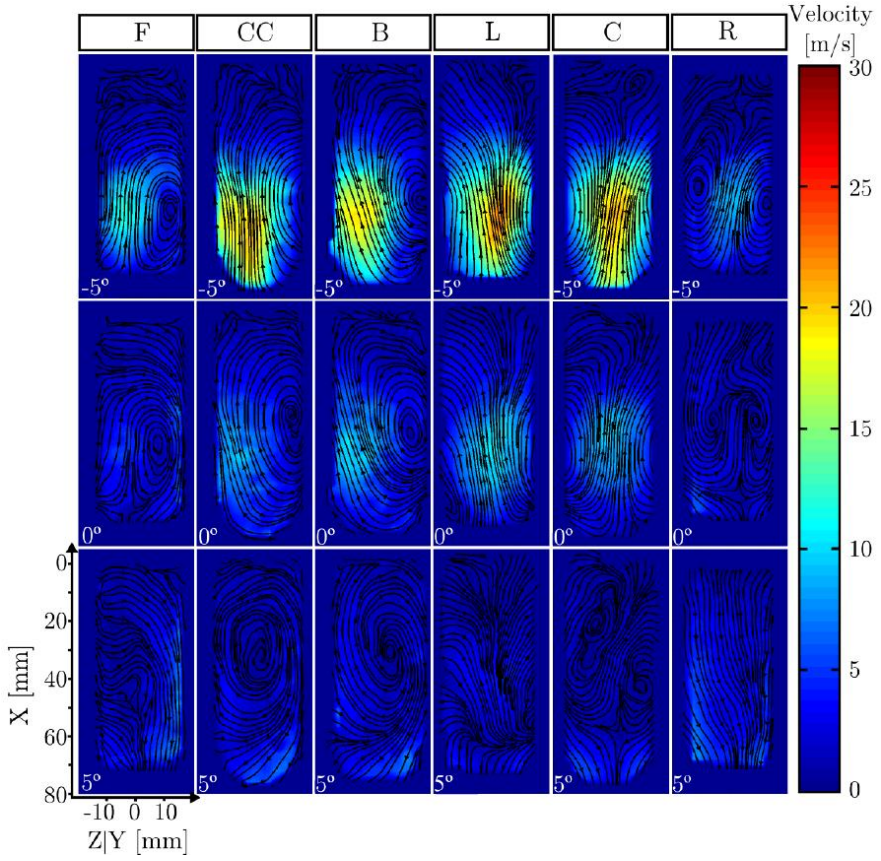

Figure 3.10. Evolution of the Airflow velocity at the 6 measuring planes. Adapted from [10].

The main conclusion that can be drawn from this comparison is that the flow field has resulted to be asymmetric within the combustion chamber. Velocities at L and B are usually higher than at R and F respectively. Moreover, it is possible to see that the vortices which appear at the right part of F and B (0 CAD), are also visible at R (around 10 and -10 mm) but not at L or C. When the piston moves down (5 CAD), these vortices move to the center of the combustion chamber and appear at C. These observations have confirmed the lack of symmetry in both Y and Z directions, even though such asymmetry seems to dilute as the piston approaches TDC.

As main consequence of the results reported from [10], it can be stated that, since the spray is injected in the interval between -5 and +10 CAD, the spray tip can be slowed down by the airflow and even displaced towards one side of the combustion chamber. Despite low velocities have been measured at 0 CAD (as expected) the air momentum can be high in comparisons with the more diluted parts of the spray (its edges). Such effect will be later discussed more in detail when considering the results analysis of Chapter 5.

3.2.5.2 Cycle-to-cycle flow field

For what concerns the analysis of the cycle-to-cycle flow field variability, as attained from the results reported in [10], the obtained standard deviation maps are here shown in Figure 3.11 and Figure 3.12. For such maps, it has been distinguished between the velocity magnitude (M), the component aligned with spray axis (U) and the component perpendicular to spray axis (V), as so it could be described both variations of the velocity magnitude and of its directions.

Considering the results reported in Figure 3.11, it can be seen how between -10 and 0 CAD, M and U shows similar values, as the X-axis is the main direction of propagation of the flow. In both cases, it is appreciable that as CAD increases, the region of higher deviation moves towards the nozzle.

After 0 CAD, the flow field becomes more uniform and the observed variability decreases drastically. The deviation of component V is usually higher at the mid-lower part of the combustion chamber, especially during the compression stroke. From such results it can be inferred that air entrainment into the combustion chamber is different from cycle-to-cycle. This could explain the differences observed in the rest of the combustion chamber.

Finally, it must be noted that, from the results presented by [10], the standard deviation reaches local values of the same order of magnitude as the corresponding average velocity.

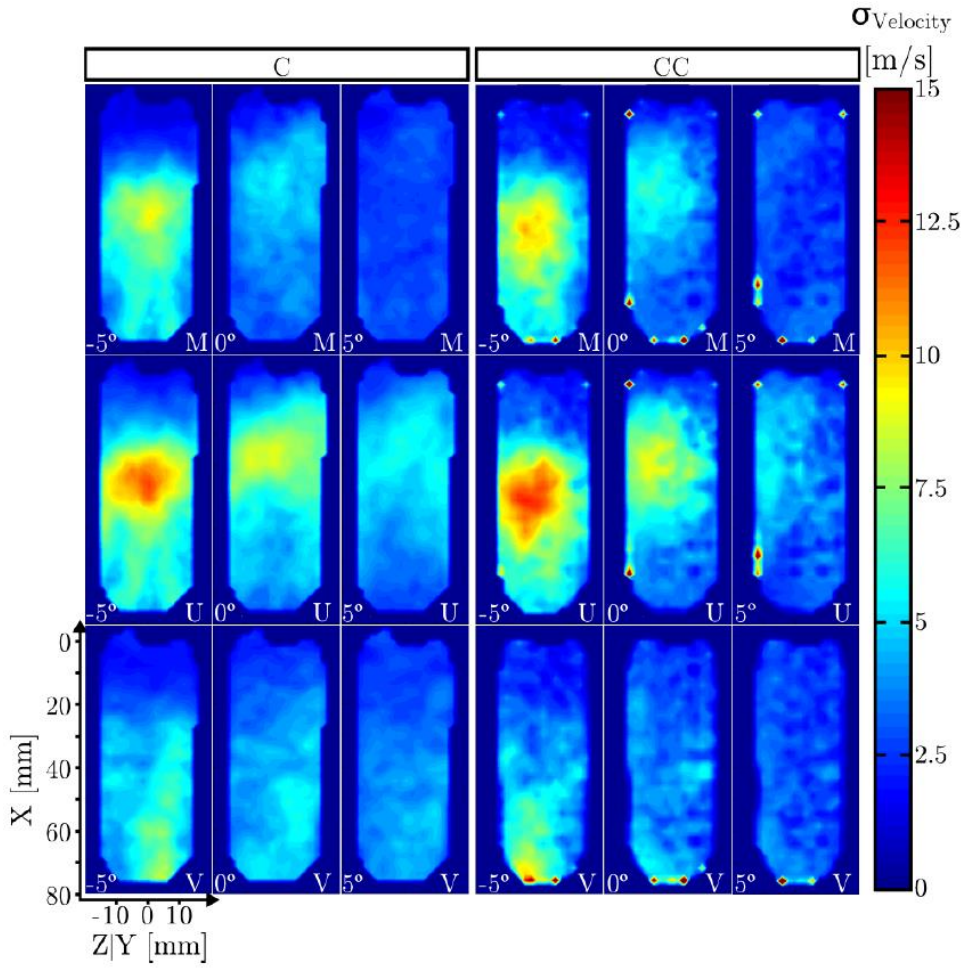

Figure 3.11. Evolution of the airflow standard deviation for M,V and U at the C and CC measuring plane. Adapted from [10].

Moreover, in order to illustrate the variability of the airflow, Micó [10] also reports a set of single cycle images, here shown in Figure 3.12 (bottom), together with the corresponding average velocity magnitude and standard deviation (top). As aforementioned, also in this case the colormap of the single-cycle images corresponds to the velocity magnitude, while the black lines with arrows represents flow streamlines. Such images correspond to plane CC, at -3 CAD (being this a typical injection location).

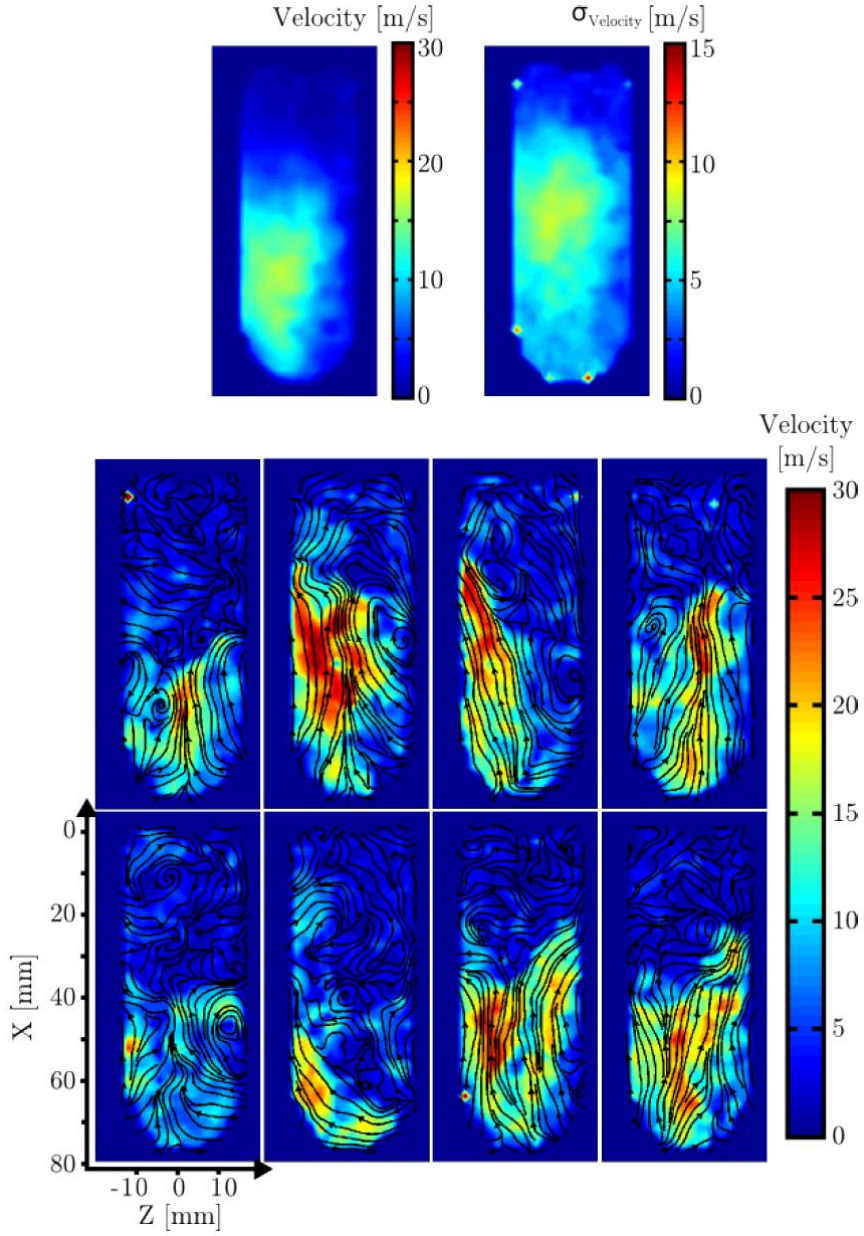

Figure 3.12. Average and Standard deviation of the airflow velocity module (top) at -3 CAD. Airflow velocity magnitude from 8 out of 75 cycle (bottom). Data corresponds to plane CC. Adapted from [10].

Considering such results, it can so be expected that the large reported scattering would cause cycle-to-cycle variations on the spray mixing process and eventually also on the combustion development. Therefore, this effect is here reported as it should be taken into account for a proper analysis of measurements presented later in Chapter 5.

3.2.6 Injection System

The injection system employed for the realization of the experimental study was a Bosch common rail injector with a cylindrical single hole of 140 µm that has been previously characterized geometrically and hydraulically in a commercial EVI_IAV system (Bosch method).

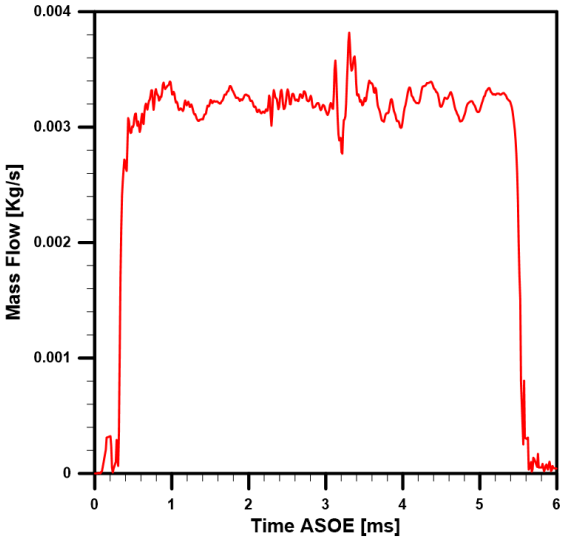

Figure 3.13 Measured mass flow rate for the specific configuration of the Bosch 140 µm common rail injector.

Standard European Diesel (Euro 6) fuel has been used for this work, injected at a rail pressure of 50 MPa and 100 MPa during the different set of tests. The measured Injection Rate is here reported as plotted in Figure 3.13,

while the injection system fundamental characteristics are summarized in Table 3.1.

Single Nozzle Injector Specifications	
Injection Pressure	50/100 MPa
Fuel Injected	Diesel B
Nozzle Diameter	140 µm
Discharge Coefficient	0.833
Velocity Reduction Coefficient	0.9819

Table 3.1. Injector principal characteristics as measured as the 2-injection pressure configuration used in the realization of the experimental tests.

3.3 Laser Induced Plasma (LIP) Ignition System

The ignition system under study and design during the development of this thesis consists in a pulsed laser, the optical elements necessary for the determination of the optical path of the emitted beam and the elements that have enabled its focus in the combustion chamber. In addition to these main components, it is also necessary to consider a series of auxiliary elements necessary for the realization of the optical assembly, such as holders, lenses, mirrors and positioning rails. In the following paragraph a brief description of each of these elements will be reported, with a special focus on the characteristics of the laser devices used in the study.

3.3.1 Laser Systems

From a practical point of view, it is possible to consider a laser system as a "black box", a light source that emits a beam of collimated light with a very narrow spectral bandwidth, at a certain frequency, power and with a precise time duration, repetitiveness and directionality. In contrast to the other common light sources, the beam emitted from a laser source has unique

characteristics thanks to the combination of its spectral purity, energy and coherence. In fact, the beam from a laser of a single spectral line has such a small range of emission wavelengths that it can be considered monochromatic in almost all its practical applications. In the case of lasers with multiple spectral lines, each of the lines at the laser output can be treated as a separate monochromatic beam.

Most lasers, on average, have a divergence angle of around 1 *mrad*, which means that their beam diameter increases by 1 meter after having traveled 1 kilometer. This indicates that the laser power is concentrated in a very small area. To clarify this important aspect, the following example is presented: the luminous intensity of a common laser would be equivalent to 1 million times the emission of a candle at a distance of 1 meter.

One of the most characteristic properties of the laser beam is its coherence, that is, the property of containing waves of light that are in phase with each other. In other words, the photons that make up the beam are of the same "type" and their coherence length (the propagation distance along which a coherent wave maintains a specific degree of coherence) can be converted into fractions of meters or more [11]. A wave with a long coherence length is considered close to a perfect sinusoidal wave. For a conventional light source, the coherence length turns out to be effectively zero.

The word laser is an acronym for "Light Amplification by Stimulated Emission of Radiation", which defines its principle of basic operation, as shown in Figure 3.14. A laser consists, in the simplest form possible, in an active, or gain medium, environment and a set of mirrors. Some photons generated in the active medium through a process known as stimulated emission (or as pumping or excitation) thanks to the effect of other elements (for example a flashlamp).

These electrons are in phase with each other, in the same polarized state, and propagate in the same direction. Then their quantity is amplified in the amplification medium through the optical feedback provided by some

reflecting surfaces (mirrors in most cases) or by other eventual physical processes (for example a *quantum drop laser*).

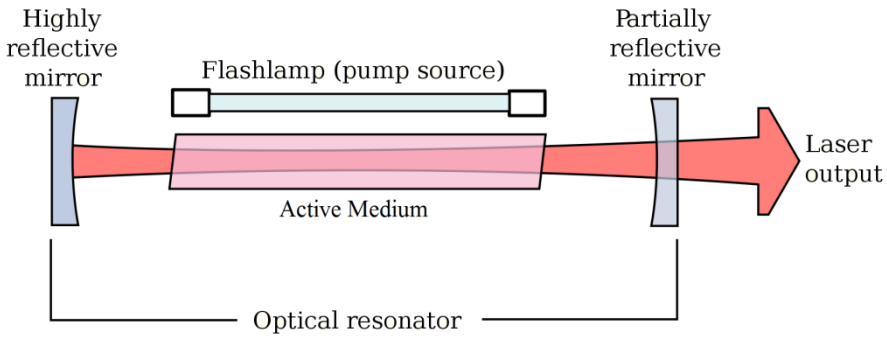

Figure 3.14 Schematic of the basic elements of a laser optical cavity.

The active medium, which is the medium which effectively produces the laser emission, contains atomic and molecular species that are the finals emitters. In general, they are mixed with several components and can be found in gaseous, liquid or solid form.

For a stimulated emission to occur, known as *lasing*, it is necessary to create a *population inversion* in the active media. In a condition of equilibrium, the application of the Boltzmann statistical equation implies that the successive energy states at higher energy, of a molecule or atom, must be respectively less populated. Rather, the population of each state decays with the negative exponential energy of that state. Now, considering the interaction between radiation and matter in a thermal equilibrium, the absorption becomes greater than the stimulated emission due to the difference in population between the states, which decreases as the energy level increases. That is why the radiation is attenuated by propagating through the medium itself. For an amplification to take place, it is necessary that the stimulated emission exceeds the absorption, that is, the density of the particles present in a state with higher energy exceeds that of the state with less energy. This concept is valid under the Einstein's invariance of the *state transition probability* for a *stimulated emission* [12]. If this happens, the

population inversion occurs, which means obtaining a greater density of population in a more energetic state than in a less energetic one. This is the reason why an unbalance condition is necessary. It can be caused by electric discharges, chemical reactions or by pumping a visible radiation. In addition, a *population inversion* cannot be produced in only two energy levels. That is why systems of three or four levels are generally used, as shown in Figure 3.15.

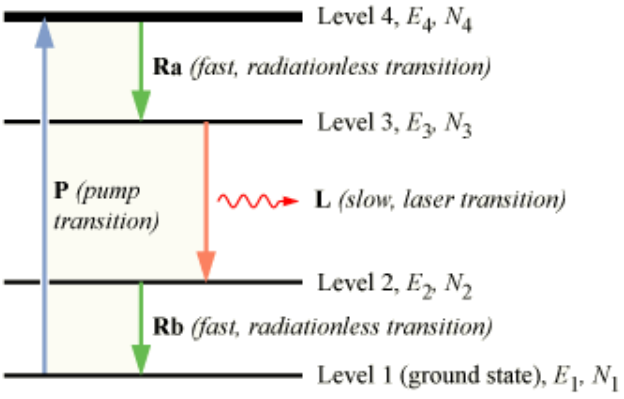

Figure 3.15 Energy levels system for a 4-level laser.

Another fundamental aspect of the stimulated emission, which provides the characteristic coherence of the laser system, is the fact that the stimulated radiation is emitted in phase and in the same direction as the incident stimulating radiation. The characteristics of directionality and power are obtained thanks to an *optical cavity* (or *optical resonator*) placed around the active medium. This important element is basically composed of two aligned mirrors, one facing the other, which provides what is called *optical feedback* along the axis that joins them. Laser emission occurs initially from a spontaneous emission, which basically consists at first in noise. This can significantly be amplified already in a single step through the cavity, which allows only a small amount of energy to be extracted, since the gaining of the active medium is not saturated yet.

Thanks to the optical feedback of the resonant cavity, the optical wave propagating along the axis between the mirrors allows it to rise to higher energy levels and, with a suitable design of the cavity, can saturate the medium's gaining, extracting thus a significant percentage of the energy stored in the population inversion that occurred previously. The optical power thus generated is finally extracted from the cavity by making one of the mirrors to transmit in partial reflection condition.

Since the first successful demonstration of a ruby laser made by Maiman in July 1960, it has been invented a variety of different laser systems, ranging from a small semiconductor laser for telecommunications to the most powerful military applications. These can be grouped, according to the amplification medium used, in: solid state lasers, gas lasers and liquid lasers or, alternatively, as continuous or pulsed lasers when considering its operation mode.

Throughout the development of this project, the main objective of the research has been pursued with two different lasers, each one chosen for a precise reason. In both cases, these are Nd:YAG pulsed laser with an amplifier-oscillator system that allows the use of a technique called *Q-switching*. This technique allows to create strongly energetic laser pulses of reduced duration. For the so called "*Q-Switched*" laser systems pulses of durations from microseconds up to nanosecond are usually available. Throughout a normal operation of laser emission, the gain obtained from the population inversion decreases due to the inevitable effect of the same stimulated emission, which produces an impoverishment of the population in the highest energetic states of the active medium. Now, by limiting the increase in the radiation field of the stimulated emission, it is possible to create a greater population inversion in the media. This is obtained by keeping low the cavity's *Q factor*, which represents a measure of the relationship between the energy of the radiation stored in the cavity and the power losses that occurs in it. In order to reduce the *Q factor*, the cavity losses are intentionally increased using several methods. By keeping low the *Q factor*, it is possible to obtain a much higher gain in the active medium

than what is normally found in a normal laser emission. At this point, the instantaneous increase of the *Q factor* can produce a very intense laser emission with a very short duration of time, due to the very high levels of gaining reached by the medium. This leads to generate laser pulses with an extremely high-power peak. For this reason, the name of the technique is "*Q-switching*" and is usually put into operation taking advantage of polarization techniques of the elements of the optical cavity, which allows to quickly vary its optical power losses.

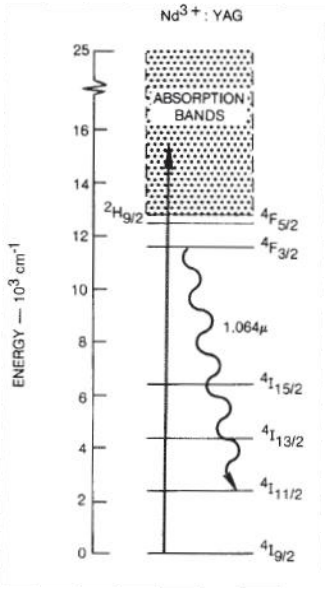

Figure 3.16 Diagrams of the Neodimium's energy levels and laser emission in its trivalent ions.

As regards the active medium of these lasers, the Nd:YAG, the phenomenon of laser emission takes place in trivalent Nd^{3+} neodymium ions, located in a yttrium aluminum crystal ($Y_3AL_5O_{12}$), which in fact is defined as "doped" with neodymium, as it could be seen in the scheme reported in Figure 3.16. For these lasers, the disequilibrium in the medium, that is to say, its excitation, is provoked through a *flashlamp*, which is typical of high energy applications. They produce a primary emission at a wavelength of

1064 nm but are often used to generate laser beams at four different wavelengths in the visible and ultraviolet region, by doubling, tripling or even quadrupling the frequency in the optical crystals. The three wavelengths corresponding to the second, third and fourth harmonic are respectively 532 nm, 355 nm and 266 nm. These lasers operate normally with fixed repetition frequencies, between 10 and 20 Hz, and with internal and external triggers, according to the user's synchronization needs.

It is also possible to use a double trigger, necessary to control the discharge of the flash lamp and the *Q-switch* independently. Typically, the delay between the two pulses is set by the manufacturer, as an optimum value for the quality and power of the beam, with the possibility to vary them so to control the power emitted as required.

Two different Nd:YAG laser systems have been used in this work.

3.3.1.1 *Q-Switched* pulsed Nd:YAG "Litron Lasers – Nano L 135-15 PIV"

As suggested by its name, it is a laser produced by Litron Lasers and designed specifically for PIV (Particle Image Velocimetry) applications. It is a pulsed laser, with an active Nd:YAG medium and has two heads, that is, two groups of active media - optical resonator. These are independent and can work alternatively or simultaneously to form a single beam.

The natural output wavelength is 1064 nm (which is the case of Nd: YAG), with the possibility of doubling, tripling or quadrupling. The detailed parameters of the laser system are reported in Table 3.2. In this project it has been used with a duplicator, working at 532 nm, that is, with a "green beam", mainly due to the advantage of working with a wavelength beam in the visible field of the spectrum when it comes to aligning optical devices that requires high precision. Moreover, as reported in Chapter 2, the independence from the wavelength of the selected plasma induction

mechanisms gives freedom in operating wavelength election. An image of the laser head is presented in Figure 3.17.

Figure 3.17 Nano L 135-15 PIV laser head.

The basic idea for the initial choice of this device for the project was focused on taking advantage of a very compact device and, therefore, to benefit from the fact that it could be moved between the different facilities designed for the use of optical techniques.

Parameter	**Value**
Repetition Rate	0-15 Hz
Output Energy @ 532nm	135 mJ
Pulse - Pulse Energy Stability	2 (±%)
Beam Diameter	5 mm
Beam Divergence	~ 3 mrad
Pulse Length @ 1064 nm	6-9 ns
Pointing Stability	< ±100 µrad
Resonator Type	Stable
Timing Jitter	<0.5 ns

Table 3.2. Parameters of the Nano L 135-15 PIV system, referred to single head operations.

In this way, it could be possible to take advantage in all the facilities of this new study possibilities: being able to freely choose the position and the delay of a combustion caused through the LIP ignition system. Moreover, the compact design of this system makes it easier to apply and align even in the same facility, if compared with bigger systems.

Despite the advantages provided by its compactness, the disadvantages and problems in the application of "Nano L135-15 PIV" system have proven to be much more relevant, which has inevitably led to its discard in the selection process of a laser device that would carry out the project. Fundamentally, with this system, it has not been possible to obtain a stable and repetitive plasma generation in air; a prerequisite to ensure that, in the process of laser ignition, an eventual phenomenon of misfire does not depend on a fault in the plasma generation at the ignition system's focal spot. In Chapter 4, the process that led to the final selection of the laser equipment will be described in detail, highlighting the critical problems that led to the need to discard this equipment and all the intermediate solutions tested.

3.1.1.1 Q-Switched pulsed Nd:YAG "Continuum Lasers – Surelite II-10"

It is a laser with similar constructive characteristics as the Litron, but with parameters that meet the highest quality requirements. It is also a pulsed Nd:YAG active medium laser with two independent heads that can work simultaneously or alternatively, and with a natural wavelength at the output of 1064 nm, which also can be duplicated, triplicated or quadruplicated.

The main difference that can be seen at first sight with respect to the Litron laser is its size. The Surelite II-10 occupies part of the testing room of the optical test rig installation of the optical engine, as can be seen in Figure 3.18 (a), making it very difficult to be moved and applied to different optical installations.

Parameter	**Value at 1064nm**	**Value at 532nm**	**Value at 355nm**	**Value at 266nm**
Repetition Rate	10 Hz	10 Hz	10 Hz	10 Hz
Output Energy	660mJ	280mJ	102mJ	70mJ
Pulse Length[1]	5-7 ns	4-6 ns	4-6 ns	4-6 ns
Pulse-Pulse Energy Stability	2,5 (±%)	3,5 (±%)	4,0 (±%)	7,0 (±%)
RMS Energy Stability	0,8 (±%)	1,2 (±%)	1,3 (±%)	2,3 (±%)
Beam Diameter	7 mm	7 mm	7 mm	7 mm
Beam Divergence[2]	~0.5mrad	~0.5mrad	~0.5mrad	~0.5mrad
Beam Pointing Stability	±30µrad	±30µrad	±30µrad	±30µrad
Timing Jitter[3]	±0.5 ns	±0.5 ns	±0.5 ns	±0.5 ns
Near Field Beam Spatial Profile[4] (<1m)	0,70	0,70	0,70	0,70
Far Field Beam Spatial Profile[4] (∞)	0,95	0,95	0,95	0,95
Deviation from Gaussian in Near Field[5]	30	30	30	30
Polarization	Horizontal	Vertical	Horizontal	Horizontal

Table 3.3. Parameter of the Surelite II-10 system, referred to a single head operation. Notes: 1 – Full Width, Half Maximum; 2 – Full Angle for 86% of Energy; 3 – With respect to the External Trigger; 4 – At Least Squares Fit to a Gaussian Profile. A perfect fit would have a coefficient of 1; 5 – Maximum Deviation at Beam Center.

Despite this disadvantage, as already aforementioned, its choice has proved to be unavoidable after the determination of the impossibility of

obtaining stable plasma with any of the configurations tested for the Litron system.

In the next chapter, the difference of operation between the two laser equipments and the final configuration defined will be analyzed in detail. Moreover, the detailed characteristics of the Continuum laser system are reported in Table 3.3.

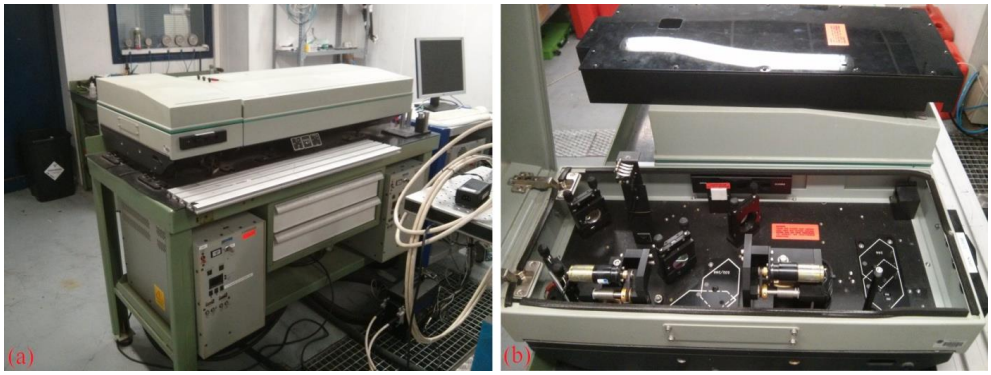

Figure 3.18. Laser Surelite II-10 system in the optical test rig installation (a). View of the SSP (Surelite Separation Package), where the optical duplicator for the output wavelength tuning are mounted (b).

3.1.2 Optical mirrors for Laser beam guidance

The optical beam path that leads from the output of the laser device to the vicinity of the combustion chamber, has been conducted using a series of specific laser line mirrors. These are flat mirrors designed specifically to work with high power lasers, which have as main characteristics a high resistance to damage caused by a very low absorbance and a very high reflectivity of the incident radiation.

More specifically, Thorlabs® mirrors for YAG lasers have been used. These mirrors, defined as dual-order laser mirrors, allows working at two different wavelengths, corresponding to the fundamental first and second

harmonics of a YAG laser (1064 nm and 532 nm). They have a damage threshold of respectively 8 and 5 J/cm^2 for pulses of 10 ns and frequency of 10 Hz, at 532 and 1064 nm. The reflectivity characteristics provided by the manufacturer are presented in Figure 3.19.

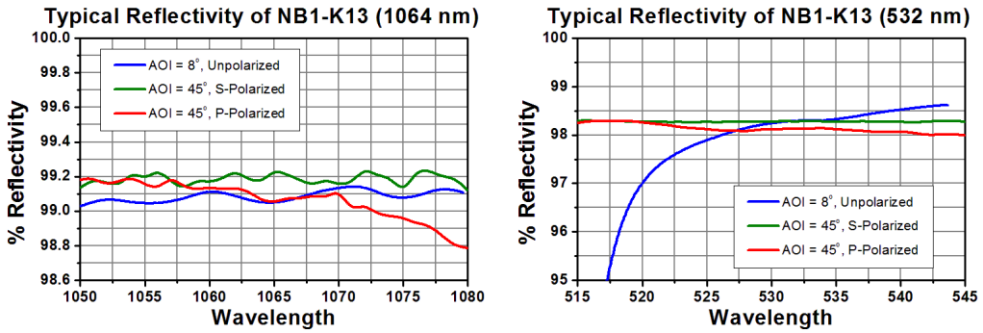

Figure 3.19. Reflectivity characteristic of the laser beam redirection mirrors used in the ignition system. (AOI = Angle of Incidence).

It could be particularly noted how the mirrors presents reflectivity levels superior to 99% for different angles of incidence and condition of radiation polarization.

3.1.3 Laser beam focusing Lens

Due to the experimental needs related to the geometrical parameters of the facilities where the ignition tests were carried out, for focusing the laser beam it was necessary to use a lens with a minimum focal length of 300 mm. In the next chapter, the practical consequences and problems arising from this requirement will be highlighted.

In addition to the focusing lens finally selected for the design of the ignition system, other lenses with the same geometrical characteristics, construction and the same material, but with a different focal lenght, have been used in the first phase of the system design and development. In Table 3.4, the common characteristics to the lenses used are reported.

N-BK7 Plano-Convex Spherical Singlets	
Lens Shape	Plano / Convex
Substrate Material	N-BK7 (Grade A)
Wavelength Range	350 nm - 2.0 μm (Uncoated)
Diameter Tolerance	+0.00/-0.10 mm
Design Wavelength	587.6 nm
Index of Refraction @633 nm	1.515
Surface Quality	40-20 Scratch-Dig
Surface Flatness (Plano Side)	λ/2
Spherical Surface Power (Convex Side)	3λ/2
Surface Irregularity (Peak to Valley)	λ/4
Abbe Number	$v_d = 64.17$
Centration	≤3 arcmin
Clear Aperture	>90% of Diameter
Focal Length Tolerance	±1%

Table 3.4. Common characteristics of the lenses used in the development of the LIP ignition system.

As the mirrors, lenses specifically designed to work with high power lasers have been used. They have very high damage thresholds and adequate transmittance characteristics for the wavelength in use. Moreover, the elevated quality of the utilized lenses guarantees high aperture, needed to avoid spherical aberration phenomenon and possible variations of the effective focal length.

3.2 Optical Techniques

In this section, the optical techniques applied in the realization of the experimental measurements of this thesis work will be described. For the study of the reactive spray, Schlieren and Natural Luminosity were used. The

Schlieren techniques was applied both for vapour penetration and ignition delay time detection.

The digital images have been analyzed by means of purpose-developed processing software, which delivers the spray/flame geometrical parameters. Examples of Schlieren and broadband radiation images are shown in Figure 3.21 and Figure 3.22.

3.2.1 Schlieren visualization

The spray evolution inside the combustion chamber has been recorded by Schlieren imaging [13]. This technique shows the boundary between vaporized liquid and background gas because of the refractive index differences that exist between them, additionally, density gradients are also created in the chamber as the vaporized liquid cools the ambient gas [14][15]; such refractive index gradients are also present during combustion, as the high temperature creates low density regions.

The technique is based on the ability to make a given optical visualization system sensitive to the first spatial derivative of density for a given media. In fact, considering a light beam crossing different medias, each one characterized by a proper refractive index, this will suffer a series of deviation, provoked by its refraction at crossing the different interfaces between the medias. This effect is known as *beam steering*. Now, it can be demonstrated that such deviation will be proportional to the variation of the refraction index at the interface or, in other words, to the refraction index gradient [13]. If the considered media is air or other gases, the density of the media is in linear relationship with its refractive index.

Considering the combustion chamber of a DI engine, the fuel injection itself generates density gradients, and so refractive index gradients. If such volume is illuminated with a uniform and collimated light beam, such gradients will produce a beam steering effect on each ray that is crossing it, producing what is defined as shadowgram. A direct visualization of this

shadowgram, is usually defined as *Shadowgraphy* and its a visualization technique applicable by itself. However, the sensitivity of this phenomenon is usually low, generally not enough for the application to the study of a diesel spray vapour phase. Schlieren visualization is considered to be an evolution of such technique, that, with the application of a more complex optical set up, allows to increase the sensitivity to the density gradients, allowing to obtain a better visualization of them. While *shadowgraphy* is sensitive to the displacement of the light rays caused by the deflection angles associated to the refractive index gradients, schlieren results to be sensitive to the deflection angles themselves. In order to do so, a modification of the optical set up is required. As a title of example, a generic schlieren system is reported in Figure 3.20.

The schlieren visualization system is always formed, in general, by a light source, a collimating lens, a collecting lens, a knife-edge located exactly at the focal plane of the collecting lens and finally a focusing lens. One of the basis of this technique resides in the fact that the light source and the knife-edge plane, as well as the test area and the screen plane, always form sets of conjugate optical planes. This means that what happens in one of the conjugated planes also happens undistorted in the other, but scale transformation factors are applicable. An ideally collimated light beam would be generated by a punctual light source, located at the focal distance of the collimating lens. As a real light source presents a finite dimension, such ideal collimation results to be impossible, implying that the light rays are not perfectly parallel. For this reason, as every point of the test area is illuminated by countless rays within a cone angle limited by the physical dimensions of the light source and that all light crossing each point of the test area will form an image of the light source at the knife-edge plane, a composite image of the light-source is formed. Such image is the results of the superposition of weaker elementary images of it. As a consequence, if the test area is blocked by a pinhole, the image formed at the knife-edge plane will have less intensity than the original one. Now, if light crosses the media without experiencing any refractive index gradient, all the elementary images will be formed at the same position.

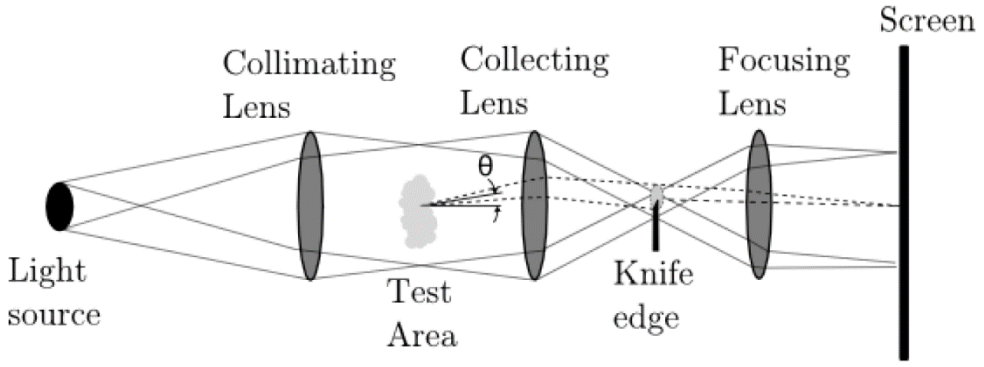

Figure 3.20. Diagram representation of a generic Schlieren system with a real light source and ray traces. Source: Settles [13].

If a knife-edge will cut all the elementary images equally, the image obtained in the screen will darken uniformly. But, when some of these light rays suffers refraction (dashed lines of Figure 3.20) and are deviated by a certain angle θ, they still form an elementary image of the light source at the knife-edge plane, but displaced from the original one just due to the experienced refraction effect. The focusing lens will still focus any bundle of rays coming from the test area at the same relative position on the screen. Therefore, the optical system designed in this way offers the possibility to spatially separate the deviated and non-deviated rays at the knife-edge plane. Additionally, for a fixed position of the knife-edge, each bundle of deviated light rays experiences a different amount of cutoff before being recombined at the screen plane, producing so a variation of luminosity with respect to the background. It is precisely in this procedure that resides the major difference when comparing the system to an ideal point light source. As a consequence of it, the image obtained at the screen, and so collected by the optical device used for the schlieren imaging visualization, results to be smoothed and in gray scale, in comparison with a perfect binary schlieren image obtainable in the ideal condition of an illumination granted by a point light source, where the image formed at the knife-edge plane could not be partially marked by the cutoff. It can so also be stated that the smaller the light source applied, the sharper will be the resulting schlieren image. An

example of a schlieren image of a direct injected diesel spray can be seen in Figure 3.21.

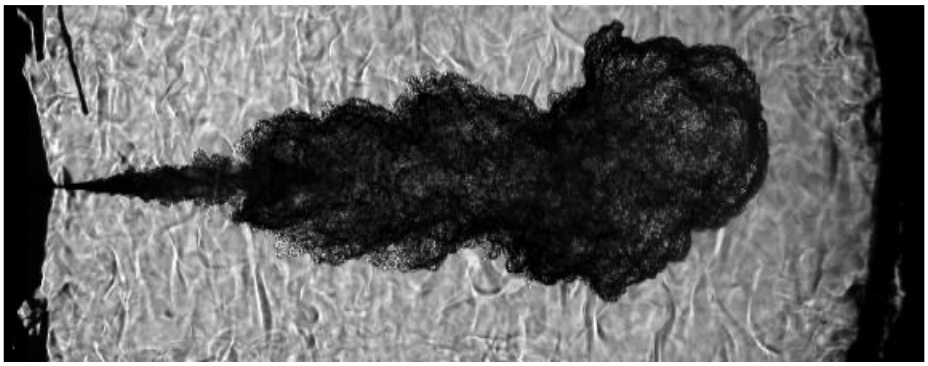

Figure 3.21. Sample image of the schlieren technique at 3000 μs after SoI.

The routine used for the processing was internally developed in the department, and adequately modified during years by various contributions [16] [17] [18] [19], in order to obtain the best data extraction from all different possible set of schlieren images. The code is based on the successive calculation of two standard deviation images to remove the schlieren effect of the hot ambient gases around the spray cone, and to detect the spray boundary. For every instant (I_t), the processing routine subtracts the two preceding images (I_{t-1} & I_{t-2}), then a two-step derivative process highlights the zones where the pixels have changed due to either spray or background gas movement, then the image is segmented [16] [20]. Once the boundaries have been defined, the spray penetration is calculated by the procedure shown in [15].

3.2.2 Natural Luminosity (Broadband Radiation)

The flame soot emission inside the combustion chamber has been recorded by means of direct imaging, also defined as Natural Luminosity technique. This technique records the flame broadband radiation, which corresponds to the soot thermal emission during the diffusion combustion

phase. This type of radiation has actually to different kinds of contributions, chemiluminescence and incandescence. Under most of the operating conditions, the second is the fundamental one as it depends on the amount of soot and its temperature. Therefore, the technique has been used for a qualitative analysis of such parameters. Moreover, it allows the calculation of soot onset length and flame length. Figure 3.22 shows a sample image of broadband radiation.

Figure 3.22. Sample of the natural luminosity imaging at 3000 μs after SoI.

For what concerns the image processing, as obtained from this kind of visualization method, an average background image is calculated for each repetition. Based on that image and two fixed thresholds, a mask is generated, allowing to define the region of interest. It is important to clarify that given the strong difference between the intensity levels in the soot onset area (in the vicinity of the lift-off length) and further downstream, two threshold values (a lower one for the onset and a higher one for the tip) were selected in order to accurately detect the contour.

Then, the area of the flame and cumulative digital intensity are computed and, based on those two values, the specific intensity is finally obtained. Also, and in a similar way to the spray penetration, the soot onset length and soot penetration (or flame length) are obtained as the distance from the nozzle to the points closest and furthest away from the injector, respectively.

Moreover, being the laser induced plasma emission both broadband extended and similar in intensity as the registered soot emission, the same visualization set up as the one used for this technique, has been exploited for

its registration, during the realization of the ignition system optimization and validation tests.

3.3 One-Dimensional Spray Model

As described in detail in Chapter 2 of this document, one of the main purposes of this experimental work consists in the application of a laser plasma ignition system to force the combustion of a direct injected diesel spray, varying timing and position of the ignition position in order to study the effects of the local conditions on the combustion development. Pursuing this purpose, it was decided to rely on the use of a spray modeling code in order to be able to determine such spray local conditions, at which ignition has been later forced, particularly in terms of local air/fuel ratios at which the ignitions attempts will be tested.

In this sense, a one-dimensional (1D) spray model was considered enough accurate in terms of the spray evolution prediction under quiescent boundary conditions to fit with the thesis purposes. The one-dimensional approach helps to simplify the problems involved in a three-dimensional real-world spray while still providing accurate results in relatively short times, if compared to a much more complex CFD model. In particular, it was decided to use a 1D-Model developed at CMT-Motores Térmicos [20], which has been previously successfully utilized for the prediction of the spray evolution under similar boundary configuration and for similar test environment [8][10][21].

In the following section, a general overview of the model details will be presented at first. Then, a brief description of the state relationship calculation will be also reported, as considered interesting for the determination of the spray evolution applied to the results analysis that will be later discussed in Chapter 5.

3.3.1 General Model Description

For the considered 1D-Model, the spray is assumed to be injected into a quiescent air volume. Such volume is supposed to be large enough so that flow evolution does not modify air conditions far away from the nozzle (which is considered to be fairly acceptable for the test installation described before).

The basic configuration of the modeled spray can be seen in Figure 3.23 and it is described here as follows. The fuel stream velocity profile is assumed to be uniform at the nozzle exit. The injected flow exchanges momentum with the ambient air, setting it in motion. In this way, its width increases with the axial distance from the nozzle. Such radial growth is defined by the spray cone half angle (or spreading angle) $\alpha/2$ and represents one of the model inputs. Together with the nozzle diameter d_0, the spray angle defines the virtual origin of the spray, which is expressed in terms of $x_0 = d_0/2/\tan(\alpha/x)$. The spray domain is axially divided into cells with a defined thickness (Δx) that spans the whole spray cross-section. Each cell is limited by the inlet and the outlet sections (i and $i+1$, respectively) so that $x_{i+1} = x_i + \Delta x$. At every time instant, the spray size is defined in terms of the tip penetration (S), represented by the farthest cell from the nozzle with inlet velocity different from zero and outlet velocity equal to zero.

Moreover, in the description of the spray model the following hypotheses are also assumed:

- Symmetry on the spray axis [22], i.e. no swirl motion.
- The flow is assumed to be turbulent and fully developed. This means that self-similar radial profiles can be defined for the conserved variables. In particular, for the present approach, a radial Gaussian profile is assumed.
- The spray cone angle is calculated from the spray contour. This is defined as the location where the axial velocity is $\zeta = 1\%$ of the value on the spray axis.

- The turbulent Lewis number is assumed to be equal to one. Consequently, the local enthalpy, for which no conservation equation is solved, can be expressed as:

  (3.3) $$h(x,r,t) = h_{a,\infty} + f(x,r,t)(h_{f,0} - h_{a,\infty})$$

  where $f(x,r,t)$ is the local mixture fraction value and $h_{f,0}$ and $h_{a,\infty}$ are the enthalpy of pure fuel (nozzle outlet conditions) and pure air (far away from nozzle), respectively. This relationship is independent from the general flow calculations, so that state relationship can be calculated *a priori*.

- Pressure is assumed to be constant all over the spray.

- The flow is assumed to be locally homogeneous, i.e., local equilibrium exists both in thermal and velocity conditions.

The conservation equations of axial momentum and fuel mass are formulated for each cell of the dominium (*Figure 3.23*). To solve them, it is needed a definition for the local density. Formally, this is expressed as a function of the type $\rho = g(f)$, which falls into the category of so-called "state relationships". As a general definition, a state relationship defines the local composition, temperature, and density of the spray in terms of the mixture fraction (f), by means of an ideal adiabatic mixing process of pure fuel stream (nozzle conditions) and pure air. Such boundary conditions can be considered either constant or variable with time. The calculation of the state relationships is independent from the solution of flow conservation equations.

The so defined relationships are utilized to solve the conservation equations at each cell. This permits to obtain the on-axis velocity and the mixture fraction. With these hypotheses, the radial profiles can be defined. In order to do so, additional information is required. In detail, the momentum (M_0) and mass ($\dot{m}_0$) fluxes at the nozzle exit and the radial integration of radial profiles, coupled to the local density. To calculate such integrals, the spray cone angle (α) and local density (ρ) (obtained from the state

relationship) are needed. Ultimately, once the mixture fraction f is obtained at one location, local temperature, density and composition can be extracted from the application of the state relationships.

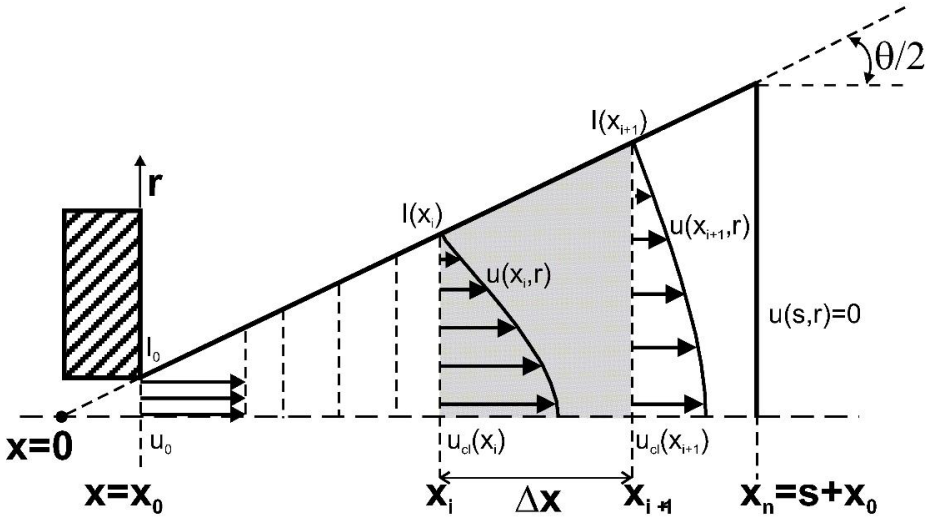

Figure 3.23. Schematic of the spray structure for the 1-D Model description. Source [23].

3.3.2 State relationship

The state relationship, as defined previously, consists of composition *(Y_i)*, temperature *(T)*, and density *(ρ)* tabulations as a function of the mixture fraction parameter *(f)*. In order to calculate these dependencies, the general procedure reported here is followed:

1. The main underlying assumption made is that the mixture state corresponds to the result of an adiabatic mixing process. In the case of inert sprays, this hypothesis derives in the following corollary:

    a. The local mixture enthalpy is calculated by means of the equation (3.3).

b. The local composition can be obtained from the mixture fraction as:

$$Y_i = Y_{i,inf} + f \cdot (Y_{i,0} - Y_{i,inf}) \quad (3.4)$$

where Y_i is the mass fraction of i species in the mixture, when the contribution of both liquid and vapor phases are considered.

2. In order to define the local composition, it has to be found the contribution of both liquid (Y_i^L) and vapour/gas (Y^V) phases to each of the components, with $Y_i = Y_i^L + Y_i^V$. If the mixture is in a single-phase region, the solution is trivial $(Y_i = Y_i^V)$. Whilst, considering the liquid-vapour region, the spray is assumed to be in adiabatic saturation conditions. Therefore, liquid and vapour phase conditions are respectively those of bubble and dew curves. This requires a calculation of the L-V equilibrium, which can be found in detail in [23]. In practice, the local composition for each phase is obtained from L-V flash calculation as a function of pressure, local temperature and mixture fraction.

3. A real-gas mixture is assumed by means of the following equation:

$$h(T, f) = \sum_{i=1}^{n} Y_i \cdot \bar{h}_i(T) \quad (3.5)$$

where $\bar{h}_i$ is the partial enthalpy of component i in the mixture. This partial enthalpy is obtained by means of the equation:

$$\bar{h}_i = h_i^0 - RT^2 \left(\frac{d\, ln\hat{\phi}_i}{dT}\right)_{p,x_i} \quad (3.6)$$

where h_i^0 is the perfect gas enthalpy, and $\hat{\phi}_i$ is the fugacity coefficient of component i in the mixture.

4. Considering the single-phase region of the spray, where composition is fully defined, the local temperature is the only unknown parameter

left when equating enthalpy from equation (3.3) to the real gas mixture enthalpy of equation (3.5). Meanwhile, in the two-phase region, L-V equilibrium is coupled to the enthalpy calculation in order to fully resolve both temperature and composition for each phase.

5. Once that temperature and composition are known, the mixture density can be obtained by means of the equation:

$$\frac{1}{\rho} = \frac{\Sigma_i Y_i^L}{\rho^L} + \frac{\Sigma_i Y_i^V}{\rho^V} \qquad (3.7)$$

where ρ^L and ρ^V are respectively the liquid and vapour phase densities obtained from local temperature, pressure, composition, and compressibility factors for each phase.

The previous reported formulation is valid for any equation of state (EoS), from which the following necessary parameters can be derived:

- The fugacity coefficient for each mixture component for the L-V equilibrium $\hat{\phi}_i$.
- The departure term in the real enthalpy calculation, i.e. $\left(d \ln(\hat{\phi}_i)/dT\right)_{p,x_i}$ (Equation *(3.6)*.
- The compressibility factors of both phases, to then derive ρ^L and ρ^V (Equation *(3.7)*.

As final consideration, it has to be reported that the model considered in this work utilizes the Peng-Robinson equation of state for both liquid and vapour phases, of which relative detailed expressions can be found in [23].

3.4 Summary & Conclusions

In this chapter the experimental and theoretical tools used in the realization of the study have been presented. The exploited experimental

resources have been described, with a particular detail and attention to the utilized test rig. The installation main characteristics have been described; the experimental facility layout have been presented together with the combustion chamber conditions. Both thermodynamic and flow field characteristics of the test rig have been presented and should be later considered for the results' analysis.

Moreover, the detailed characteristics of the two lasers systems employed in the study have been presented, in order to permit a comparison between them for all the considerations that will be later reported upon their applicability to the specific purposes if this work. All the fundamental optical components used in the laser ignition system setup have also been described, detailing their fundamental characteristics.

The optical techniques applied during the realization of the experimental study have been also detailed. For each technique, the theoretical foundations has been explained in detail, joined with its purposes and ideals applications. Finally, the spray mixing 1D-Model has been described and will be later used in the results analysis as both a predictive tool and a validation method.

3.5 Bibliography

[1] V. Bermúdez, J. García, E. Juliá and S. Martínez, "Engine with optically accessible cylinder head: A research tool for injection and combustion processes", *SAE Technical Paper*, 2003.

[2] J.-G. Nerva, "An assessment of fuel physical and chemical properties in the combustion of a Diesel spray", Valencia: *Doctoral Thesis*, Universitat Politècnica de València, 2013.

[3] O. Armas, J. Rodríguez, F. Payri, J. Martín and J. Agudelo, "Effect of the trapped mass and its composition on the heat transfer in the compression cycle of a reciprocating engine", *Applied Thermal Engineering*, vol. 26, pp. 2842-53, 2005.

[4] M. Ikegami and T. Kamimoto, “Flow and Combustion in Reciprocating Engines”, *Springer-Verlag*, 2009.

[5] P. Holland and R. Welsch, "Robust Regression Using Iteratively Reweighted Least-Squares", *Commun. Statis.-Theor. Method*, vol. A6, 1977, pp. 813-827.

[6] W. DuMouchel and F. O'Brien, "Integrating a Robust Option into a Multiple Regression Computing Environment", *Computer Science and Statistics: Proceedings of the 21st Symposium on the Interface*, Alexandria, VA, 1989.

[7] F. Payri, J. Pastor, N. J.-G. and J. García-Oliver, "Lift-Off Length and KL Extinction Measurements of Biodiesel and Fischer-Tropsch Fuels under Quasi-Steady Diesel Engine Conditions", *SAE International Journal of Engines*, vol. 4, no. 2, pp. 2278-2297, 2011.

[8] R. Payri, J. García-Oliver, M. Bardi and J. Manin, "Fuel temperature influence on diesel sprays in inert and reacting conditions", *Applied Thermal Engineering*, vol. 35, no. 1, pp. 185-195, 2012.

[9] F. Payri, J. Pastor, J. García-Oliver and J. Pastor, "Contribution to the application of two-colour imaging to diesel combustion", *Measurement Science and Technology*, vol. 18, no. 8, pp. 2579-2598, 2007.

[10] C. Micó Reche, “Development of Measurement and Visualization Techniques for Characterization of Mixing and Combustion Process with Surrogate Fuels”, *Doctoral Thesis*, Universitat Politecnica de Valencia, 2015.

[11] H. Zhao, “Laser Diagnostics and Optical Measurement Techniques (in Internal Combustion Engines)”, Warrendale, PA 15096-0001: *SAE International*, 2012, pp. 13-21.

[12] A. C. Eckbreth, “Laser Diagnostics for Combustion Temperature and Species”, A. G. a. D. Lilley, Ed., *Cambridge*, Mass 02139: Abacus Press, 1988.

[13] G. Settles, “Schlieren and Shadowgraph Techniques: Visualizing Phenomena in Transparent Media”, Berlin: *Springer-Verlag*, 2001.

[14] L. Pickett, S. Kook and T. Williams, "Visualization of diesel spray penetration, cool-flame, ignition, high-temperature combustion, and soot formation using hig-speed imaging", *SAE International Journal of Engines*, vol. 2, no. 2009-01-0658, pp. 439-459, 2009.

[15] J. Naber and D. Siebers, "Effects of gas density and vaporization on penetration and dispersion of diesel sprays", *SAE Technical Paper*, no. 960034, 1996.

[16] J. V. Pastor, R. Payri, J. M. Garcia-Oliver and F. J. Briceño, "Schlieren Methodology for the Analysis of Transient Diesel Flame Evolution", *SAE Technical Paper*, 8 September 2013.

[17] J. Benajes, R. Payri, M. Bardi and P. Martí-Aldaraví, "Experimental characterization of diesel ignition and lift-off length using a single-hole ECN injector", *Applied Thermal Engeneering*, no. 58, pp. 554-563, 2013.

[18] R. Payri, J. M. García-Oliver, T. Xuan and M. Bardi, "A study on diesel spray tip penetration and radial expansion under reacting conditions", *Applied Thermal Enegeneering*, no. 90, pp. 619-629, 2015.

[19] R. Payri, J. S. Giraldo, S. Ayyapureddi and Z. Versey, "Experimental and analytical study on vapor phase and liquid penetration for a high pressure diesel injector", *Applied Thermal Engeneering*, no. 137, pp. 721-728, 2018.

[20] J. Pastor, J. López and J. P. J. García, "A 1D model for the description of mixing-controlled inert diesel sprays", *Fuel*, vol. 87, no. 13-14, pp. 2871-2885, 2008.

[21] F. Payri, R. Payri, M. Bardi and M. Carreres, "Engine combustion network: Influence of the gas properties on the spray penetration and spreading angle", *Experimental Thermal and Fluid Science*, vol. 53, pp. 236-243, 2014.

[22] J. Borée, N. Atassi and G. Charnay, "Measurements and image analysis of the turbulent field in an axisymmetric jet subject to a sudden velocity decrease", *Experimental Thermal and Fluid Science*, vol. 14, pp. 45-51, 1997.

[23] J. Pastor, J. García-Oliver, J. Pastor and W. Vera-Tudela, "One-dimensional diesel spray modeling for multicomponent fuels", *Atomization and Sprays*, vol. 25, no. 2, pp. 485-517, 2015.

Chapter 4

Laser Induced Plasma Ignition: System Optimization

Contents

4.1 Introduction

This section presents the experimental results obtained from the plasma induction system optimization process for the application of such system to a direct injection spray.

The application of a high reliability ignition system is considered as a matter of major importance in any engine application, especially if the main objective is to study its impact on the combustion development in comparison with a conventional spark plug. Indeed, a high effectiveness system in terms of plasma formation, timing and spatial precision, will allow to discard any failure in the breakdown generation from the causes of eventual variations between different forced ignition conditions, that such system is permitting to test. This allows ascribing such variations just to the fuel spray local conditions of the ignition region discarding a second order factor of uncertainty. To get this sort of high-reliability system, both optical system settings and thermodynamic conditions in the combustion chamber were considered in a parametric variation study to find the highest laser plasma formation effectiveness experimental conditions. This study was performed by taking plasma images with the high-speed CMOS camera synchronized with the laser system by an external trigger, which virtually wants to simulate the ignition trigger signal. The tests were carried out both under engine-like and atmospheric ambient conditions, in the latter case with and without the optical access window mounted as an element of the laser beam path.

4.2 Laser induced plasma system set up

In the following paragraph the laser system setup needed for the plasma formation studies and the later ignition application are reported. The characteristics of the tested laser system for the plasma induction will be

presented, as well as the tested configurations and eventual considerations upon its applicability to different systems.

4.2.1 Previous considerations for the Laser ignition system design

The design of the system starts with taking into consideration the fundamental parameters that should allow to obtain plasma in a reliable form, as extensively explained in Chapter 2. Such parameters will then be adapted to the experimental limitations of the systems in use, which are reported in Chapter 3. For completion, a resume of the principal characteristics for a reliable induced plasma generation under engine-like conditions is defined as follows:

- The most reliable and applicable induction mechanism is the non-resonant breakdown, as reported in Chapter 2. Even if it requires a higher energy concentration, its advantages of not requiring neither a match between emission and absorption wavelengths nor an absorption element to heat up the ignition volume, are much more significant, making it the common first choice for this kind of applications.

- High local pressure should be a favorable condition for the plasma induction. As reported in detail in Chapter 2, increasing pressure in a media under laser plasma induction will lead to a reduction in the necessary Minimum Ignition Energy (MIE).

- Combustion chamber conditions should be generally favorable. However, important variations could be identified, specifically related to the local in-chamber conditions at the induction spot. As reported in Chapter 2:

  - The eventual presence of impurities in the focal volume should be a favorable condition to provoke breakdown.
  - High local flow velocity could lead to a high MIE required for a local rich mixture condition to ignite, but MIE should be lower for lean mixtures. Overall, the effect of local flow condition on the plasma induction and consequent ignition could be considered not decisive, especially if compared to the local equivalence ratio effect.
  - The local equivalence ratio dependence has been considered in detail in 4.2.3. Just as a brief resume, it can be stated how a laser plasma induction system seems to be favored in the ignition process of rich mixtures and penalized in the one of lean mixtures if compared to a traditional spark ignition system.

- The use of a short focal length lens should be considered always favorable and a primary importance factor to define. The focusing lens' focal length has been shown, as explained in Chapter 2, to be a major importance factor for the determination of the energy density achievable with the laser system, and it influences in primary form the possibility to reach the media's threshold for breakdown.

On the other hand, as already showed in Chapter 3, the optical test rig installation presents a fundamental limitation for the design of the optical system for the plasma induction, which is the minimum distance from the injector nozzle at which the incident laser beam should be focused. In this case, as previously reported in the plane of Figure 3.2, this minimum distance is 300 mm. As already reported before and detailed in Chapter 2, this represents a great limitation for the entire system, as the focal length is inversely dependent to the energy deposition capability of the system.

Thus, a better, more efficient and fundamentally greater energy generation system is needed in order to compensate this limitation. Moreover, as detailed in Chapter 2 of this document, the one needed for the realization of this study represents one of the largest focal length with which a stable plasma generation for an ignition system has never been attempted.

4.2.2 Set up: Laser system selection for the induced plasma generation

The first laser system tried for the plasma induction studies, as reported in Chapter 3, has been a Nd:YAG Nano L 135-15, from Litron Lasers, due to its advantages in terms of compactness and easy alignment and possible applicability to different tests rigs. Firstly, to study the laser system applicability to the current objective, a wide set of plasma induction test in ambient air were carried out. The aim of this first set of tests was to both optimize the laser output to obtain the minimum energy necessary for the plasma generation and to control the system reliability in the plasma induction process, in order to ensure a 100% effectiveness under the aforementioned restriction related to the tests facilities in use. In particular, the minimum applicable focal distance of 300 mm from the injector nozzle axis inside the combustion chamber. During these tests, the Nano L laser system was not able to generate plasma in a reliable form in ambient air condition, making it no exploitable for the final design of the ignition system.

More in detail, two specific parameters have been identified as critical points for the failure of the system in the plasma induction. These parameters are the divergence angle of the beam and the maximum output power at 10 Hz and 532 nm wavelength. In fact, it is the combination of these two parameters, with the focal length limitation, that has led to the impossibility of generating plasma under the required test conditions, not allowing to obtain a sufficient local energy density for breakdown. So, not having options to increase the energy available for laser output and with the need to achieve a power density value comparable to that reported by several authors [1] [2]

[3] [4] and already defined in Chapter 2, the only possible variation to apply to the system was reducing the focal volume at the focusing spot. The principal way to doing it, not modifying the lens' focal length, is to operate on the beam diameter and beam divergence at the incidental plane of the lens, where it can affect the focusing capability of the same optical element within the diffraction limit. In this sense, it should be noted how the size of the focal volume at the focusing spot of a laser beam is strongly affected by its divergence. This dependency is better represented by the M^2 parameter, which is defined as the quality factor, or propagation factor, of a laser beam and takes into account the diameter d_i, the divergence angle θ and the emission wavelength λ, as detailed in equation (4.1):

(4.1) $$M^2 = \frac{0.25\, d_i\, \theta\, \pi}{\lambda}$$

Actually, to define its quality, a laser beam is generally defined as "M^2 times limited by diffraction", referring to the fact that an ideal laser beam limited by diffraction, also perfectly Gaussian, has an M^2 factor of 1. The M^2 values lower than 1 is physically impossible while obtaining a beam of unitary M^2 is impossible at the practical act. In any case, the more a laser beam is characterized by an M^2 factor close to the unit, the greater it will be its quality. On a practical level, the beam quality factor limits its possibilities of approach to a certain angle of divergence. For the Nano 135-15 laser system under analysis, it presents a beam divergence of 3 milliradians, thus generating an M^2 factor at 532 nm close to 22. For what already said, this represents a very high value by itself, symptom of a rough quality laser beam. Moreover, this beam quality factor value results much higher to the ones directly reported, or calculable starting from the reported laser parameters, of different authors. In general, considering the more common literature for the laser plasma induction process reported in Chapter 2, the M^2 results to be around a value of 6 as maximum [1] [2] [3] [4]. It can so be stated how, for the case of analysis, although only for comparison between the characteristics of the equipment under analysis with the ones reported by various other authors, the main limitation when considering the size of the focal point that

the laser-lens assembly could produce was represented from the low quality of the beam, particularly from its high divergence.

At this point, a common way to limit and decrease the divergence of a collimated beam is to increase its diameter, as reported by Bradley et al. [1]. With this operation, by keeping the beam collimated through an optical system, is the same beam expansion or reduction system that defines the new angle of divergence of the beam. This type of optical system is usually called beam expander and can be realized as a *galilean* type telescope, composed of a plane-concave lens that allows to enlarge the beam diameter and another plano-convex lens that, put at the adequate distance from the first lens, allows to collect the expanded beam and collimate it again. Such beam expander, in addition to decreasing the M^2 parameter of the laser by decreasing the divergence of the beam, is able to reduce the size of the focal point also thanks to the effect of having increased the global diameter of the beam at the focal lens plane.

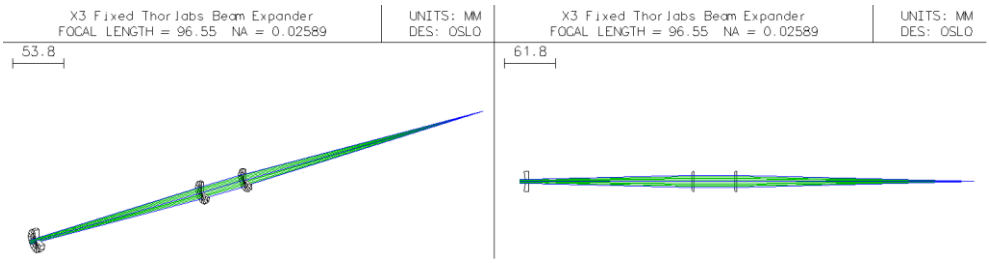

Figure 4.1. Graphic representation realized with the OSLO® optical software of the lenses system forming the galileian X3 beam expander.

This should always be valid under the consideration that the focusing condition is not limited by spherical aberration of the lens in use. The spherical aberration phenomenon is due to geometrical imperfections of the lens that, for constructive limitations, isn't typically able to maintain the exact curvature along all its surface, so not providing in some points the nominal focal. This effect usually happens in the outer area of the lenses where this curvature turns out to be more distorted, and it is in that area

where the greatest effects of spherical aberration occur. The lens that has been used in this project presents a good constructive characteristic, which allows to take advantage of 90% of its diameter without suffering aberration. In other words, if the beam expansion is still in the lens' clear aperture, the reduction effect on the focal spot should be ensured by the combination of the aforementioned two factors.

Therefore, in the study of possible beam expander configurations to apply to the laser beam, being fixed the diameter of 25.4 mm of the focusing lens, it has been limited the beam expansion to 3 times the initial size (5 mm), thus ensuring not to limit the focusing process by spherical aberration. The design of the beam expander has been made with the aid of the OSLO® software (Optics Software for Layout and Optimization), developed by Lambda Research Corporation. This software has allowed to analyze different combinations of lenses for different degrees of diameter expansion. The final choice has fallen on a plane-concave lens of -100 mm focal, used to expand the beam, and another plano-convex lens of 300 mm focal, identical to the focusing one, necessary to re-collide the beam. The characteristics of these lenses are reported in the alleged paragraph of Chapter 3. The two lenses have been mounted at a distance of 200 mm between them, in a configuration that can be appreciated in Figure 4.1. The beam expansion system proved to be effective in the focal spot reduction. Proof of that has been obtained by various plasma generation tests, performed with different focal length shorter than 300 mm, where the plasma induction has been always achieved with laser powers largely smaller than the one used before the expander application. However, using the 300 mm focal lens, even the increased beam diameter and the decreased beam divergence has not been enough to compensate the lack of power of the laser device.

In conclusion, it has been necessary to take note of the practical impossibility of implementing this laser equipment in the plasma induction ignition system, which has led to the selection of the Continuum Surelite II laser system for the implementation of the ignition system. All detailed characteristics of the selected laser are reported in Chapter 3.

4.2.3 Set up: final Laser induced plasma system configuration

Switching to the Surelite II laser system has permitted to easily obtain reliable plasma induction in ambient air, principally due to his low M^2 parameter (around 6) and higher power level than the first tested Nano 135-15. Once defined the system selection, all the optical configuration for the beam guidance and focusing have been fixed and tested. In particular, laser-grade mirrors have been used for defining the optical beam path in order to have freedom for its movement along the vertical axis, being so able to focusing it on different positions along the spray axis inside the combustion chamber. In order to achieve it, a fine vertical alignment of the beam has been carried on. A couple of motorized travel stages have been employed in the final focusing lens setup for the horizontal alignment and vertical movement. In this way it has been able to maintain the alignment of the beam path while the vertical position of the focusing lens was variated.

Once the optical setup was settled, a brief set of tests was carried out in order to establish possible beam deviation effects due to the optical windows position. These tests, carried out in ambient air conditions, have showed how the optical access deviation effect on the focused laser beam is practically negligible. This seems reasonable once taken into account the relatively small thickness of the rig's optical accesses (28 mm) and the own proper variation of the plasma induction position within the focusing volume, already fixed by the limitation of the large focal length applied.

Then, plasma induction tests at different engine like conditions have been carried out, in order to establish the capacity of the system in a reliable plasma induction. All these tests results, both in air and under engine-like condition, will be later reported in detail in this same chapter. However, it is worth mentioning in this paragraph that moving from the ambient air condition to any of the engine-like ones has evidenced a phenomenon to take into account when considering the design of the system: the windows damage threshold variation with pressure and temperature. Moving from ambient air condition to engine conditions, has led to provoke damages in the optical access windows of the test rig at the exact same laser configuration at which

it was able to obtain a 100% plasma induction. An example of the obtained damages is shown in the pictures of Figure 4.2. As those damages were largely random, it was not exactly predictable which chamber conditions were more or less favorable to damage. Moreover, once the damage was done, it creates a hot spot along the beam focusing axis, absorbing almost all the beam energy and completely preventing a breakdown event to take place inside the chamber. So, considering that the damage threshold for the windows at 1064nm was largely higher than the one at 532nm, at which under high-pressure high-temperature the focused beam was evidently very close, it has been taken the decision to switch from visible to infrared wavelength for the design of the laser induced plasma ignition system. This has completely prevented all possibilities of windows damages, raised the available peak power for breakdown with the drawback of needing a more cared attention at the time of align the beam path during the experimental tests.

Figure 4.2. Pictures of an optical access windows as damaged by the laser beam focused trough it under engine-like conditions, at 532 nm and with 350 mW of peak power.

4.3 Laser induced plasma system validation and optimization

As reported before in section 4.2.1, theoretical consideration about breakdown thresholds and energy density at the focal spot were the starting point for the design process of the plasma induction system. This initial setup was then extensively tested at different experimental conditions where its reliability, both in terms of effective induction capability and plasma position stability, were quantified. The results of the first study, as well as the experimental configuration and methodology applied for the performed tests, are reported in the next section.

4.3.1 Experimental set up and methodology

In this section, a description of the utilized experimental setup and the applied experimental methodology will be presented. The experiments for the validation and optimization of the designed LIP system were conducted in an optical test rig which detailed characteristics have already been reported extensively in Chapter 3 of this document. Is still important to underline that during the realization of this first test on the ignition system fuel injection was not applied inside the combustion chamber, as these results are part of the secondary major task of the research work and will be detailed in Chapter 5. All details regarding single systems and optical components used for the experimental setup have also been reported in Chapter 3.

The methodologies used for the experiment development will also be here reported. Natural luminosity visualization has been employed for registering plasma images when evaluating the performance of the laser induced plasma system in the absence of injection. The plasma images registration and processing detail will be presented in two specific paragraphs.

4.3.1.1 Operating conditions

The first tests carried out for configuring the induction system and quantify its effectiveness were done in ambient air conditions. The alignment of the plasma generation system with the injector position in the combustion chamber has allowed the evaluation of the positional stability of the air breakdown, as will be later analyzed in detail trough this same chapter.

For the tests carried out under engine-like conditions, the test matrix defined in terms of TDC pressure, temperature and density is here reported in Table 4.1, joined with the proper case names assigned to each thermodynamic configuration considered.

Temperature [K]	Pressure [bar]	ρ [kg/m3]	Case Name
900	53	20.8	53900
700	43	21.7	43700
800	53	23.4	53800
700	53	26.7	53700
700	63	31.8	63700

Table 4.1. Operating engine's conditions at TDC used in the plasma induction effectiveness tests.

4.3.1.2 Experimental system synchronization

System synchronization was performed with the help of ad-hoc system, known as DISCA, especially designed to control both flash lamp and Q-switch pulses of the laser system to ensure stable operating conditions and to minimize laser shot energy fluctuations. This system enabled synchronization of laser together with the camera, injection system and pressure transducer. Even though the injection system was not used in the realization of this set of tests, a simulated injection trigger was generated in order to have a main trigger to which refer all the synchronization parameters of the experimental

process. The schematic of Figure 4.3 shows the whole synchronization system used.

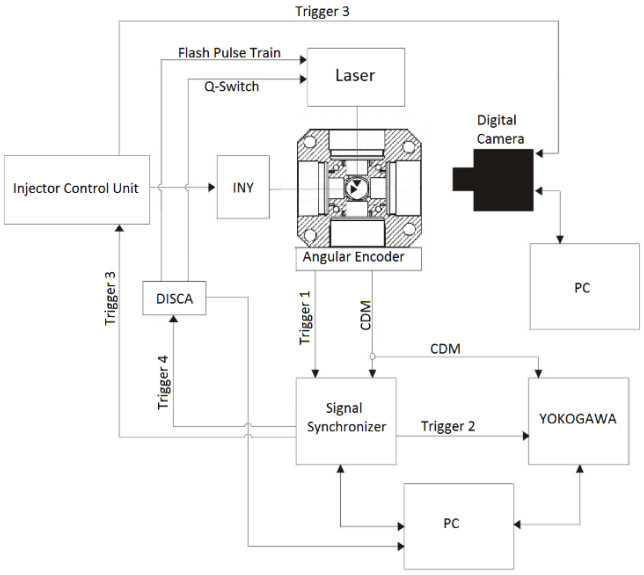

Figure 4.3. Experimental control and measuring signal synchronization system employed during the tests performed in the optical test rig.

4.3.1.3 Plasma images registration

The visualization of the plasma formation has been carried out by registering its broadband high intensity emission by means of a high-speed CMOS camera (Phantom V12.0) coupled with a 100 mm *f*:2 camera lens (Zeiss Makro-Planar T*2). The plasma emission was collected outside the optical access to the cylinder, by a 150 mm diameter lens with a focal length of 450 mm, sufficient to guarantee a minimal light dispersion while maintaining a good tradeoff between global magnification of the zone under focus and the possibility to still have a full visualization of the combustion chamber. Details regarding the importance of this factor are later reported. A schematic representation of the final experimental setup used for the LIP system validation and optimization process in presented in Figure 4.4.

The registration of plasma images will allow the quantification of both effectiveness and reliability of the designed plasma induction system. So, registering them with a good spatial resolution and a fixed spatial reference has resulted to be of primal importance. Giving the right attention to such factor, permits not only to account for the overall shot by shot effectiveness of the system in provoking the breakdown of the medium, but also to account for the positional stability of the obtained induced plasma. Positional stability is in fact considered to be another fundamental factor in order to determine the system's ignition capabilities of direct injection sprays.

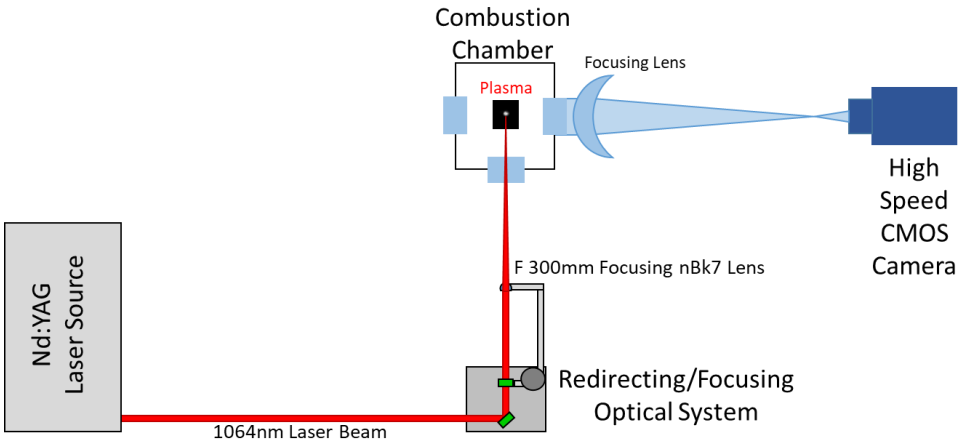

Figure 4.4. Schematic representation of the optical setup used in the plasma images registration for the validation and optimization of the LIP ignition system under design.

The plasma generation tests have been realized both in ambient air conditions and engine like conditions, as will be later detailed. For every tested condition, the plasma induction was attempted at five different distances from the injector nozzle, all along the injector axis and inside the combustion chamber. Every induction position was spaced 5 mm from the previous one. This variation of the plasma generation position has allowed to test the precise vertical alignment of the system with the injector axis, ensuring the possibility to obtain plasma reliable formation within the spray

cone all along the combustion chamber volume. The spatial resolution obtained from the setup combination of the camera focusing lens and light collecting lens was of 10.28 pixels/mm. This resolution has been selected in order to be enough focused for a detailed visualization of the plasma formation area while still maintaining the possibility to visualize the entire combustion chamber. This has resulted to be very important in order to ensure a common reference through all the executed plasma induction tests at the time to determine the spatial stability of the plasma formation process.

Figure 4.5. Image of recorded plasma obtained during the laser induction system optimization test. This image has been recorded in ambient air condition and shows an example of a multipoint induction event.

The camera was synchronized with the laser pulse by a single trigger signal, virtually representing the injector's start of energizing. To avoid any synchronization error, the camera was always fired earlier than the laser system and was set up to register the maximum number of images in the selected time interval. Each image frame was collected with a minimum exposure time of 8 µs higher than the plasma lifetime, as commonly reported in literature to be around 105 ns [5], and, more in general, in the same order of a laser pulse duration [2]. Pickett et al. [3], for a comparable optical setup, has reported to use similar parameters of a 10 µs framing period and 4 µs exposure time for registering plasma images. Once the camera configuration was selected as reported, the combination of recording speed and shutter time parameters were tuned up always to maintain a fixed image resolution of 384x800 pixels, allowing so to visualize the entire combustion chamber. This has permitted, during the subsequent image processing phase, to refer the

registered induced plasma position with the volume effectively occupied by the spray cone inside the combustion chamber. For each tested condition, 75 repetitions were performed. An example of the recorded plasma images is here reported in Figure 4.5.

4.3.1.4 Plasma images processing

The plasma induction system's effectiveness has been quantified through the application of a specific plasma images processing, which has allowed to obtain the defined "plasma probability maps", such as the ones later reported in Figure 4.7 for the atmospheric air condition tests.

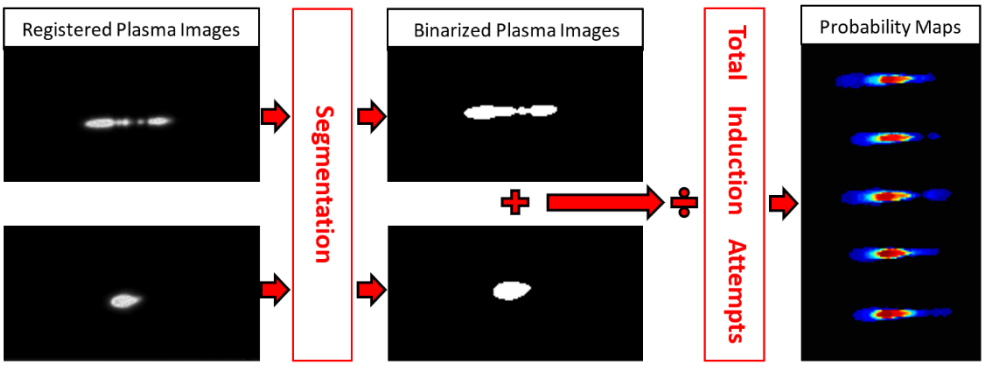

Figure 4.6. Schematization of the process followed by the plasma image processing algorithm in order to obtain the plasma probability maps. The plasma images are first selected among all the registered repetition, then binarized in order to distinguish the image background from the area occupied by the plasma emission. The binarized images are cumulated and divided by the total number of the induction attempts. The results are then plotted in color-map showing in red the 100% and in black the 0% plasma occurrence probability pixel by pixel.

These probability maps represent the effectively calculated probability of finding plasma in a concrete position of the combustion chamber, with respect to the total plasma induction attempts. Such maps were obtained

from the processing of the plasma images registered with the camera through a specific algorithm. For every image registered, the algorithm first identifies plasma presence and, if detected, it segments the image by dividing the region occupied by the plasma emission from that of the background. This procedure was carried out, after a series of different processing attempts, using a fixed threshold value of 20% higher than the average background digital level, both for the plasma presence detection and for the segmentation. The fixed threshold selected was considered to be optimal and not so critical for the image segmentation, thanks to the high intensity emission of the plasma in comparison with the surroundings. The binarized images where then accumulated and divided by the total number of breakdown attempts, permitting to estimate plasma occurrence probability.

A visual schematization of the process followed by the image processing algorithm is reported in Figure 4.6. The results of this operation, shown in a 0–100% color map, represent the number of times that plasma could be detected at a specific pixel position, and allows the estimation of both the overall breakdown success rate and the positional stability of the induction event. Both factors will be later considered in detail for the results analysis. The relatively small size of the registered plasma, when compared with the total resolution of the registered image, has not allowed any discrimination between the real plasma kernel zone and a blooming effect zone registered by the camera sensor due to the high intensity emission. In any case, for the purpose of this study, the spatial resolution is considered to be enough in order to determine whether the plasma induction position was or not included within the spray cone boundaries, as represented in Figure 4.7 (left).

4.3.2 Laser induced plasma system effectiveness in atmospheric conditions

The first test was performed at atmospheric conditions, having the complete optical guidance and focusing system mounted. The aim of this first setup test was its optimization for the maximum effectiveness in overall

plasma generation. Indeed, the large focal length of the employed focusing lens (300 mm), forced by the test rig geometry, was one of the biggest limitations for such kind of application.

As explained before in section 4.2.1, larger focal lengths limit both minimum size and depth of focus of the focusing spot, and it has been defined by various authors how properly the minimization of the focal spot's dimensions represents a crucial factor for the success of such stochastic induced breakdown event [2] [6] [7]. In fact, most of the studies carried out in this same research field have reported a design of optical set-up with focal lengths shorter than 300 mm, the one used for this study. Test rig limitations, in terms of space and disposition of the optical elements, has restricted the possibilities of further reduction of this parameter, leading to the necessity of using a higher energy beam in order to reach an optimal breakdown configuration. In fact, the results obtained from the plasma generation tests reported in Figure 4.7, have shown the proper capability of the setup to reach 100% effectiveness in plasma induction, both in terms of molecule breakdown effect and positional stability. Figure 4.7 (right) reports the obtained results for atmospheric air conditions breakdown attempts, with the rig's fused silica window mounted as an element of the optical system in the laser beam path. The results are here reported as a probability map, which shows the probability of finding plasma in a certain region along the spray axis with respect to the total plasma generations attempted.

Complementary to the information reported in Figure 4.7, Figure 4.8 presents the same probability maps in terms of one-dimensional plots. Here, the horizontal axis represents the distance to the spray axis, where the beam is theoretically focused, and each profile corresponds to a different distance from the injector's nozzle where the laser was targeted by the optical guidance system. The effective dimension of the area where it is always possible to find induced plasma can be quantified with such plots.

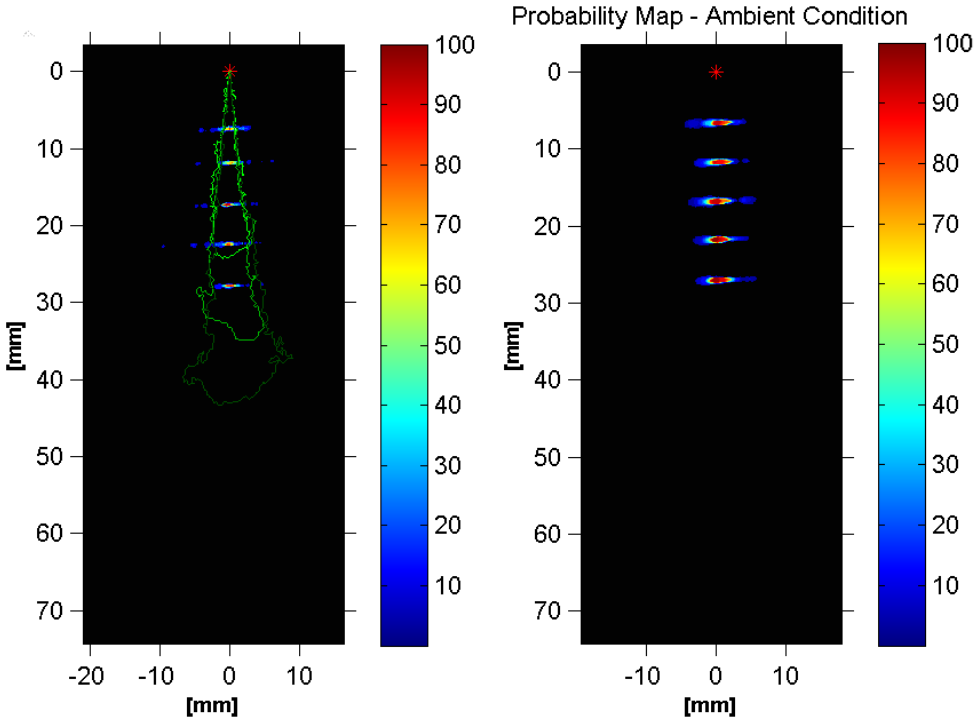

Figure 4.7. Plasma Generation Probability Maps. On the right: probability maps obtained for the plasma induction under atmospheric conditions, without fuel injection, at different distances from the injector nozzle (marked as a red asterisk). On the left: probability maps obtained under engine-like condition, without fuel injection. As an indication of the volume occupied by a real spray cone under the same conditions, some examples of real spray contours have been reported in the figure. The area of 81 x 28 mm visible in the reported images is the total available access to the combustion chamber.

For each tested location along the spray axis 75 repetition attempts were recorded. Even if the spatial resolution of the registered images is not adequate to determine the effective plasma dimensions, due to the impossibility of distinguishing between the real plasma volume and the blooming effect also registered by the camera sensor, it's at least sufficient to determine whether or not the plasma generation location was included within

the spray boundaries, which is in the end the main purpose of the previous optimization study. This was considered as the fundamental parameter to take in account in order to ensure the effectiveness of the ignition system under design.

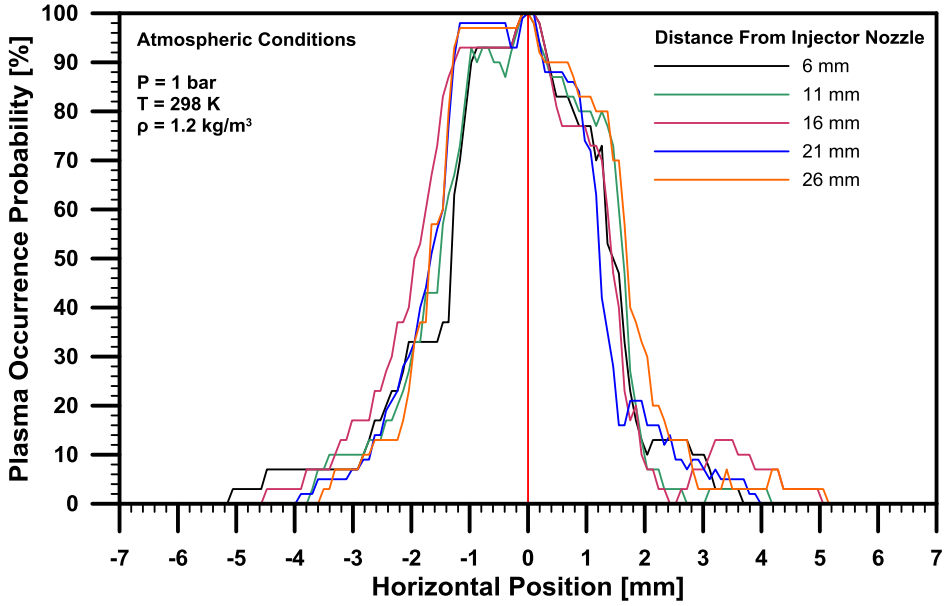

Figure 4.8: Plasma Occurrence Probability as obtained from the probability map method. The injector nozzle position is nominally located at 0 mm. The graphic shows the probability of inducting plasma at the focal axis and permits the determination of its positional stability.

Looking at the plasma occurrence probability graph reported in Figure 4.8, it results clear that the system can reach a plasma generation effectiveness of 100% with excellent positional stability, in air at atmospheric conditions, for the finally chosen laser system and applied optical settings. In this particular case, the typical gaussian shape of the probability curve, with the highest generation probability always on the axis with respect to the borderline, is due to the variation of the obtained plasma dimensions between subsequent firing attempts.

4.3.3 Laser induced plasma system effectiveness in engine-like conditions

For the evaluation of the system's plasma generation capability under engine-like conditions, the tests were performed following exactly the same experimental procedure as earlier described for the atmospheric conditions. The investigated in-cylinder conditions are reported in Table 4.2 with its respective overall success rate (SR). The Success Rate (SR) is obtained as here reported in equation (4.2).

(4.2) $$Success\ Rate = \frac{Induction\ Succes\ Events}{Total\ Number\ of\ Induction\ Attempts}$$

Case	P [bar]	T [K]	ρ[kg/m3]	Total Rep	No Plasma	Success
Atm	1	298	1.2	75	0	100%
53900	53	900	20.8	75	32	57%
43700	43	765	21.7	75	10	87%
53800	53	800	23.4	75	19	75%
53700	53	765	26.7	75	0	100%
63700	63	765	31.8	75	4	95%

Table 4.2. Overall plasma induction success rate for all the tested engine-like conditions. The reported pressure, temperature and density values are always referred to Top Dead Center position in the engine cycle.

For completing these results section, in addition to the results presented in Table 4.2, plasma occurrence probability graphs are depicted in Figure 4.9. It has to be noted that the defined success rate only considers the possibility of the breakdown to occur, not its spatial repeatability, which is rather described in the plasma occurrence probability graphs of Figure 4.9.

Observing the reported results, both in terms of absolute overall effectiveness and positional stability, an important loss in effectiveness in the transition from atmospheric to engine conditions can be clearly appreciated. Applying the induction system to the lowest density case, 53 bar 900 K 20.8 kg/m^3, has caused a 43% effectiveness loss of the induction process if compared to the results obtained in atmospheric conditions, even though a high density ambient should be theoretically more favorable to the induction process due to a lower breakdown threshold of the media. For this reason, the observed effectiveness loss must be only related to the laser focusing process.

Once the engine is running, both the elevated density gradient and air movement inside the combustion chamber lowers the focusing capability of an optical system, mostly for an accumulation of beam steering and beam expansions effects. Considering this factor, the lower possibility to focus the beam in a sufficient small spot evidently overcomes the advantage of lowering the energy threshold for the plasma breakdown event to take place. This leads to the well observed decrease of the induction effectiveness. Moreover, from the plasma probability maps reported in Figure 4.9, a large variation in the positional stability can be also appreciated. If compared to the atmospheric ambient test, every single engine condition shows a greater "plasma probability area", which indicates the possibility to find plasma in the chamber farther away from the theoretical focal position of the beam at the spray axis.

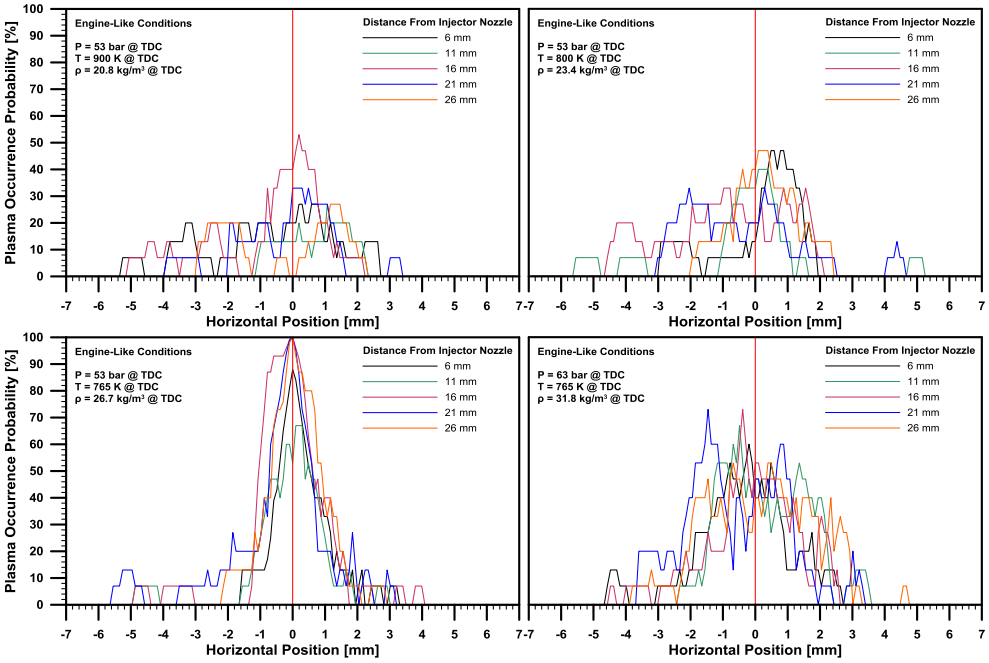

Figure 4.9. Plasma Generation Probability for pressure and temperature variations under engine-like conditions. For every engine-like tested conditions the plasma induction was attempted at five different generation locations along the injector axis, nominally at 6, 11, 16, 21, 26 mm from the injector nozzle. The 0 mm position in the graphics represents the injector axis position in the combustion chamber.

Once made these considerations, the parametric study has also shown the possibilities to obtain 100% effectiveness in plasma generation even under engine conditions. This has led to select 700 K and 53 bar as the best thermodynamics configuration for performing the spray ignition tests, at which the highest positional stability and overall effectiveness of the induction process could be appreciated. The detailed results, in terms of probability maps and distribution along the spray axis at the selected engine condition, are reported in Figure 4.10. In fact, among all the tested engine conditions, it was the only one where local areas of 100% plasma generation probability are still appreciable.

Considering the reported results, it can be distinguished two potential leading factors for the observed difference among the probability maps at different conditions. The first one is density, which came to be the most influencing factor for breakdown occurrence, even though in literature such variations are most commonly related to ambient pressure. In this sense, Table 4.2 reveals how by changing temperature at constant pressure it can anyhow be observed a variation in induction success rate, establishing here the role of density rather than pressure as a governing factor.

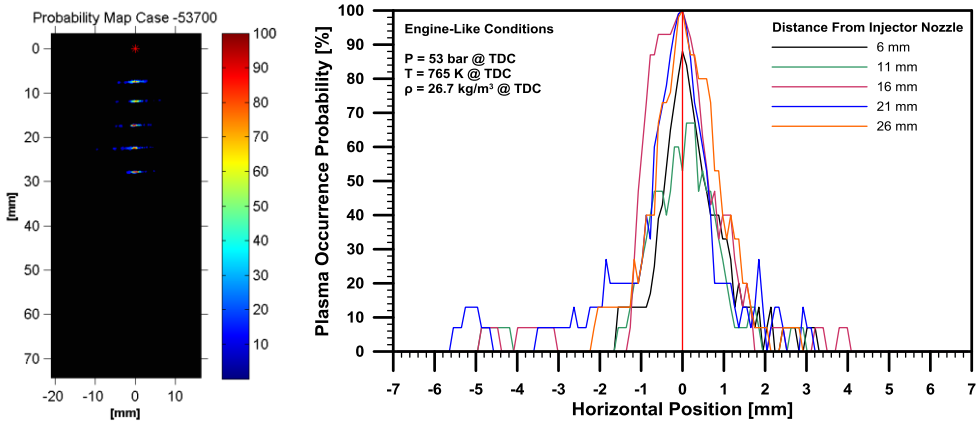

Figure 4.10. Plasma probability map (left) and Plasma Occurrence Probability (right) at the focal axis of each respective tested distance from the injector nozzle for the Engine condition case of 53 bar and 765 K at the TDC. This engine condition was finally selected as test case for the ignition attempts, thanks to the possibility to obtain full success rate at different distance with minimum positional variation if compared with the other reported cases.

In the end, it could be considered as both things to be real: it is true, as reported in literature, that pressure variation is the leading factor in terms of energy threshold variation for breakdown occurrence; but it is also true how, in this particular study case, density variation plays a bigger role than pressure, by compensating the energy threshold variations with the in-

chamber focusing efficiency of the system, leading to a higher impact in overall plasma generation terms.

The parametric variation has also shown how, starting from the lowest density condition, both the overall effectiveness in the plasma generation and the positional stability increases with the ambient density until it reaches its peak (100%) at 26.7 kg/m^3. After this point, it can be appreciated a slight reduction in the success rate (95%) at the highest tested density of 31.5 kg/m^3, also with a more disperse induction position. This puts more evidence on the second major factor influencing the results: the beam steering effect. This light deviation effect caused by density gradients is clearly limiting the performance of the beam focusing process at high density, making more difficult to accumulate energy at the focal point. A difficulty that increases with temperature and density, offsetting the previously discussed decrease in energy breakdown threshold. As a result, at the highest density case, even if the energy breakdown threshold should be the lowest, the energy density accumulation is also the worst. This takes the system near the limit of the breakdown event occurrence. A worsen beam focusing also implies a higher local focal volume, which is reflected in a bigger focal spot diameter and bigger depth of focus, which is a measure of the focal volume in the direction of the lens focal axis. This effect, paired with the lowered energy threshold and the higher in-cylinder air movement, could be an explanation of the observed loss in the induced plasma positional stability and for the large spatial variation observed in the focusing plane. This fact becomes even more clear if it is considered how for the 53700 case, at which a 100% success rate is obtainable, that peak is appreciable only in a few and very small local zones of the probability map.

Another interesting fact to report, and another indication in the same direction for the analysis of the plasma induction event in engines, is the appearance of multi-point induction, for which an example could be seen in Figure 4.11. An explanation for such events fits perfectly with what already here reported before: with the raising of the in-chamber pressure, the breakdown threshold of the media is lowered to the point where the local

energy density results to be far over the breakdown limit. So, there will be a higher volume where the energy density outmatches the threshold and so a higher volume where it is probable that a molecule reaches breakdown randomly. This enlargement of the "probability volume" is fundamentally caused both by the effects of the pressure on the energy threshold and by the effect of the density on the beam scatter and focusing efficiency. Both effects contribute to enlarging the volume around the focal spot where the probability of a stochastic breakdown event reaches 100%. Anyhow this still does not explain how, for the tested cases, the registered success rate decreases for the 63700 case once has already reached 100% at the 53700 case, even if the thermodynamic conditions should be more favorable. Since the purpose of these preliminary tests was to ensure the possibility to reach a plasma generation stability of 100%, the fact of losing effectiveness was not further investigated in this work but, referring to Picket's analysis [1], we can generally justify such behavior as due to additional interactions effects between the quartz optical access window and the laser radiation.

Figure 4.11. Example of Multipoint Plasma Induction registered for the condition of 63bar and 700K at 6mm from the injector Nozzle.

These interactions should be caused by the behavior of the quartz material subject to mechanical and thermal stresses, as it happens along an engine cycle, which can provoke a variation of its optical properties interfering with the beam focusing and so lowering the obtainable local energy density more than what could be only caused by the density gradient effect.

As a conclusion, this preliminary study, aimed at the optimization of the experimental thermodynamics and optical conditions for the subsequent spray ignition tests, has permitted to:

- Infer the importance of the density as a main factor leading the variation of the breakdown probability in engines, considered as a coupled effect of both pressure on energy thresholds and density gradients on beam scatter and focusing efficiency.

- Select an optimal configuration for the realization of spray ignition tests. A configuration which ensures 100% laser breakdown repeatability, so that differences found in the subsequent results should be related only to the local flow conditions of the fuel spray and not to possible further variation of the ignition system, that could be considered reliable after this analysis and optimizations.

4.4 Summary & Conclusions

An optimized, reliable and controllable non-intrusive ignition system has been developed on the basis of the laser plasma induction process.

A method for the quantification, control and optimization of reliability and effectiveness of such laser induced plasma ignition system (LIP) has been experimentally tested in an optical test rig, by means of the application of Natural Luminosity visualization techniques to record plasma images. Such images have been then processed using a specific algorithm which has led to the determination of plasma probability maps, allowing the quantification of the overall efficiency and positional stability of the induced plasma.

The optical design of the elements needed for the realization of the laser plasma induction system has been performed and finalized, starting from some literature considerations upon plasma formation and non-resonant breakdown generation in air. The laser pulse energy was then optimized, in order to limit the total amount of energy density generated at the focal spot, avoiding eventual overkill effects that could provoke multipoint induction processes and so lowering the positional stability of the induced plasma.

To pursue this optimization purpose, laser induced plasma was generated in two different environments, sequentially:

- Atmospheric conditions: In order to define a methodology to ensure the required reliability of the induction system for engine combustion's parametric studies. Thus, LIP system settings were defined to ensure full success rate (100%) in terms of plasma generation and optimal positional stability, guaranteeing the induction just in the region of the spray cone, all along the injector axis. Such results have been finally obtained with a configuration of a laser beam of 300 mJ energy peak, emitted at 1064 nm and focused through a plano-convex n-BK7 lens of 300 mm focal length.

- Engine-like conditions: in-cylinder pressure and temperature conditions have been varied in an optical test rig, permitting to reproduce in a parametric study real engine density conditions, ranging from 20.8 to 31.8 kg/m^3. By applying the previously developed methodology of probability maps, the following conclusions have been drawn:

    - Compared to the results at atmospheric air, the engine-like condition of 20.8 kg/m^3 has shown a 43% loss in the system effectiveness to induce plasma, even though, as reported in literature, the higher density should more be favorable for the occurrence of a breakdown event. This behavior has been explained through the consideration of a high decay in the system focusing ability caused by the strong beam steering effect induced by both the internal air flow and the refraction index variation in the last part of the focusing beam path, though the test rig.

    - Different induction success rate values were obtained for different chamber densities from 56% at 20.8 kg/m^3 to 100% at 26.7 kg/m^3. Thus, higher densities imply higher success

rate, and it has been confirmed that the full success rate could be reached also under engine-like conditions. Consequently, the increase of the air density seems to be the main parameter governing the laser induced breakdown success.

Positional stability of the induced plasma has resulted to be also affected by the density variations, as shown in the above reported probability maps and graphs. In particular, the lowering effect on the breakdown energy threshold together with the increase of the local density has led to an "overkill" condition for the 31.8 kg/m3 case. In this condition the local energy density is far beyond that needed for the plasma induction, meaning that a bigger local volume should contains enough energy to provoke a breakdown. In such condition, the stochastic nature of the breakdown event implies that randomly any molecule contained within the volume could break-up, generating the electron cascade that leads to the plasma induction and so lowering the positional stability of the ignition system and its general final reliability.

4.5 Bibliography

[1] D. Bradley, C. Sheppard, I. Suardjaja and R. Woolley, "Fundamentals of high-energy spark ignition with lasers", *Combustion and Flame*, no. 138, pp. 55-77, 11 May 2004.

[2] J. L. Beduneau, B. Kim, L. Zimmer and Y. Ikeda, "Measurements of minimum ignition energy in premixed laminar methane/air flow by using laser induced spark", *Combustion and Flame*, vol. 132, no. 4, pp. 653-665, 2003.

[3] L. M. Pickett, A. A. Hoops and J. M. Headrick, "Laser Ignition of multi-injection gasoline sprays", *SAE Technical Paper*, no. 2011-01-0659, pp. 1-26, 2011.

[4] T. X. Phuoc and F. P. White, "An Optical and Spectroscopic Study of Laser-Induced Sparks to Determine Avaible Ignition Energy", vol. 29, pp. 1621-1628, 2002.

[5] J. Ma, D. Alexander and D. Poulain, "Laser Spark Ignition and Combustion Characteristics of Methane-Air Mixtures", *Combustion and Flame*, no. 112, pp. 492-506, 1998.

[6] T. Phuoc and F. White, "Laser induced spark ignition of CH4/air mixtures", *Combustion and Flame*, no. 119, pp. 203-216, 1999.

[7] T.-W. Lee, V. Jain and S. Kozola, "Measurements of Minimum Ignition Energy By Using Laser Sparks for Hydrocarbon Fuels in Air : Propane, Dodecane, and Jet-A Fuel", *Combustion and Flame*, vol. 125, pp. 1320-1328, 2001.

[8] L. M. Pickett and M. P. Musculus, "Diagnostic considerations for optical laser-extinction measurements of soot in high-pressure transient combustion environments", *Combustion and Flame*, no. 141, p. 371–391, March 2005.

Chapter 5

Laser Induced Plasma Ignition: application to Diesel sprays

Contents

5.1 Introduction

This chapter is focused on the application of the Laser Induced Plasma ignition system to a direct injected Diesel spray. After the parametric study for the optimization and the evaluation of efficiency and reliability of the system in the plasma generation, reported in the previous chapter, its application to a real Diesel spray is described in the following sections.

With the twofold objective of both considering the viability and efficiency of the LIP system in a typical engine application and also studying the effect of the local condition at ignition on the subsequent development of the Diesel combustion, the system will be used to provoke ignition of a typical Diesel spray under different conditions.

At first, the experimental setup and the followed experimental methodology for the realization of this research will be detailed. Then, the first study on the effectiveness of the system on a general Diesel spray will be carried out, in order to ensure its ignition capability in a real scenario. Later, in order to define the characteristics of the reference case, results on the combustion and ignition of a Diesel spray under typical autoignition conditions are reported at the same engine conditions selected for the LIP system application. This will also ensure the determination of an adequate test matrix, where the selection of the location and timings for the plasma ignition will be first compared with the real in-chamber spray development before and after the autoignition reference event.

Moreover, the determination of the basics of autoignition Diesel combustion characteristics will later be fundamental for the analysis of the obtained provoked plasma ignition results upon combustion development. Furthermore, the reference spray under study has been modeled with a 1D spray model in order to obtain the local air/fuel ratio evolution at the spray axis in space and time, as the spray penetrates the combustion chamber before autoignition takes place. This information has been used to determine

under which local conditions the spray ignition will be later forced with the application of the designed ignition system. Finally, from the application of the LIP ignition system, a parametric study on the effect of local conditions at ignition on the combustion development is reported in the last paragraph of this chapter. In particular, the study is focused on the effects of local ignition conditions upon delay time, heat release, spray tip penetration and soot evolution in the flame.

5.2 Experimental set up and methodology

In this section the experimental setup applied to the reported measurements and the followed experimental procedure will be presented. As detailed in Chapter 4 of this document, the LIP system design has led to a final configuration that will be then applied to the ignition of direct injected diesel sprays under a wide variety of thermodynamic conditions. It will be considered that all details reported in Chapter 4 regarding the experimental setup, are still valid, and only the measurement tools needed to study the application of the ignition system to a real diesel spray will be here presented.

5.2.1 Spray and flame visualization set up

A single optical setup was used both for the plasma and spray combustion visualization by applying two different optical techniques, namely Schlieren visualization and Natural Luminosity imaging. A diagram of the arrangement is shown in Figure 5.1.

For Schlieren analysis a collimated light beam was used for illumination by focusing the light source (300 W Xe continuous lamp, Karl Storz Xenon Nova 300) with a liquid light guide through a pinhole of 0.15 mm, to form a light spot at the focal plane of a 150 mm diameter spherical mirror with a focal length of 610 mm. The mirror collimates the beam that then enters the combustion chamber reflected through another redirecting mirror.

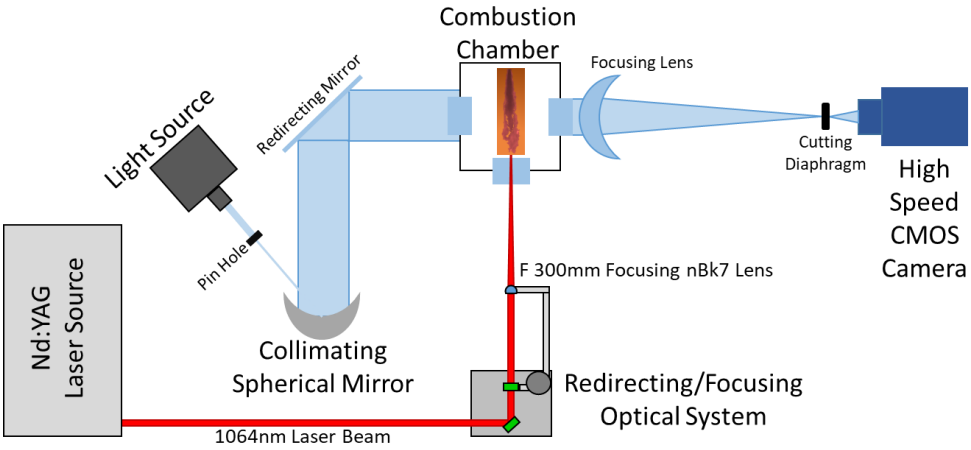

Figure 5.1. Schematic representation of the optical system obtained for Schlieren imaging acquisition, Natural Luminosity images acquisition and Laser Induced Plasma ignition.

On the other side of the combustion chamber, light was collected by a 150 mm diameter lens with a focal length of 450 mm, sufficient to guarantee a minimal light dispersion. A cutting diaphragm was positioned at the lens focal length to apply a spatial filtering to the focalized beam in the Fourier's plane. Both the light source and the cutoff diaphragm were only used in Schlieren visualization tests, the latter one being replaced by a neutral density filter when carrying out broadband radiation imaging. Images where taken with a high-speed CMOS camera (Phantom V12.0) equipped with a 100 mm *f*:2 camera lens (Zeiss Makro- Planar T*2) to collect all the light into the camera sensor, allowing a very sharp definition of the focusing zone.

The aim of this technique is to register images of spray combustion, particularly focusing on the determination of the spray penetration in the combustion chamber. Spray auto-ignition and provoked ignition cases were both registered with the high-speed CMOS camera synchronized with the injection signal while the combustion chamber was continuously illuminated with the collimated beam.

The same setup was used to register the high intensity broadband radiation produced by the incandescence of the soot particles in the flame, with the objective of complementing the visualization of the spray combustion already realized with the Schlieren method comparing the auto-ignition with the laser plasma provoked ignition. The natural luminosity images were registered by maintaining the optical parameters of the setup (in this case, the light source was kept off) and slightly modifying the camera acquisition parameters, where the shutter time was increased in 2 µs thanks to the application of a neutral density filter to limit the soot emission collection. The camera acquisition parameters for the combustion visualization applied techniques are listed in Table 5.1.

Phantom V12.0 CMOS Camera Acquisition set-up	
Image resolution	384 x 800 pix
Pixel/mm ratio	10.28 pix/mm
Acquisition Framerate	16000 fps
Image-Image Interval	62.5 µs
Exposure time (Schlieren Imaging)	6 µs
Exposure time (Natural Luminosity)	8 µs

Table 5.1. High-speed CMOS camera settings used for the images acquisition for the two different imaging techniques applied, Schlieren and Natural Luminosity.

5.2.2 Pressure signal processing

The evolution of the thermodynamic conditions during compression have been calculated following the standard procedure described in [1], from the cylinder pressure using a first-law thermodynamic analysis considering blow-by, heat transfer and mechanical deformations. The instantaneous in-cylinder pressure evolution registered during the combustion tests was principally used for the quantification of the spray ignition delay, in order to

determine if the laser plasma ignition system was effectively provoking an earlier ignition of the Diesel spray before the natural auto-ignition event takes place.

An AVL GU13P pressure transducer coupled to a Kistler 5011 charge amplifier was used to measure the cylinder pressure with a sampling frequency of 100 kHz. Every registered pressure acquisition event consists of a pair of engine cycles, the first one under motored, the second one under firing conditions. The direct comparison of the two consecutive pressure curves, permits the detection of the ignition event when the in-cylinder pressure evolution starts to raise over the engine motored compression pressure curve, as can be seen in Figure 5.2.

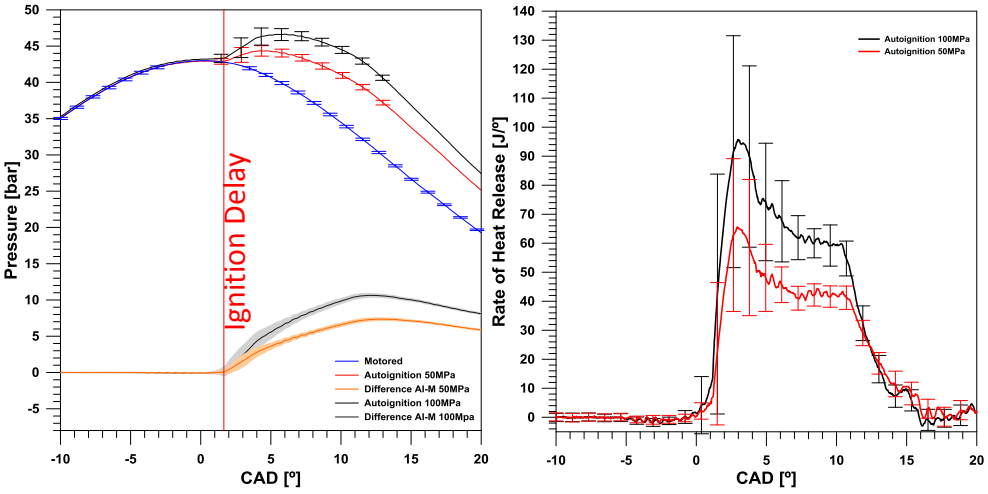

Figure 5.2. Evolution of In-cylinder pressure (left) and Rate of Heat Release (right) for the autoignition reference combustion event at the two injection pressures. The curves showed here are an average of 50 different cycles. The standard deviation is reported as vertical error bars along the average curves. The difference between firing and motored cycles is also reported at the bottom, as a clear indicator of the start of combustion (SOC).

The ignition delay is defined as the time elapsed from the start of injection (SoI) until a steep rise of the pressure in the chamber is detected

two times greater than the standard deviation of the pressure difference, and could be visualized on the pressure curves. As an example, this figure shows the evolution of pressure in the combustion chamber in comparison with a motored pressure curve (i.e. without fuel injection), and the rate of heat release evolution, calculated with a combustion diagnostic code, for the same reference combustion event.

5.2.3 Diesel Autoignition: Laser induced plasma ignition conditions definition

The Schlieren visualization technique has been proven by a great number of authors [2] [3] as a fair tool to track the spray tip penetration of a direct injected fuel spray (Diesel in this particular case). A fair tool to track penetration not only under inert conditions, but also in reacting sprays before ignition or when the flame has progressed. However, whenever the spray density becomes the same as the bulk gas inside the combustion chamber, which may occur just before, during or just after fuel ignition, the detection of the actual spray boundaries is not always easy, if even possible [2]. To overcome such a difficulty, every repetition of every tested case was registered with the high-speed CMOS camera using both the Schlieren method and the Natural Flame Luminosity emission, obtaining both spray and sooting flame visualization. An example of the obtained visualization images and sprays evolution are here reported in Figure 5.3 for the Schlieren imaging and in Figure 5.4 for the soot radiation.

Both applied techniques were focused on the analysis of the spray evolution under reactive conditions, with the aim to see how plasma induced ignition affected spray and flame development. Although the settings of the Schlieren can be chosen in such a way that flame luminosity is suppressed and automatic detection of the spray's boundaries could be made confidently [2], in this work Schlieren systems settings were chosen just to avoid blooming effects on the camera and making the sooting flame clearly visible. Actually, it was found being such settings more convenient as it enhances the effects

of the plasma induced ignition. However, this configuration decreased the accuracy of the segmentation procedures and wrong boundaries' flame detection quite often occurred, as could be seen in the last frames reported in Figure 5.3. In order to bypass this processing problem, a different procedure was instead applied.

The information obtained from the two imaging methods were combined together, permitting to be still able to obtain a penetration curve for the entire visible range by not only relying on Schlieren imaging and discard those Schlieren images where flame boundaries were not properly detected. In this sense, as the failure in the contour detection only appears, for the Schlieren images, under strong soot emission, only in that cases half of the penetration curve was obtained from the Schlieren processing until the soot appearance, and the last half from the NL processing method. As NL was detecting only the soot emission and it was registered simultaneously, it has been obtained a perfect match in the penetration curves.

Thus, in Figure 5.5 the penetration curve is reported for the spray under conventional combustion (with autoignition) for both injection pressures, combining experimental information from different sources: first, spray penetration from the Schlieren technique is drawn; then flame penetration is plotted with a solid line, representing the average value as obtained either from Schlieren measurements (when it is possible) and/or natural luminosity imaging (i.e. broadband emission imaging). The shadowed area width corresponds to ± the measured standard deviation. In addition, spray penetration of the liquid and vapor phases as obtained respectively from Mie scattering and Schlieren imaging of the spray injected into an inert ambient, at the same thermodynamics and injection conditions, are plotted for the first 1500 us ASOE.

First of all, for the sake of the subsequent analysis regarding the plasma ignition event, it is important to underline how in a normal autoignition event the soot signal, registered with the natural luminosity technique, is considered to be a good indicator for the in-chamber spray penetration, since

are the local conditions at the spray tip that allows the ignition and successive combustion of the mixture.

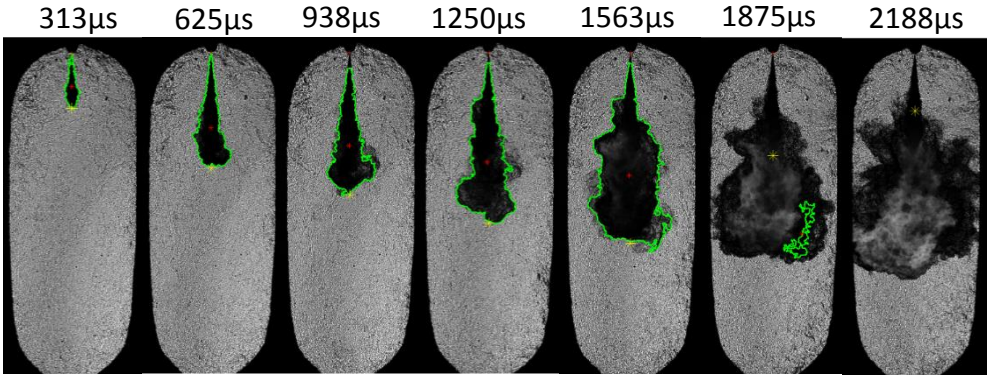

Figure 5.3. Example of images of spray vapor phase evolution inside the combustion chamber as derived from the application of the Schlieren technique. Spray contours as obtained by the image processing code are overlaid on the images in order to show the difficulties in the contour detection algorithm after ignition, when appears the emission of the soot cloud. The red and yellow dots also come from the processing code and indicates the center of mass of the detected contour area (red) and the spray penetration as detected by a secondary processing method (yellow). The reported images are taken from a 5.3 MPa, 765 K at TDC case, with Diesel injected at 50 MPa and ignited with LIP located at 11 mm from the nozzle at 0.8 ms. All the reported times are defined ASOE.

So, if the flame kernel is formed at the spray tip, the broadband emission signal recorded can be directly linked to the spray tip position and used to measure the spray penetration, usually as a substitute of the Schlieren imaging after ignition takes place. This permits to avoid saturation effects and post-processing problems that could arise from the application of only Schlieren visualization in presence of the broadband emission of the flame. In this sense, later in this section, it will be shown how forcing the ignition with plasma could instead cause a positional shift between the registered soot signal and the real tip of the spray, since the generation of the flame kernel

could still not occur at the spray tip. This has led to the impossibility to match the Schlieren and Natural Luminosity penetration curves for certain provoked ignition conditions, as it will be later detailed.

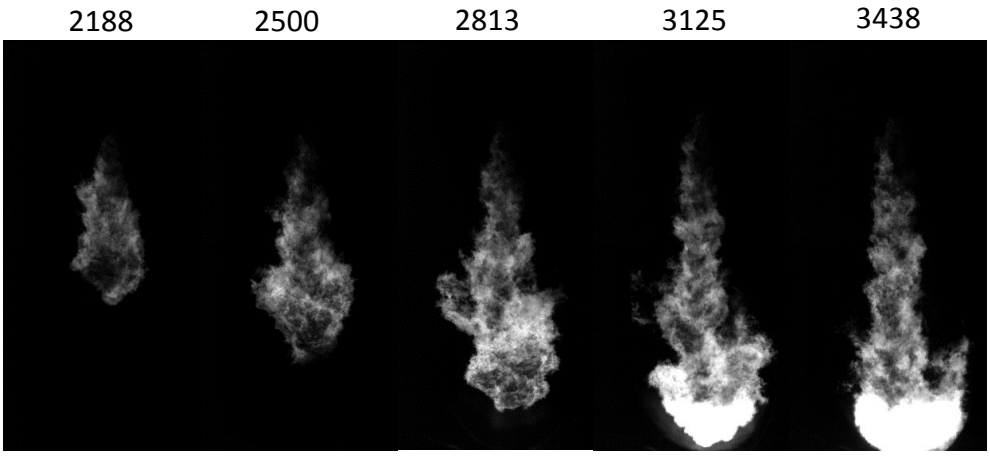

Figure 5.4. Example of spray evolution inside the combustion chamber as derived from the application of Natural Luminosity technique once the soot emission appears. The reported image sequence is taken from the 5.3 MPa, 765K at TDC case, with Diesel injected at 50 MPa and ignited with laser induced plasma at 11mm from the nozzle and 0.8 ms. All the reported times are defined After Start of Energizing (ASOE).

A second point to state before any further discussion: by comparing the penetration curves obtained for the autoignition condition in inert and reactive cases under tests, it cannot be clearly seen the expected spray acceleration in the reacting versus the inert spray as reported in [4]. This is probably due to the peculiarities of the in-chamber air flow movement of the used test rig, causing an appreciable slowdown of the spray [3]. This feature of the experimental facility, which was described in Chapter 3, has been taken into account when the positions and timings of the laser plasma ignition where defined, so that the start of ignition was always forced in a location where the air flow intensity magnitude scale was not so high as to mainly disturb the spray/flame structure.

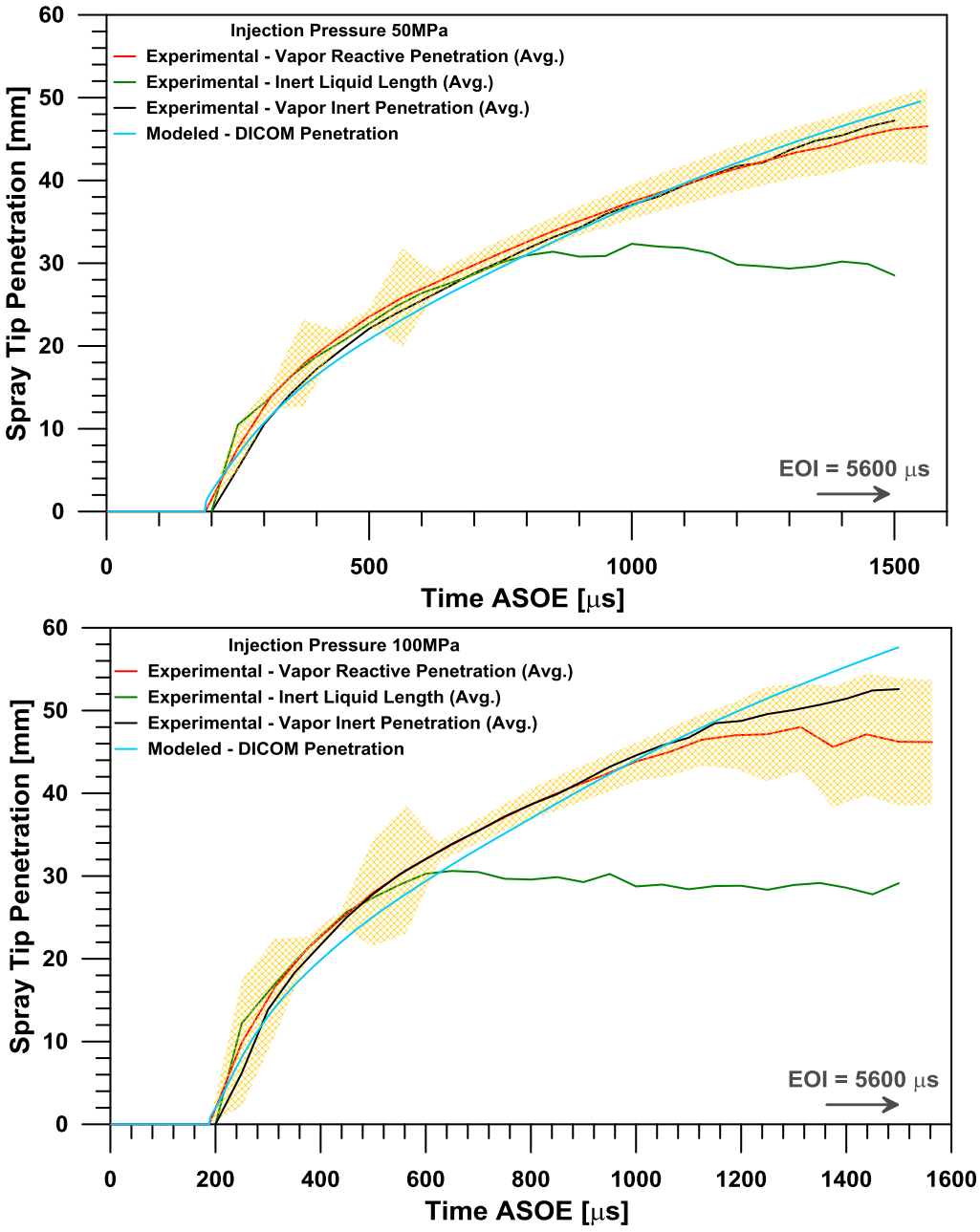

Figure 5.5 Modeled/Experimental Spray Penetration curves comparison for the DICOM model spray evolution validation.

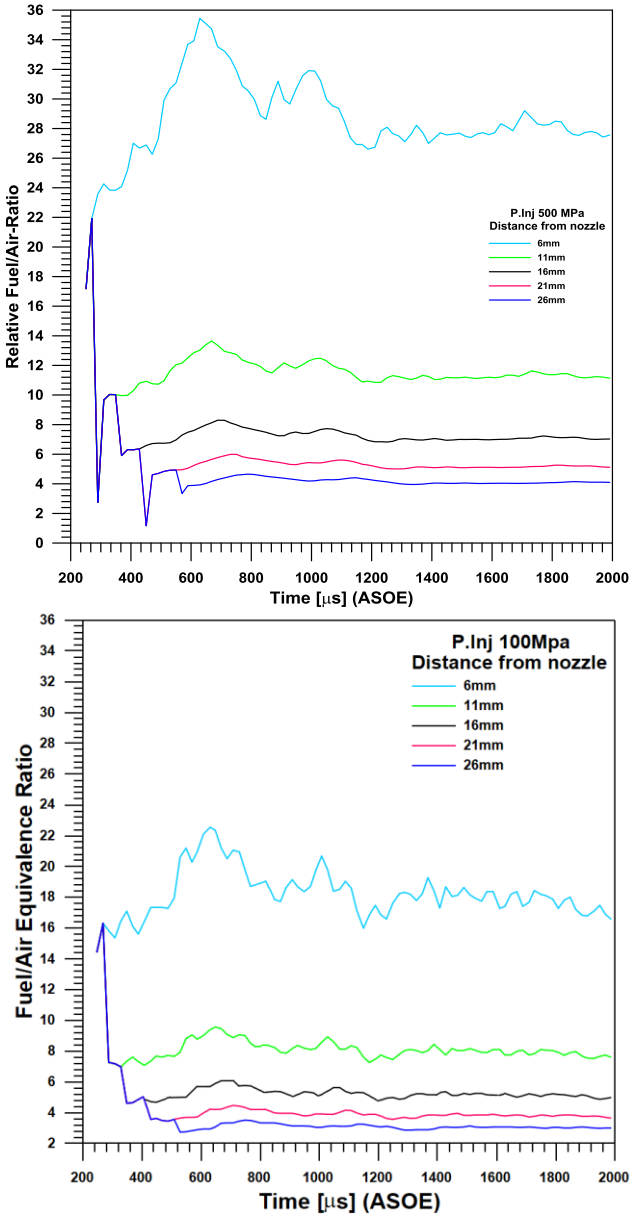

Figure 5.6 Local Fuel/Air Equivalence Ratio evolution, as obtained from the DICOM 1D spray model, for the two tested injection pressures (50 MPa upper and 100 MPa lower) at 5,3 MPa and 700 K conditions at TDC.

Then, in order to get a better idea about the local conditions at the locations where plasma should be created and to facilitate further analysis, the spray evolution was simulated with a 1-D spray model [5] [6] . The applied model uses injection rate and spray cone angle as inputs to solve the mass and momentum conservation equations. The penetration curve obtained from this simulation is also plotted in Figure 5.5, and the local relative equivalence ratio at the spray centerline is reported then in Figure 5.6.

5.2.4 Baseline case definition

On the basis of the results of the parametric study for the optimization and reliability determination of the ignition system detailed in Chapter 4, the case of 53 bar and 700 K was selected as the best engine conditions combination for the realization of ignition tests on a direct injection Diesel spray.

Then, before the application of the ignition system to the spray, a series of auto-ignition tests were performed to determine the reference conditions in terms of auto-ignition delay, auto-ignition position and heat release. For these reference tests, 200 different auto-ignition repetitions were registered for each optical setup (Schlieren and Natural Luminosity), with a total amount of 400 valid repetitions for the ignition delay determination obtained from the pressure curves analysis.

Once the reference for the Diesel auto-ignition characteristics at the selected engine conditions were determined, a set of 200 tests for the provoked ignition with laser induced plasma were carried out. The laser was synchronized to be fired 0.8 ms ASOE. Taking in account that the first registered auto ignition event does not occur until 2.2 ms ASOE, the selected plasma induction timing was early enough with respect the auto-ignition event to permit a clear distinction between the two combustions, but not too early to have a local condition in the induction point of a too high air/fuel ratio which would have made impossible the success of the ignition.

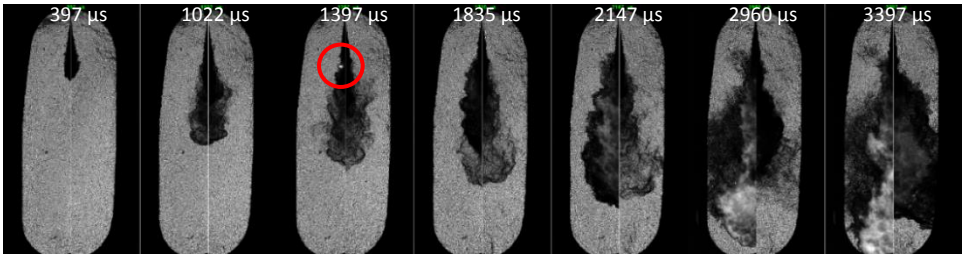

Figure 5.7. Combustion comparison evolution between a provoked ignition attempts with a laser plasma system (left) and a natural auto-ignition event of Diesel spray (right). In the third picture, registered at 1397 µs ASOE, the plasma spark is visible in the spray (evidenced with a red circle).

As a preliminary attempt of applying such ignition system to a direct-injected Diesel spray, it can be concluded from the tests that the laser plasma ignition system works in a reliable form, being able to ignite the fuel spray with a success rate of 100%. As an example, two different combustion cycles recorded with the Schlieren visualization method, with and without plasma ignition are shown in Figure 5.7.

A plasma spark in the spray is appreciable in the third picture of Figure 5.7, taken at 1397 µs ASOE. In the fourth picture, registered at 1835 µs ASOE, the combustion process for the provoked ignition test has already started (the spray angle is increased) but not for the auto-ignition case, which happens only at 2960 µs ASOE. Figure 5.8 compares the ignition timing for the auto-ignition and laser plasma provoked ignition for the investigated conditions on a cycle-to-cycle basis, which confirms the previously commented ignition success rate.

Besides the reported evidence of the system capability to provoke ignition, a stabilization of the ignition delay for the laser ignition can also be clearly noted. In fact, it is appreciable in Figure 5.8 how the ignition delay in the provoked laser plasma ignition case is nearly constant, if compared with the auto-ignition reference, which points out that it is dominated by the plasma induction timing.

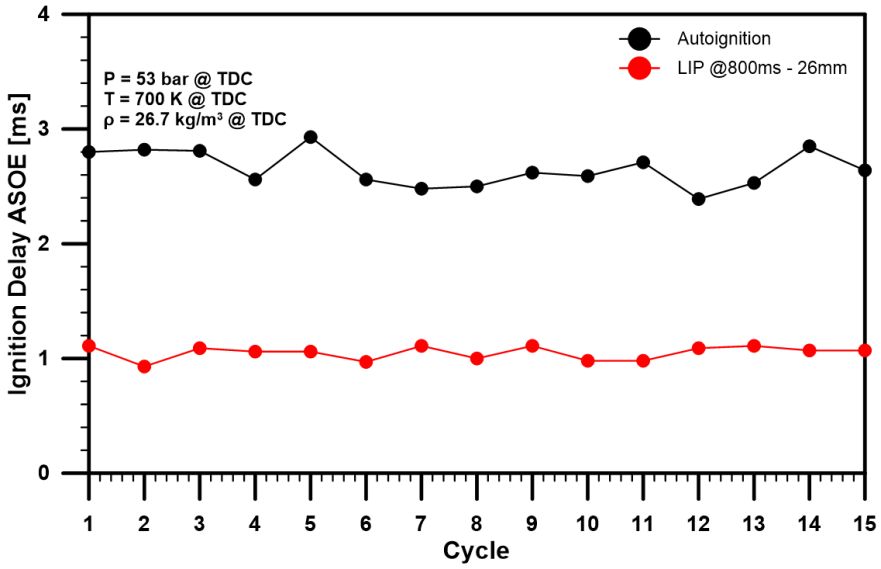

Figure 5.8. Ignition Delay comparison between provoked ignition and auto-ignition of a Diesel direct injection spray. The Ignition Delay obtained from the in-chamber pressure signal is showed cycle by cycle for the autoignition event and the provoked LIP ignition event, generated at 800 μs ASOE and at 26 mm from the injector nozzle position.

Moreover, considering the images reported in Figure 5.9, the effect of the spatial position of the induced plasma on the combustion development is another factor that could be evaluated and compared with the auto-ignition event. From the images, for the autoignition case, the light emission of the soot cloud is observed to be located at the fuel spray tip, where the conditions are feasible to start the ignition of the mixture and therefore the soot formation. Considering the case of the provoked laser plasma ignition, the laser position for these tests was fixed at 16 mm from the spray nozzle. Such a location was chosen taking into consideration that the spray should have already reached it at the laser timing, but the local air/fuel ratio conditions should not be critical for the ignition. Compared to the natural autoignition case, where soot cloud is first generated at the spray tip, in the laser-ignited case the reaction zone, where soot radiation is present, occurs at first around

the plasma induction location and not at the spray tip, where the spray can still be seen to progress.

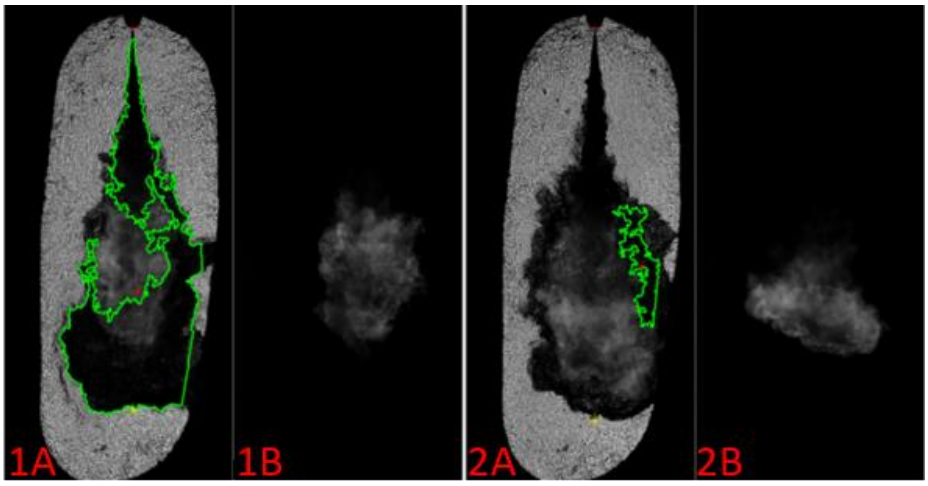

Figure 5.9. Comparison between the soot cloud position in a laser plasma provoked ignition (1A) and auto-ignition (2A). Pictures (a) of both images are obtained by the Schlieren method for combustion visualization while (b) pictures are obtained by the Natural Luminosity visualization technique. With both methods it is possible to visualize the soot radiation in the spray and so infer the position where the combustion has started.

5.2.5 Test matrix definition

All the measurements presented in this chapter have been performed at a fixed engine condition, with standard dry air (21% O_2), inside the range of operation of current automotive DI Diesel engines. Thermodynamic conditions of the intake air where selected in order to achieve, under motored conditions, in-cylinder peak pressure of 5.3 MPa and peak temperature of 700 K, which leads to an average density value of 21.7 kg/m3 during the injection process.

A single injection was performed per cycle, with an energizing time of 5600 µs and a Start of Energizing (SOE) of 6.5 CAD BTDC. Two values of injection pressure, 50 and 100 MPa, were tested, and 75 injection cycles were recorded in every condition. It must be underlined that in both cases injection duration is long if compared with more typical real engine application values. However, it was selected on purpose, in order to ensure a nearly steady spray condition, so that the effect of induced ignition upon spray combustion evolution was not masked by effects inherent to transient spray development.

The selection of two different values of injection pressure is only motivated by the need to enlarge the range of local conditions achievable to generate a laser plasma which could provoke fuel ignition. From what reported in Figure 5.2 it could be seen how, for the autoignition cases, combustion at the two different injection pressures starts almost at the same time, but due to the different amount of fuel present in the chamber, the subsequent development, although similar, is shifted to higher pressure and heat release rates for the highest injection pressure.

Regarding the determination of a reference values for the autoignition delay at the reference cases, it has shown no sensitive effect to the injection pressure, as expected. The measured differences have been far smaller than the experimental uncertainty, indicating though a low cycle to cycle repeatability. Thus, for tests done at 50 MPa injection pressure, an average auto-ignition delay time of 2613 µs was measured with a standard deviation of 200 µs. In the case of 100 MPa injection pressure, the average registered ignition delay time was 2540 µs with a standard deviation of 260 µs. It will be later shown in this same chapter how the plasma induction has an important stabilization effect on the ignition delay time when compared to the registered cycle to cycle variation typical of the autoignition conditions under analysis.

For these reference conditions, here later referred as baseline autoignition cases, several Laser Induced Plasma test cases have been considered. Plasma has been generated, maintaining the same optical

arrangement and laser settings in all the cases, at 10 different timings (between 0.4 and 1.6 ms ASOE) for a fixed distance from the nozzle (16 mm) to analyze the effect of plasma generation timing.

Whereas, in order to study the effect of laser plasma generation location in the spray, 4 different plasma positions (within 6 to 21 mm from the nozzle) at the same fixed timing (0.8 ms ASOE) have been measured.

These values, here reported in Table 5.2 and visually marked in Figure 5.10 and Figure 5.11 to facilitate the later result's discussion, were selected after a preliminary study (not detailed here for brevity), in order to sweep a fair range of fuel/air ratios at the ignition location. For every laser plasma position and timing where registered a total of 30 different cycles, applying both Schlieren visualization and flame soot broadband imaging techniques.

		LIP Generation Delay Time (ASOE) [ms]									
		0.4	0.5	0.6	0.7	0.8	0.9	1	1.2	1.4	1.6
Distance from Injector Nozzle [mm]	6					X					
	11					X					
	16	X	X	X	X	X	X	X	X	X	X
	21					X					
	26					X					

Table 5.2. Laser Induced Plasma generation timings and positions selected for the reported study.

In both figures, the symbols labeled as "LIP positions" are plotted to a visual indication of the timings and local positions along the spray axis where the plasma ignition was attempted. It must be noted that all the attempted ignition locations are located at distances to the nozzle below the spray liquid length, i.e. ignition is provoked in a region where fuel has not completely vaporized at the moment of the plasma induction.

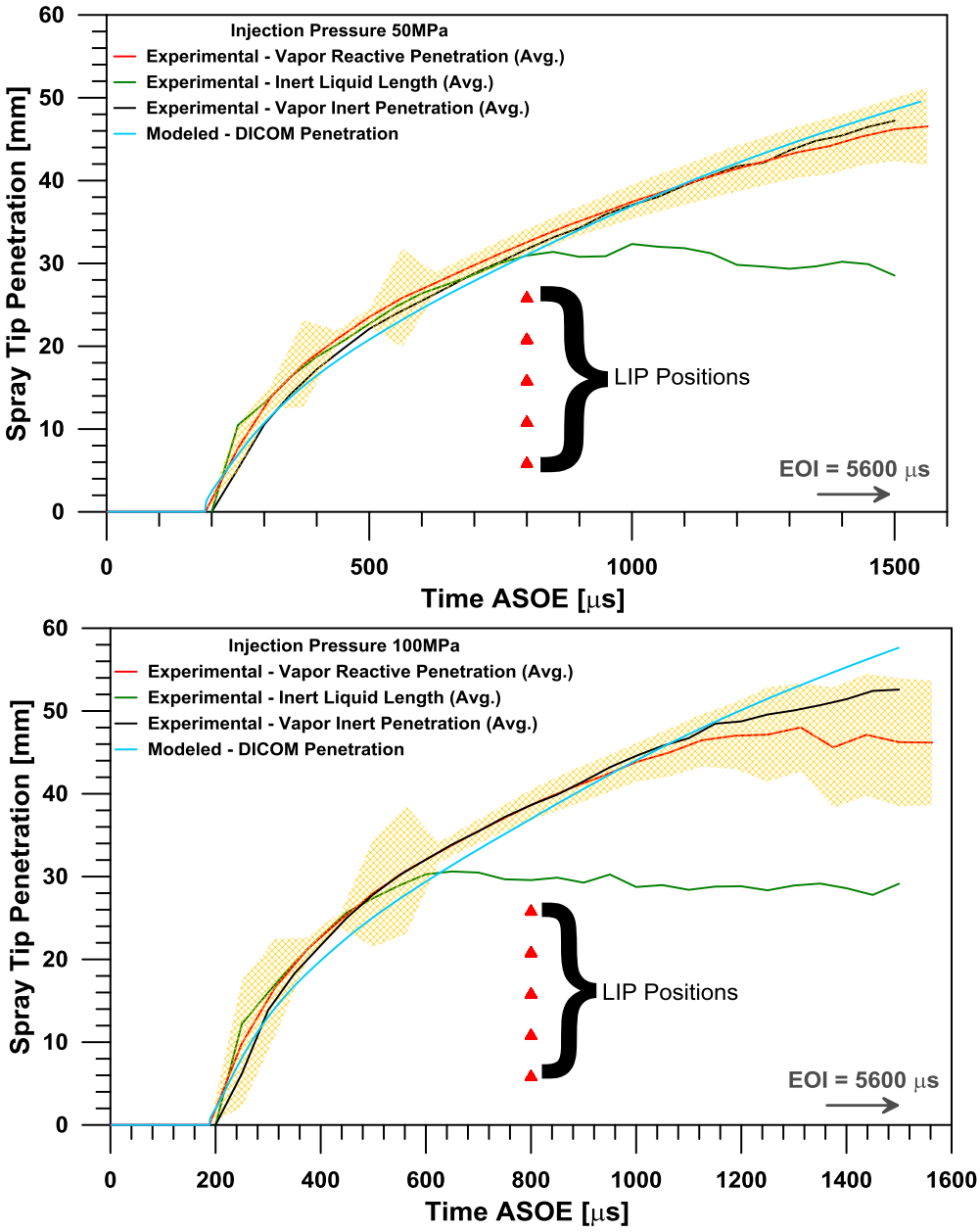

Figure 5.10 Modeled/Experimental Spray Penetration curves comparison from the DICOM model. On the graphs are indicated the attempted ignition positions at the fixed time of 800 μs ASOE.

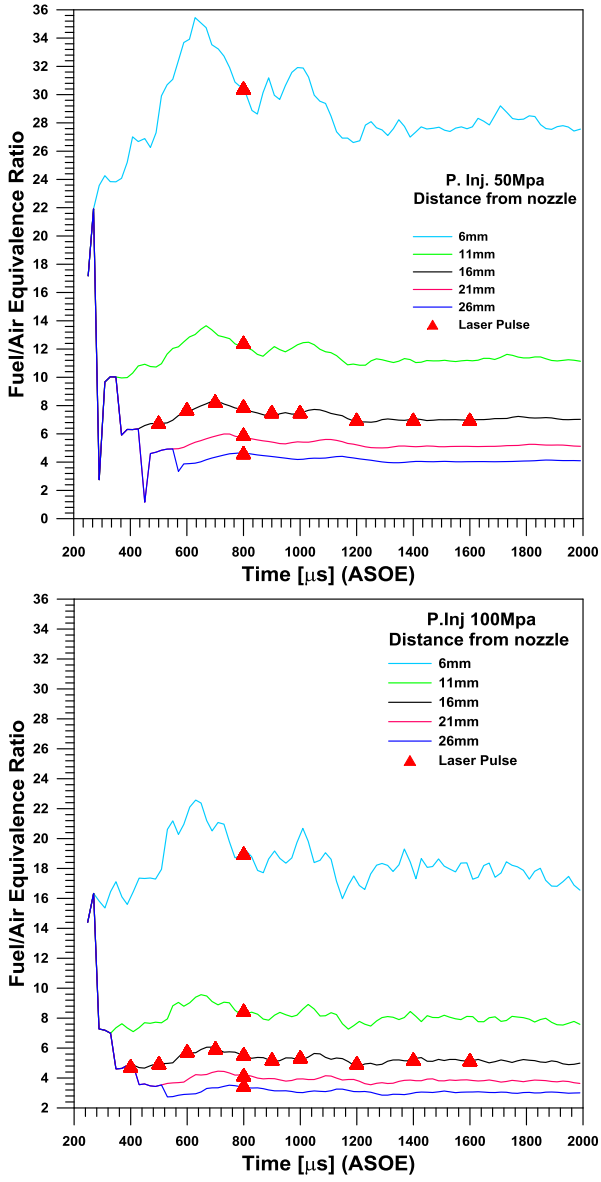

Figure 5.11 Local Fuel/Air Equivalence Ratio evolution, as obtained from the DICOM 1D spray model, for the two tested injection pressures (50 MPa upper and 100 MPa lower) at 5,3 MPa and 700 K engine condition at TDC. On the graphs are indicated all the attempted LIP ignition positions and timings.

Figure 5.11 shows the estimated equivalence ratio at the ignition locations as derived from the 1D spray model. Results indicate that all the attempted ignition tests were made in rich mixture conditions.

Despite eventual considerations regarding the precision of the quantitative values obtained from the 1-D spray modeling and the fact that equivalence ratio absolute values could be biased, it becomes clear that in all cases were ignition was attempted, the fuel mixture was very rich: relative fuel/air ratio between 28 and 2 where obtained for the 50 MPa injection pressure case, and between 18 and 2 for the 100 MPa pressure.

It should be also underlined that the highest local fuel/air ratio variation happens between the two closest points to the nozzle (6 mm and 11 mm), independently from the applied injection pressure.

It is also remarkable the fact that the time evolution of the local equivalence ratio indicates, from the simulation, a nearly constant value for all the attempted ignition at the different induction times tested at 16mm from the injector nozzle. This could be caused by the evolution of the spray under quasi-steady conditions. All these considerations about the local conditions at the plasma generation location will be later discussed in more detail for the laser ignition cases.

5.3 Laser induced plasma ignition effects, a parametric study

In the following chapters, first, the effectiveness of the ignition system for the ignition of a DI Diesel Spray will be proven; then, the effects of the variation of the local ignition conditions on the combustion development will be analyzed in detail. In particular, the analysis will be focused on:

- The ignition delay time variation with position and timing of the plasma induction.

- The heat release variation of the obtained combustion with position and timing of the ignition event.

- The spray penetration variation for each provoked combustion event.

- The soot emission evolution of the combustion flame obtained from the different local condition at the ignition location.

5.3.1 Laser induced plasma ignition efficiency and overall success rate

It is highly significant how, at the selected experimental conditions, the ignition of the Diesel spray was successfully achieved in all different local points and delay times with the only exception of the injector nozzle's nearest position, namely at 6 mm from the nozzle. This results are here summarized in Table 5.3 for the plasma position variation tests and in Table 5.4 for the plasma laser pulse timing variation tests.

LIP Position (from nozzle) [mm]	Injection pressure 50 MPa	Injection pressure 100 MPa
	Ignition Success Rate	Ignition Success Rate
6	0%	0%
11	47%	77%
16	100%	93%
21	96%	100%
26	100%	100%

Table 5.3. Summary of the success rates for the LIP ignition tests realized varying the plasma induction position at a fixed laser pulse timing of 800μs ASOE.

All the tests performed with plasma at 6 mm from the nozzle have not ignited the spray even with the maximum available laser pulse energy of

almost 800 mJ, i.e. roughly 3 times higher than the power employed for all the other cases under test. This clearly indicates an upper limit for the local equivalence ratio of the mixture that allows a successful ignition with such ignition system.

With respect of this success rate analysis, especially for which concerns the high energy used for the ignition, it must be remarked that all the provoked ignitions were attempted at distances from the nozzle shorter that the liquid length of the spray. This means that, to reach the ignition condition of the mixture, the energy provided at the local spray location was used to generate free radicals starting from a practically liquid spray or a very rich mixture. The generation of a sufficient amount of radicals seems to be the key for the success of a forced ignition event.

LIP Delay (ASOE) [µs]	Injection pressure 50 MPa	Injection pressure 100 MPa
	Ignition Success Rate	Ignition Success Rate
400	None	97%
500	90%	100%
600	97%	96%
700	93%	100%
800	100%	93%
900	97%	97%
1000	100%	97%
1200	97%	97%
1400	97%	100%
1600	97%	100%

Table 5.4 Summary of the obtained success rates for the LIP ignition tests realized varying the plasma induction timing at a fixed position of 16mm from the injector nozzle.

5.3.2 Ignition delay time

The results obtained from the registered pressure curves shows clearly how the fuel spray ignition delay, as defined above, varies with the position and the timing of the laser plasma induction. The "Ignition-Laser pulse timing" is defined as the time from the effective laser shot occurrence until the actual mixture ignition point.

The results for this kind of analysis are here reported in Figure 5.12, where the laser pulse timing, autoignition and provoked ignition delays are represented as average values, each with it correspondent standard deviations. Considering the plasma induction location variation along the spray axis, it can be clearly appreciated how the ignition delay of the mixture gets larger and the results scattering increases as the plasma induction location approaches the injector nozzle.

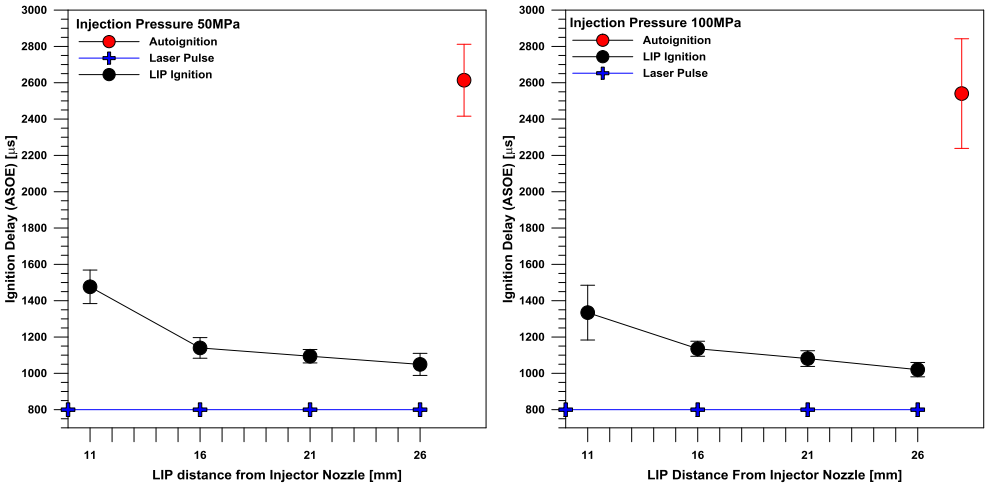

Figure 5.12. LIP position effect on combustion ignition delay. The average ignition delay of the autoignition case is also reported for comparison.

The graphs of Figure 5.12 show the evidence of how plasma ignition stabilizes ignition delay, as already reported before, limiting the dispersion around the average value of each case if compared with the autoignition

results, where the range of possible ignition delay times is highly wider. The only exception, comparing only the standard deviations, seems to be represented by the 11mm induction position case at 100 MPa injection pressure, where the spray seems to have a transitional or boundary ignitable condition. Generating plasma at 11mm from the nozzle and 0.8 ms of delay with respect the start of energizing seems to have practically the same average 70% probability of success (for the 100 MPa injection pressure) along a time range of more than 500 µs. For this reason, this is also the test that has the greater data dispersion compared with all the other cases, as appreciable from Figure 5.12.

Concerning the results obtained from the plasma laser pulse timing variation study, it has been found a constant linear increase of the ignition delay with the laser pulse timing, as appreciable from Figure 5.13. These results seem to be logical due to the similarity of the local conditions for the different cases as obtained from the 1-dimensional model already introduced before (see Figure 5.11).

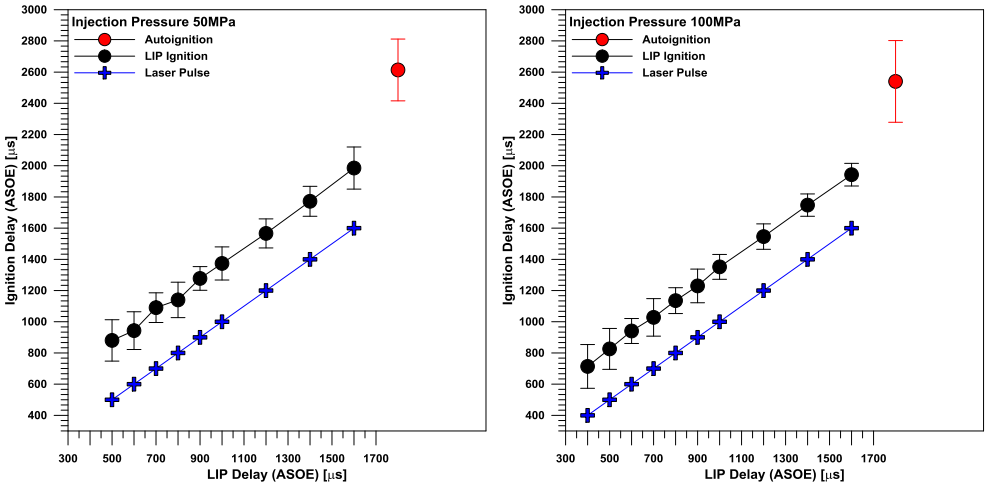

Figure 5.13. LIP Timing effect on combustion ignition delay. The average ignition delay of the autoignition case is also reported for comparison.

Standard deviation bars, reported in Figure 5.13 for the laser pulse timing variation, still clearly indicate the stabilization effect of the laser plasma induction on the ignition delay if compared with the autoignition case, as it happens for every tested ignition position.

From the analysis of all the combustion indicator parameters, it seems that the ignition delay should be considered as the main tracer for the effects of induced ignition upon fuel combustion. It also seems that the ignition delay should be linked to the local flow conditions at the ignition location and timing. However, there are other parameters which should allow understanding and quantifying the effect of local conditions at the provoked ignition location upon fuel combustion and subsequent engine performance. These are considered in the following sections.

5.3.3 Heat release rate

A fundamental parameter for the combustion diagnostic is commonly represented by the Rate of Heat Release (RoHR) curves, which have been calculated, in this case as Apparent RoHR, for each tested ignition case. This parameter will also be used as an indicator of the effects of the local condition at ignition. It must first be underlined that the shape of the curves would be quite different to those typical of Diesel engines for automotive applications, since both injection duration and combustion chamber volume are here quite different too. However, comparison of these curves between the conventional case with autoignition and those of plasma induced ignition should help to identify and illustrate the effects under study.

In terms of plasma induction location variation, it could be seen in Figure 5.14 that, as the plasma induction region approaches the injector nozzle, the energy release gets lower. The same effect could be appreciated for the laser pulse timing variation: as the laser pulse timing time gets shorter, combustion starts earlier and the total heat released in the chamber gets higher even if the theoretical local mixture equivalence ratio is constant, as obtained from the 1-D spray model.

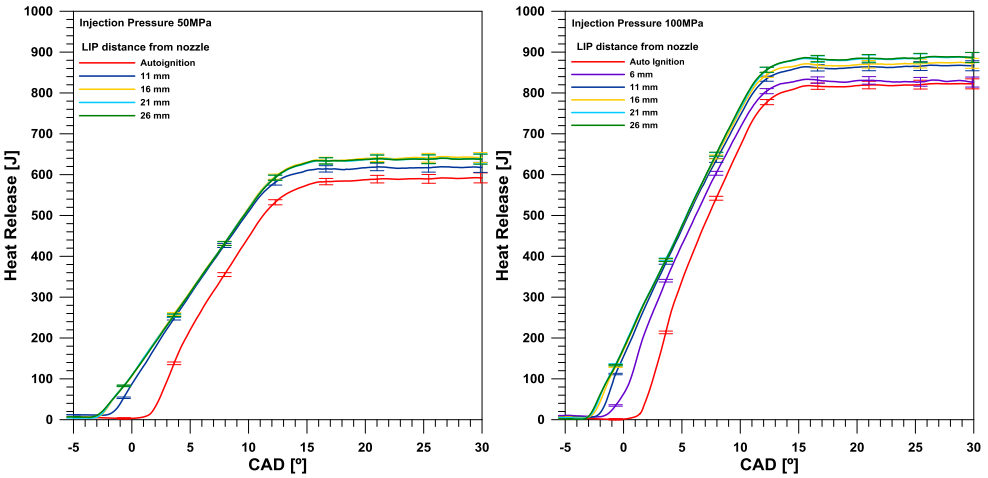

Figure 5.14. Apparent total Heat Release curves for the two injection pressure as obtained for the variation of the induced plasma position. AHR curve for the autoignition case is also reported as reference.

Again, from the ARoHR curves reported for the plasma position variation in Figure 5.15, it could be seen how, as the induction position moves farther from the nozzle, the resulting combustion varies progressively from a typical premixed combustion, similar to the one of the autoignition case, to a more homogeneous diffusive combustion, with a first rapid mixing-controlled phase and a subsequent steady phase that lasts till the end of injection.

The same behavior could be appreciated in Figure 5.16 for the plasma induction time variation tests, where the premixed peak progressively disappears as the laser pulse timing time gets shorter. In both cases the disappearance of the premixed peak in the ARoHR curves is paired with a higher total heat release for the combustion, as could be appreciated from the Heat Release curves depicted in Figure 5.14. All the tests were realized with the same injection parameters in terms of fuel quantity (energizing time) and timing (SoE). In a more detailed analysis it can be appreciated that, for the low injection pressure test at the furthest induction position from the nozzle (26 mm), and for the high injection pressure at the shortest laser pulse

timing time (0.4ms), the ARoHR curves do not present any premixed-combustion peak at all. Those are the only conditions of the whole test matrix that presents a pure diffusive combustion development, reflected in the highest heat release obtained for both injection pressures.

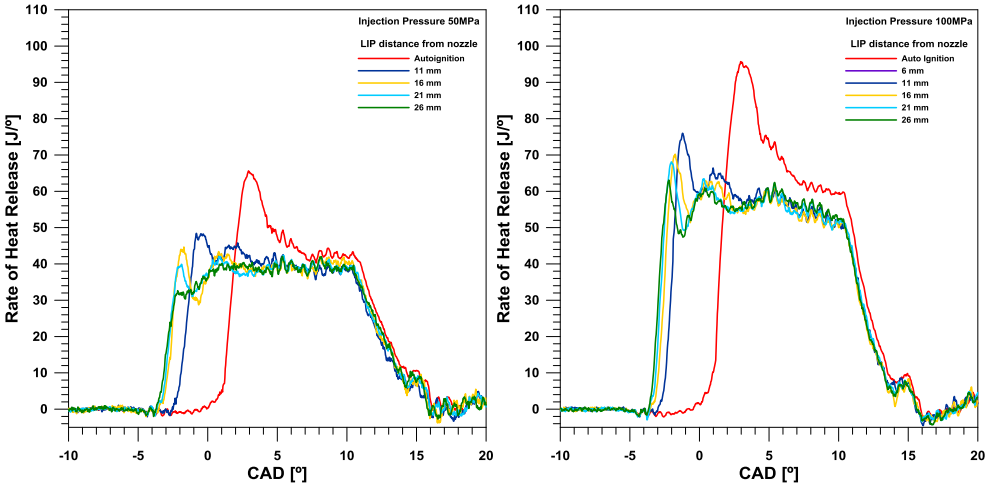

Figure 5.15. Apparent Rate of Heat Release curves for the two injection pressure as obtained for the variation of the induced plasma position. ARoHR curve for the autoignition case is also reported as reference.

This could be considered an indicator of how the relative ignition delays of 1049 µs, for the 26 mm/0.8 ms plasma induction at 50 MPa of injection, and 713 µs, for the 16 mm/0.4 ms induction at 100 MPa of injection, are not allowing a sufficient mixture formation before the start of combustion. Even so, for the 50 MPa injection pressure case, from the analysis of all the obtained ignition delay values, this ignition condition does not correspond to the lowest ignition or ignition-laser pulse timing achieved, but it is the only case where the premixed peak cannot be found. As an example, an earlier ignition attempt at 0.5 ms of delay ASOE at 16 mm from the nozzle, which involves a shorter laser pulse timing of 880 µs, still presents a small premixed combustion peak whereas the before commented case does not. The reason for the observed difference should be probably ascribed to the relative position of the plasma with respect the spray tip and the current local

equivalence ratio of the mixture. As could be seen from the already reported Figure 5.10 and Figure 5.11, the induction position at 0.5 ms and 16 mm from the nozzle is located in the tip zone of the spray and the local equivalence ratio should be higher than the one at 0.8 ms and 26 mm from the nozzle.

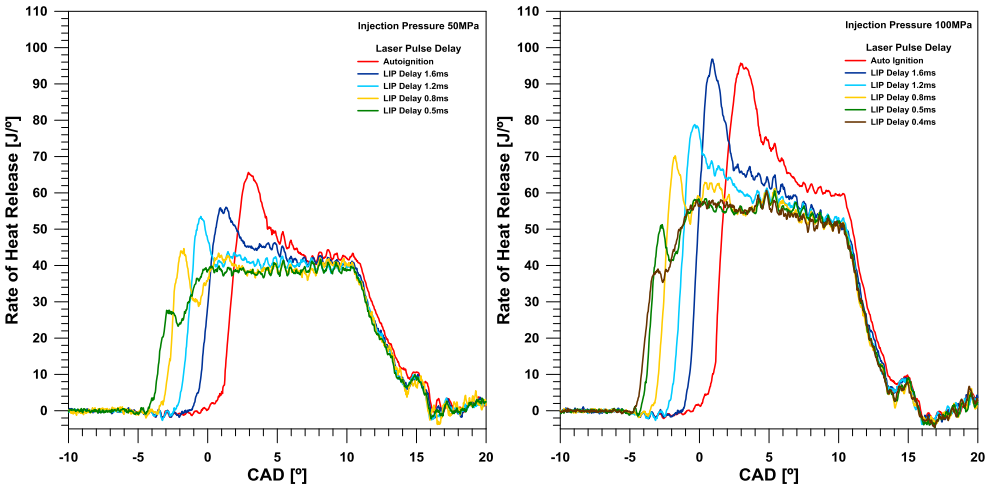

Figure 5.16. Apparent Rate of Heat Release curves for the two injection pressure as obtained for the variation of the induced plasma timing from the start of energizing. RoHR curve for the autoignition case is also reported as reference.

Moreover, for a complete analysis, also the effect of the local temperature variation must be considered. In a closer position to the injector nozzle the local temperature should be lower, which implies that some part of the deposed plasma energy should be there used to raise the temperature to reach the fuel vaporization level. This is acting as a local energy sink, in the end lowering the total energy available for the radical generation in that local zone. On the other hand, this temperature effect should be negligible if compared to the very large variation in terms of local equivalence ratio predicted from the 1D model. For this reason, it should be still considered that the same amount of energy is used in this case for generating radicals, but for a richer mixture and at a position closer to the nozzle.

With all these considerations it can be explained why such delay in the start of combustion has been observed. As the ignition occurs only when a critical amount of radicals has been achieved, the richer mixture condition paired with a higher energy request, caused by the lower local temperature, leads to a higher combustion delay. For this reason, the flame effective kernel formation take place in a zone further from nozzle. Meanwhile, the time elapsed to reach a critical amount of radicals has allowed the formation of a local leaner mixture, that now burns as soon as the combustion starts, causing the typical premixed peak of the ARoHR. In the other case under analysis things are slightly different: the further position and the leaner local mixture of the spray at the plasma induction location lead to ignition in a zone where the local mixture is not yet completely formed, and so it cannot burn at the very beginning of the combustion. This leads to a diffusion driven combustion, as observable from the ARoHR curve. In this case the flame kernel can grow only as long as the fuel injection continues. This analysis puts in evidence how only the ignition delay parameter for a combustion diagnostic cannot explain just by itself all the differences in the obtained combustion evolution.

From all the obtained short ignition delay cases it is clear how a reduction in the premixed combustion peak comes paired with a second rapid combustion phase. This indicates a fast mixture formation during the combustion development, particularly in the instants immediately following the first generation of the flame kernel.

5.3.4 Spray tip penetration

The spray tip penetration is a relevant parameter of comparison in the analysis of the laser ignition effect and, more in general, in the analysis of a provoked earlier ignition effect with respect to the conventional autoignition reference case.

From the penetration graph, reported in Figure 5.17 for the plasma position variation and in Figure 5.18 for the laser pulse timing variation, at

both injection pressures, it can be observed that all the provoked ignition cases are characterized by a faster penetration than the one of the autoignition reference. For a further analysis in this sense, a more detailed comparison between the spray tip penetration for the LIP provoked ignition cases is reported as relative penetration evolution (the difference between the LIP provoked ignition spray penetration and the autoignition reference) for both injection pressures in Figure 5.19 and Figure 5.20, respectively for the LIP position variation and LIP timing variation. The faster penetration for the LIP cases could be expected since an earlier start of combustion would lead earlier to a penetration curve driven by the flame expansion, and so to an earlier acceleration of the penetration curve as discussed in [7].

The results obtained here show that the provoked ignition penetration curves get progressively away from the autoignition one as the ignition delay time is reduced. It is important to remind, for the complete understanding of the reported penetration curves, how the slowdown effect of the air flow in the internal combustion chamber, caused by the piston movement, affects the penetrations curves. This effect is particularly evident for the 100 MPa injection pressure cases where it is amplified by the higher penetration velocity due to the higher momentum of the spray. Furthermore, this difference is emphasized by the fact that the autoignition presents an average ignition timing that occurs when the spray has already penetrated in the slowdown zone while, thanks to the shortest provoked ignitions delays, in the laser ignition cases the combustion starts upstream of such zone. This leads to even more important differences in the penetration curves, as it could be clearly appreciated in the results reported as relative penetration in Figure 5.19 and Figure 5.20, especially for the 100 MPa injection cases.

Despite the very different ignition delays registered, this result could anyhow indicates that all the penetration curves accelerated by the flame penetration at different instants will collapse at the same ideal penetration curve. This ideal limit penetration curve should be the theoretical flame penetration curve, already stated in [2], and so an asymptote limit for the spray penetration velocity, under any possible ignition condition.

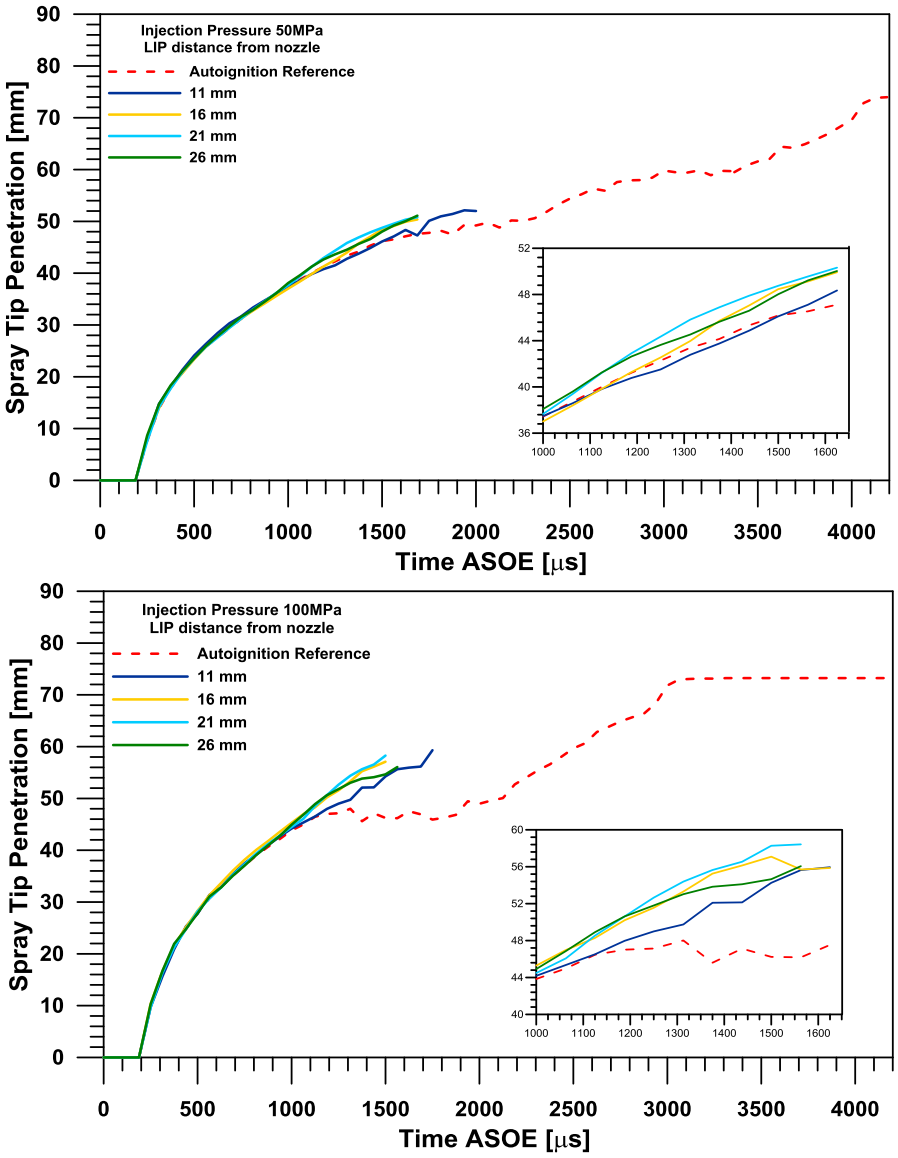

Figure 5.17. Tip penetration curves comparisons for the induced plasma position variation tests at 50 MPa (left) and 100 MPa (right) injection pressure with a fixed LIP delay time of 0.8 ms ASOE. The tip spray penetration for the autoignition reference is also reported as a red dashed line. A magnification of the most interesting area is also showed.

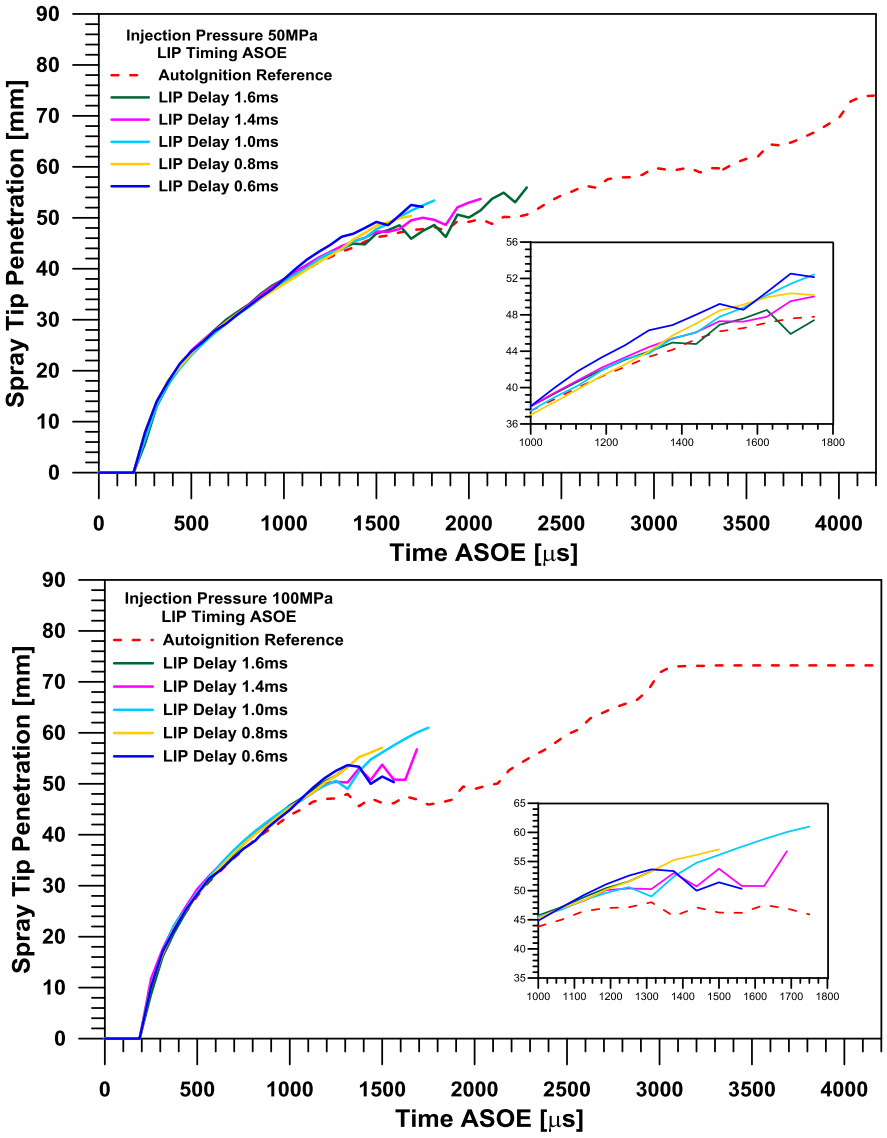

Figure 5.18. Tip penetration curves comparisons for the induced plasma delay variation tests at 50 MPa (left) and 100 MPa (right) injection pressure with a fixed LIP position of 16 mm from the injector nozzle along the spray axis. The tip spray penetration for the autoignition reference is also reported as a red dashed line. A magnification of the most interesting area is also showed.

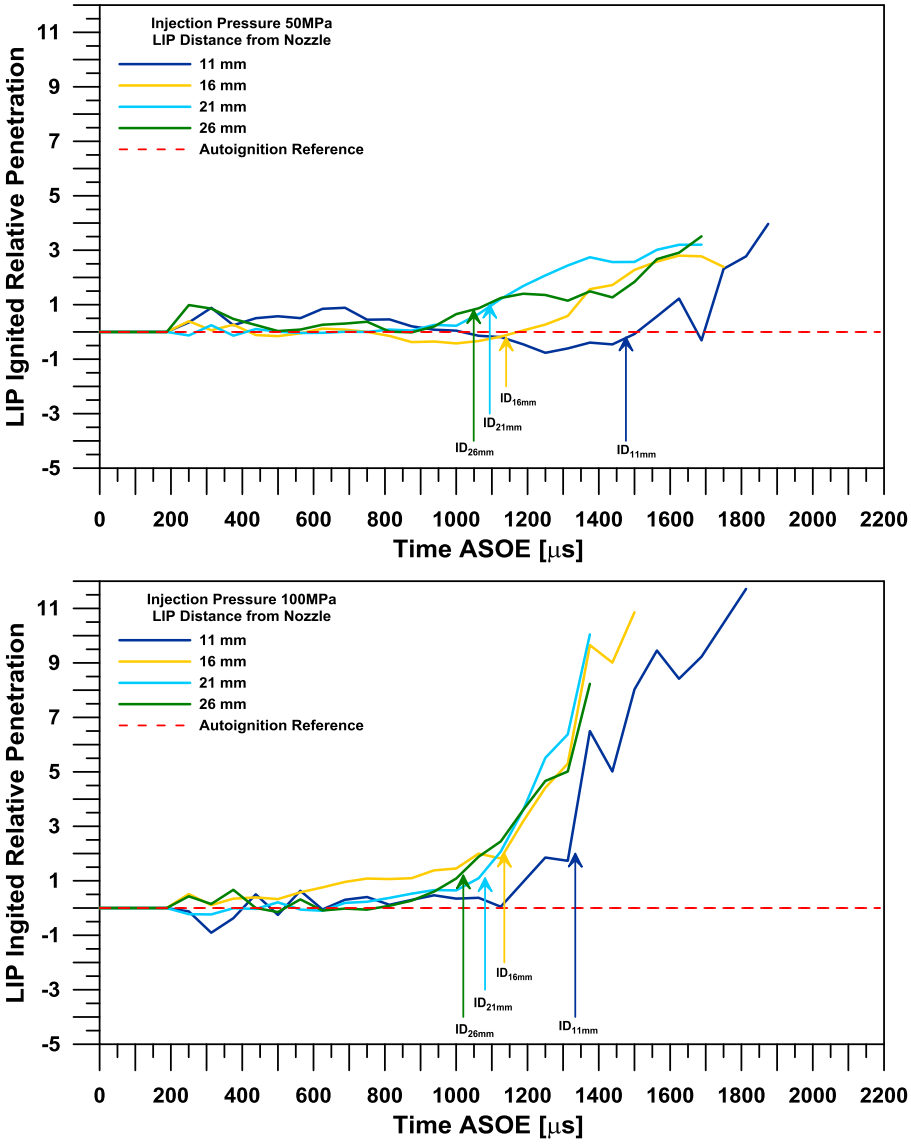

Figure 5.19. Relative penetration with respect the autoignition reference (S_{lip}-S_{auto}), obtained for the LIP position variation along the spray axis for both injection pressures of 50 MPa and 100 MPa. The obtained ignition delay for each test case is also indicated in the graphics.

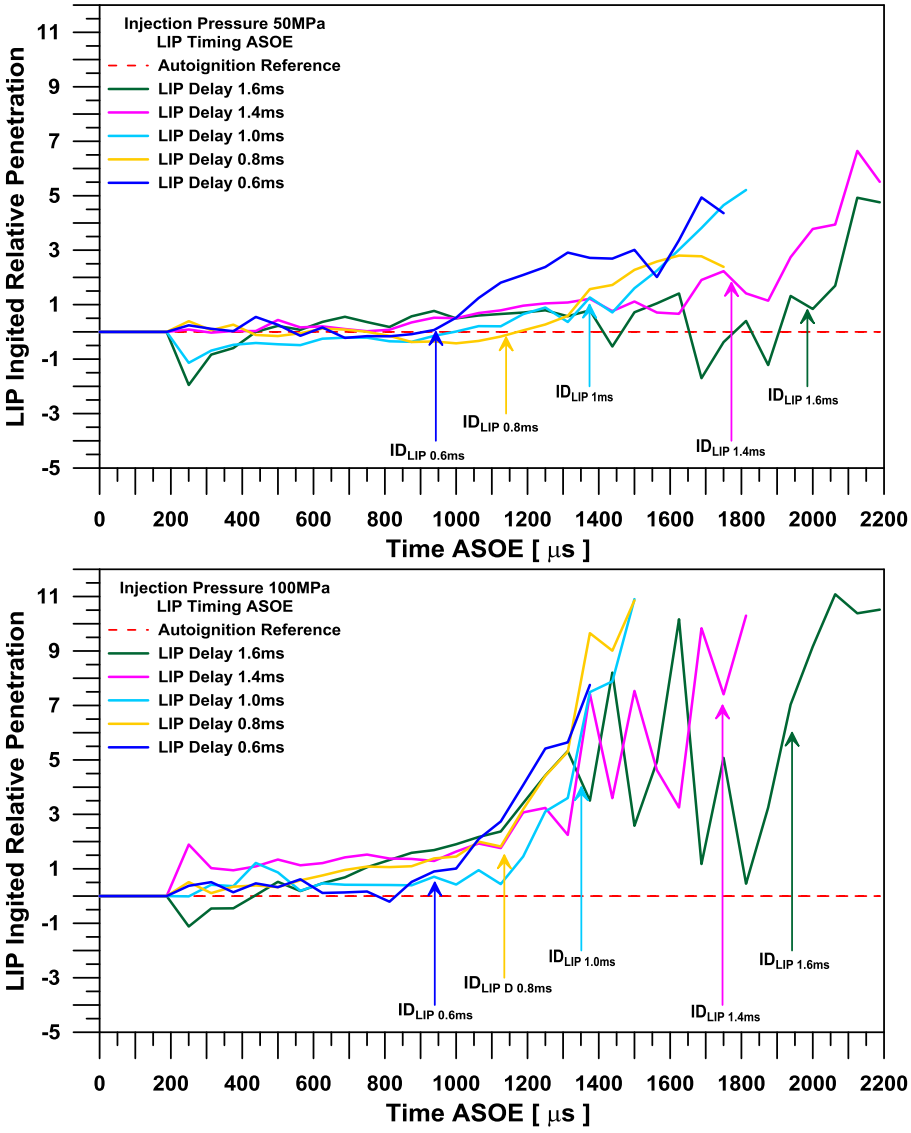

Figure 5.20. Relative penetration with respect the autoignition reference (S_{lip}-S_{auto}), obtained for the LIP delay variation along the spray axis for both injection pressures of 50 MPa and 100 MPa. The obtained ignition delay for each test case is also indicated in the graphics.

The flame penetration curve is actually fixed once given some parameters, such as fuel type, injection timing and duration and in-chamber thermodynamic conditions. So, the differences in ignition delay and combustion development induced by the plasma should not affect the curve itself. It just modifies the speed with which the penetration curve reaches the actual flame velocity limit. From the reported penetration curves, it can be seen how, from the penetration of cases with a very different ignition delays, a first acceleration phase occurs, but then the same penetration curve is reached asymptotically.

5.3.5 Soot evolution

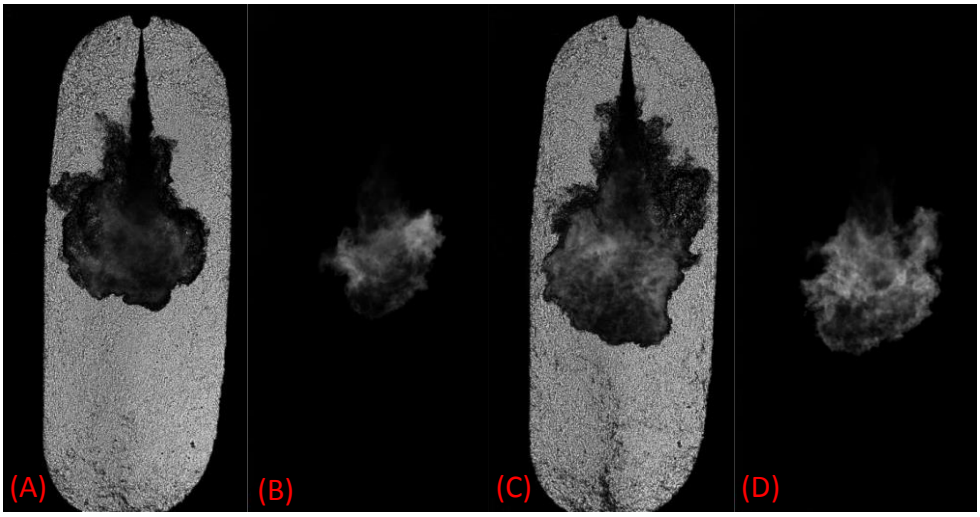

Figure 5.21. Examples of good matching between spray tip position as determined by the Schlieren imaging (images A and C) and the Natural Luminosity soot signal acquisition (images B and D). The images are taken from 4 different repetitions (A and B at 1250μs ASOE; C and D at 1500 μs ASOE) at 5.3 MPa 700 K condition, 50 MPa of injection pressure and with the laser ignition at 16 mm from nozzle and 500 μs ASOE.

The first interesting observation to be dealt for the flame soot generation, concerns the position in the flame where it could be found at first. In fact, for cases of conventional autoignition and only some of the cases with plasma induced ignition, the registered soot luminosity is found to be generated in the spray tip zone and the penetration after the start of combustion is completely driven by the flame velocity, as expectable. This is clearly shown in Figure 5.21, where images from Schlieren and NL visualization are juxtaposed to clearly show this evidence: once the combustion has started, the spray penetration should be directly considered as flame penetration in the combustion chamber, as the soot luminosity signal always stands at the tip of the spray. This is also clearly shown from the results reported in Figure 5.22.

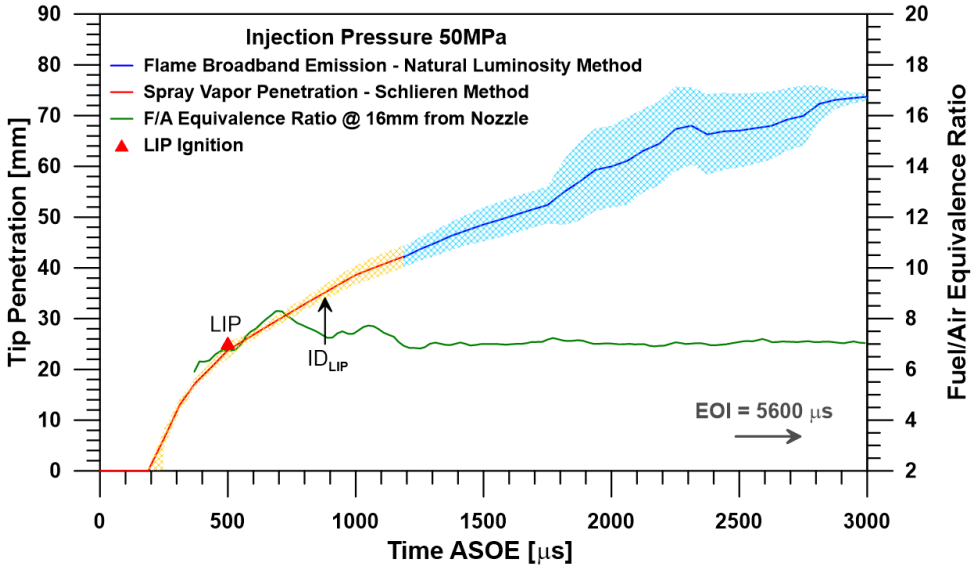

Figure 5.22. Vapor Spray Tip penetration curve and Flame Soot Emission penetration curve obtained respectively from the Schlieren and Natural Luminosity methods. The curves have been obtained from the LIP ignition case provoked at 16 mm from the nozzle and 0.5 ms delay ASOE. The relative fuel/air ratio evolution is also reported as reference as the ignition delay time.

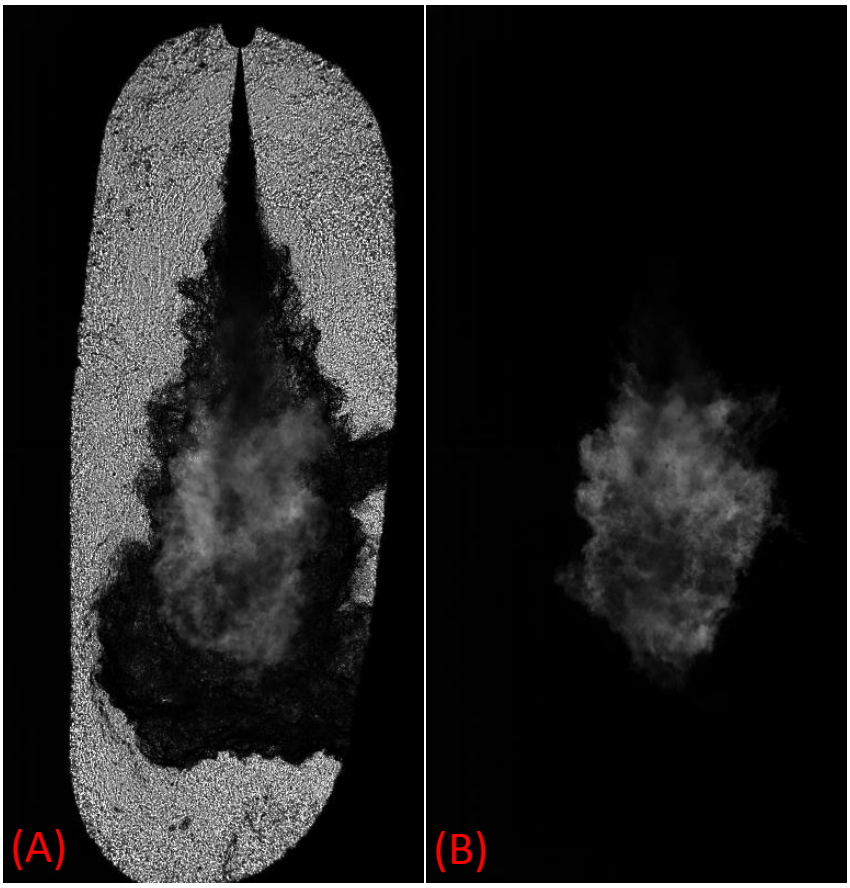

Figure 5.23. Example of the observed difference between the spray tip and the soot emission zone for large ignition delay times. Images taken from 2 different repetitions (Schlieren Visualization (A) and Natural Luminosity (B)) at 5.3 MPa and 700 K for ignition attempts at 16mm from nozzle and 1.4 ms ASOE.

More in detail, the example reported in Figure 5.21 is a laser ignition test where the laser is triggered at 16mm from the nozzle at 500 µs ASOE. Two different time instants are shown, namely 1250 µs for the images A and B and 1500 µs for the images C and D. The 1250 µs images are the first registered instant where the soot emission is detectable and it is evident how

from that instant onwards the penetration could be determined only by observing the natural luminosity images, as the soot emission always stands and represents the spray tip. The results obtained from the image processing on these example images is than detailed in Figure 5.22.

However, moving the plasma induction position along the spray axis, or varying the laser pulse timing, has shown an unexpected shifting effect between the relative position of the spray tip and the soot emission, as appreciable from Figure 5.23. The experimental penetration data analysis has shown that the curves from the two different visualization methods matched well for the shortest laser pulse timing cases but get progressively delayed as the laser pulse timing gets larger, as could be appreciated more in detail from Figure 5.24.

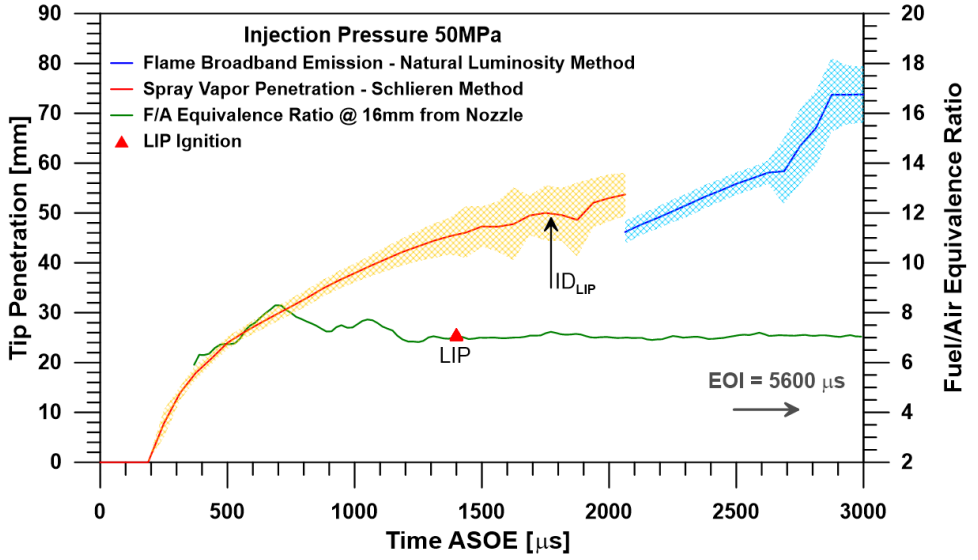

Figure 5.24. Vapor Spray Tip penetration curve and Flame Soot Emission penetration curve, obtained respectively from the Schlieren and Natural Luminosity methods. The curves have been obtained from the LIP ignition case provoked at 16 mm from the nozzle and 1.4 ms delay ASOE. The relative fuel/air ratio evolution is also reported as reference as the ignition delay time.

In fact, in the latest laser pulse timing cases, the curves were clearly unmatched, with substantial difference between the penetration obtained with both methods, as shown in Figure 5.24. This is caused by the fact that the flame was expanding from a region closer to the injector nozzle than the spray tip, as it is appreciable in Figure 5.23. The plasma generation position combined with the ignition delay time contributes to generate a flame kernel not anymore only in the "tip zone" of the spray, as typically occurs for the auto-ignition cases, but now in an upper region, igniting the mixture nearer to the injector nozzle and so generating a cloud of soot particles that are no more reaching the tip of the spray.

5.4 Summary & Conclusions

In this chapter, the purpose-designed optical system for laser induced plasma ignition has been applied to direct injected diesel spray under real engine-like conditions.

Under engine-like condition of 53 bar 765 K and 26.7 kg/m^3 at TDC the laser induced plasma ignition system presents a full induction success rate. Once applied to the ignition of a diesel spray, the LIP system has revealed also full ignition success rate. Moreover, the LIP system has shown to be able to provide temporal and spatial control of the combustion process. In particular, compared with the case of conventional auto-ignition of the Diesel spray, some results have been underlined:

- Temporal control capability: the main parameter considered for the determination of the temporal control of the system over the combustion event is the ignition delay, which can be quantified from both the in-cylinder pressure and from combustion visualization images. In every single cycle fired with the LIP ignition system at 0.8 ms ASOE and 26 mm from the injector nozzle, combustion has been observed to start earlier than in the auto-ignition reference conditions (1.1 ms compared to 2.9 ms ASOE, respectively). Moreover, igniting

the spray with the LIP system also leads to a high reduction of the variation in the ignition delay times.

- Spatial control capability: evidences obtained from the Schlieren and Natural Luminosity combustion visualization techniques have shown how the LIP induced combustion occurs closer to the injector nozzle. It was shown that, for the plasma induced ignition conditions tested, the soot cloud is generated inside the spray cone, near the plasma induction position, and not at the spray tip as occurs in an auto-ignition event.

Furthermore, the system has been able to ignite the fuel spray above the upper flammability limits and reaching the maximum local equivalence ratio of 12 for the 50 MPa injection pressure case. In almost all the tested cases, the overall rate of success of ignition in engine like conditions has been near 100%, with the only exception for some misfiring case registered at 11 mm from the nozzle and characterized by a modeled local equivalence ratio of respectively 12 and 8 for the 50 MPa and 100 MPa injection pressures, respectively. Such local conditions should represent a transition point between ignitable to non-ignitable equivalence ratios for the application of the designed ignition system.

The combustion ignition delay variation with the position and timing of the laser plasma induction has shown a clear evolution. Moving closer to the injector nozzle, and so moving through richer local equivalence ratio, has shown to have the effect of retarding the start of combustion with respect the downstream zones. The ignition delay seems to represent a good indicator for forecasting the subsequent combustion development. Nevertheless, the only exceptions to this statement have resulted to be the tested cases of 26 mm/0.8 ms and 16 mm/0.5 ms, for the 50 MPa injection pressure, which need a deeper investigation as pointed out in the Future Work section at the end of the document.

Each provoked ignition case has registered higher pressure and apparent heat release curves than the respective autoignition references. As the quantity of fuel injected in each tested case was exactly the same, the only reasonable explanation should be associated to differences in the total unburnt fuel of the different cases, that have to be higher for all the autoignition cases. This becomes an indicator of how the laser plasma ignition permits a higher efficiency in the total amount of fuel that can be burnt in a combustion event in similar conditions.

The rate of heat release has shown how, with the variation of the ignition delay, the premixed combustion's indicator peak could completely disappear. Moving through shorter delays leads to a more diffusive driven combustion development, to the point that it permits to avoid the typical diesel premixed phase.

The analysis of the spray reactive penetration has shown that it is highly influenced by the internal air flow of the engine test rig. Consequently, it has not allowed reliable measurements after a certain distance from the injector (roughly half of the combustion chamber). For this reason, the results here presented and the conclusion reported for this field of combustion diagnostics need a deeper investigation. Even though, the existence of a flame velocity limit for the reactive penetration in the combustion chamber could be speculated from the recorded penetration curves. It seems that all the different provoked ignition cases present a penetration curve that, even if it gets away from the inert reference after combustion onset, seems later to accelerate and collapse asymptotically upon the same curve. Another interesting result obtained from the analysis of the images is the determination of different soot cloud generation locations, linked to the relative position between the spray tip and the laser plasma induction. This fact became evident from the analysis of the mismatching average penetration curves obtained from the application of the two optical techniques. The difference between the soot cloud position and the real spray tip gets higher as the plasma spark timing is increased or as it is positioned closest to the injector nozzle.

5.5 Bibliography

[1] J.V. Pastor, J.M. García-Oliver, J.-G. Nerva and B. Gimenez, "Fuel effect on the liquid-phase penetration of an evaporating spray under transient diesel-like conditions", *Fuel*, no. 90, pp. 3369-3381, 2011.

[2] J. V. Pastor, R. Payri, J. M. Garcia-Oliver and F. J. Briceño, "Schlieren Methodology for the Analysis of Transient Diesel Flame Evolution", *SAE Technical Paper*, 2013-24-0041, 2013.

[3] C. Micó Reche, "Development of Measurement and Visualization Techniques for Characterization of Mixing and Combustion Process with Surrogate Fuels", *Doctoral Thesis*. Universitat Politècnica de València, 2015.

[4] J. M. Desantes, J. V. Pastor, J. M. García-Oliver and F. J. Briceño, "An experimental analysis on the evolution of the transient tip penetration in reacting Diesel sprays", *Combustion and Flame*, no. 161, pp. 2137-2150, 2014.

[5] J. V. Pastor, J. J. Lopez, J. M. Garcia and J. M. Pastor, "A 1D model for the description of mixing-controlled inert diesel sprays", *Fuel*, vol. 87, no. 13-14, p. 2871–2885, 2008.

[6] J. V. Pastor, J. M. Garcia-Oliver, J. Pastor and W. Vera-Tudela, "One-Dimensional Diesel Spray Modeling of Multicomponent Fuels", *Atomization and Sprays*, vol. 25, no. 6, pp. 485-517, January 2015.

[7] J. M. Desantes, J. V. Pastor, J. M. Garcia-Oliver and F. J. Briceño, "An experimental analysis on the evolution of the transient tip penetration in reacting Diesel sprays", *Combustion and Flame*, vol. 161, no. 8, p. 2137–2150, August 2014.

Chapter 6

Conclusions and Future Work

Contents

6.1 Introduction

This last chapter has the aim to conclude this doctoral thesis by listing and detailing the main conclusions obtained from the carried-out research work, as well as to present and enumerate eventual new open research lines emerged from it.

At first, the main results obtained from the experimental study will be summarized and synthetized, also in order to establish existent relationship between the literature-based objectives and the research results obtained.

Finally, ideas raised from the obtained results and methodologies will be presented as possible future research work applications to proceed in the experimental line marked by the current work.

6.2 Conclusions

In this doctoral thesis a method for the set-up, optimization and validation of a controlled laser induced plasma ignition system and its application to the provoked ignition of direct injected diesel spray has been developed. The main application of such system has been the study upon the effects of the local conditions at ignition on the development of the subsequent diesel combustion, focusing on some of the principal combustion diagnostics parameters variation, with respect the classical autoignition frame case.

From a methodological point of view, the main conclusions obtained to answer to the first objective of this research work are here reported as follows:

- A non-intrusive, controllable and reliable ignition system based on the laser plasma induction process has been developed for its application to the provoked combustion of direct injected diesel sprays in an optical test rig. The system designed has proven to be

highly effective in the plasma generation and capable of controlling the ignition of diesel spray under real engine-like conditions. The system has been proven to allow time and spatial control over the plasma deposition inside the combustion chamber, permitting to carry on a study upon the effects of the local conditions variation at ignition of such fuel spray. In particular, the possibility of selecting the local spatial position where to force ignition along the spray cone axis has allowed new considerations upon the obtained combustion development.

- A methodology for the optimization of the ignition system's fundamental parameters and quantification of its effectiveness in the plasma generation and fuel ignition has been developed. Such methodology has allowed not only to validate the developed laser induced plasma ignition system, but also to perform its optimization in terms of combustion control, permitting to obtain the most reliable and effective system possible for the research application. Starting from literature considerations upon plasma formation and non-resonant breakdown in air, as reported extensively in chapter 2, the established methodology has allowed to optimize the system's optical components and the laser pulse energy. In particular, with the experimental systems used in the development of this work, the developed optimization methodology has permitted to found that:

    - It is possible to obtain a 100% reliable and positionally stable laser plasma induction system, under atmospheric air conditions, with the application of a 300 mJ laser beam of coherence M^2 factor around 6, emitted at 1064 nm and focused through a plano-convex n-BK7 lens of 300 mm focal length. The experimental path followed to obtain such system configuration has showed how the beam coherence factor joined with the focusing lens' focal length limitations are the most critical factors in the energy condensation procedure

needed to obtain plasma induction through the non-resonant molecule breakdown process.

- Under an engine-like condition sweep, it has been shown how the beam steering effect, due to the joint contributions of internal air flow movement, density gradients and refraction index's variations of the optical access' windows, produce an important loss in the system plasma induction effectiveness, overcompensating the theoretical advantages of a higher local density for the generation of a non-resonant breakdown. In detail, raising from ambient air conditions to an engine like condition of 20.8 kg/m3 global density has caused a 43% loss in the system efficiency.

- It has been also demonstrated how higher densities implies higher success rates, lowering the energy threshold for breakdown, and permitting to still reach a 100% success rate in the plasma induction at a chamber density of 26.7 kg/m3. It can be so confirmed how the increase of the air density represents the main parameter governing a laser induced plasma generation success via the non-resonant breakdown process.

- Moreover than the reported considerations upon the system effectiveness, engine-like high density conditions have shown to affect also the positional stability of the induced plasma generation. In particular, it has been shown how for a combustion chamber density of 31.8 kg/m3 multipoint induction events have been registered. This has led to the consideration that, at a fixed beam energy, such conditions represent an overkill for the plasma induction process, not allowing the correct spatial control needed for its purpose application.

For what concerns the second main objective of this research work, the study of a provoked diesel combustion by the application of the developed ignition system has permitted to conclude that:

- Under engine-like conditions of 53 bar and 765 K at TDC, generating a chamber air density of 26.7 kg/m3, it has been possible to ignite a diesel spray in a repetitive and reliable form, actually producing a full ignition success rate.

- The LIP system has shown to be able to provide temporal and spatial control of the combustion process in a reliable way. If compared with the autoignition reference case, for the same boundary conditions, it has been obtained that:

    - Forcing the ignition at 0.8 ms ASOE and 26 mm from the injector nozzle has consistently permitted to advance the SOC, producing an average ignition delay time of 1.1 ms versus the 2.9 ms of the autoignition reference. Such forced ignition has permitted to highly increase the cycle to cycle stability of the diesel combustion process.

    - The forced combustion starts consistently closer to the injector nozzle than the autoignition reference. Consequently, it has been shown how the soot generation also occurs in a closer position, with the appearance of the soot cloud emission inside the spray cone and near the plasma induction location, whilst it is at the spray tip for a common autoignition event.

- The LIP system has showed to be able to ignite the fuel spray above the upper flammability limits, reaching a maximum local equivalence ratio at the ignition location of 12, for a 50 MPa injection pressure.

- The combustion ignition delay has shown a clear evolution with the position and timing of induced plasma ignition. Moving the induction

point close to the injector nozzle, and so through a richer local equivalence ratio, has presented the effect of retarding the SOC with respect to the spray downstream zone. It has finally been appreciated how the ignition delay could represent a good indicator to forecast the subsequent combustion development.

  - Directly referred to the ignition delay modulation, the rate of heat release of each provoked combustion has permitted to show the possibility of a transition from a typical diesel premixed combustion to a diffusive driven combustion, allowing to fully avoid the appearance of the typical premixed combustion peak when moving through shorter ignition delays. Such results could be accomplished both via time phasing of the ignition system and via space phasing of the plasma induction position.

- The diesel combustion derived from each provoked ignition has shown a registered higher-pressure curve than the same autoignition reference. At equal injection rates, such results underline a better combustion efficiency obtainable from the provoked ignition process, permitting to lower the unburnt fuel residual mass of the combustion process.

6.3 Future Works

In general terms, the ignition system developed and optimized along this research work should represent a very powerful and interesting methodology to expand the possibilities in the combustion study. In fact, its fundamental characteristics of being non-intrusive, power-modulable and, above all, time and position controllable, could permit a lot of new degrees of freedom in the combustion study of a direct injected spray, particularly for what concerns the analysis of its combustion development under non-conventional conditions.

Considering the implications of the application of the developed ignition system to the general combustion study, some of the possible future works are here presented as follows:

- A general deep study of the effect of local ignition conditions on the combustion development could be carried on. The here presented research works has been focused on the methodological and practice development of a non-intrusive and controllable ignition system, whose characteristics are now well known and which should be easily reproducible even under different boundary conditions, following the proposed optimization and validation methods. But in terms of its application possibilities it has been only scratched the surface. It has been shown which the system capabilities are, and its application can so produce a deeper study upon the variation of the local ignition conditions, such as:

    - Extend the parametrical variation in terms of engine-like boundary conditions at which the provoked ignition combustion study will be carried out, will allow the generation of an extense database permitting to infer more precisely the effects under study.

    - Extend the application of optical techniques to the above reported study, could lead to the possibility to analyze more in detail a lot on interesting parameters. The application of an OH-chemiluminescence technique will permit to consider lift-off length variations with the ignition spot ant timing, such as the application of a Soot-DBI technique can allow a precise determination on the variations in the soot production of the different provoked combustion modes. All this factors could lead to a better understanding of the importance of the ignition conditions for a diesel combustion.

- Deepen the investigation upon the effects of the position and timing variation of the provoked plasma ignition on the combustion parameters, in particular:

  - Ignition delay. As already pointed out in paragraph 5.4, even though it has been shown how the ignition delay parameter represents a good indicator for forecast the combustion development from the LIP ignition process, some of the results, in concrete for two points of the test matrix, have reported different consequences. The application of extended set of optical techniques, joined with the extension of the local conditions at which force and study a LIP provoked combustion, should permit to determine the reason for the obtained results.

  - Spray reactive penetration. The investigation upon the existence of a flame velocity limit for the reactive penetration into a combustion chamber still represents an open field that could lead to very interesting results and consequences. As reported with details in 5.4, in this research, the influence of the internal air flow motion has not allowed to obtain reliable measurements for the spray penetration after a certain distance from the injector, leaving to eventual future works, carried out in a different test rig or with a different set of selected conditions, the task of finally demonstrate the here reported speculations.

- As the combustion control represents in general terms the most important field of research for the active pollutant limitation procedures, it should be interesting to apply the developed LIP system to some different mixtures of different reactive fuel blends of interest for dual fuel combustion. Such kind of study could lead to infer both

the extended possibilities of combustion control for different reactive-grade fuels and to extend the basic knowledge upon different kind of combustion processes.

In particular, the study of diesel/gasoline blends will be of great interest for the future dual-fuel application in non-conventional combustion engines. Different optical techniques, such as Schlieren, OH Chemiluminescence, Soot DBI should converge for the study of different ignition conditions at different mixture percentages.

- Different diesel/gasoline blends should be used, varying the volume concentrations percentages, in order to have blends characterized by a different reactivity scaled between them. In this way, the ability of the LIP ignition system could be tested on a wider set of conditions, even some where the autoignition is impossible, allowing to better determine the system performances.

- Such different reactivity dual-fuel blends should be first tested under the same thermodynamic conditions used in this work, in order to recollect data of the baseline cases. The application of the different optical techniques should allow to determine, for each tested case, parameters such as reactive spray penetration, soot particle concentration evolution, lift-off length, ignition delay, apparent heat release and rate of heat release. Some of the tested blend should also not be ignitable in some of the conditions under study. The results of this tests should lead the possibility to determine effects and trends of the blending effect on the mixtures in use.

- Once determined the baseline autoignition characteristics for each blend and condition, the provoked LIP ignition should be applied at a set of different timings and position along the spray axis. During the application of the ignition system, the

laser power should be controlled via an adequate beam sampler/power meter combination. In this way, even though the laser energy used should be the optimal for breakdown at the selected thermodynamics conditions (as reported in this work), eventual cases of misfire could be tested with a higher energy plasma, in order to determine extended ignition limits of the applied technique.

- Once obtained all the results for the combustion parameters under study, an extended comparison between LIP provoked combustions and autoignition reference cases should be made. Such comparison, joined with the blending effect on the autoignition combustion analysis should lead to extend the comprehension of the effects of local conditions on the combustion generation and evolution for different reactive fuel blends.

Some of the here presented future work on the dual-fuel combustion has already been started following the development of the work here presented in this thesis, and will be carried on in the department in the future years.

Bibliography

[1] Pocketbook, European Commission - Transports. Statistical, "https://ec.europa.eu/transport/facts-fundings/statistics/pocketbook-2018_en," 2017. [Online].

[2] "http://www.acea.be," Europe, New passenger car registrations in Western, 2015. [Online].

[3] K. Mollenhauer and H. Tschoeke, Handbook of Diesel Engines, London, New York: *Springer Heidelberg Dordrecht*, 2010.

[4] Environmental Protection Agency, Nitrogen Oxides (NOx), why and how they are controlled, *Technical Report*, 1999.

[5] W. Wallace, M. Keane, D. Murray, W. Chisholm, A. Manyard and T. Ong, "Phospholipid lung surfactant and nanoparticle surface toxicity: Lessons from diesel soots and silicate dusts", *Journal of Nanoparticles Research*, vol. 9, no. 1, pp. 23-38, 2007.

[6] DieselNet: Diesel emissions online, "http://www.dieselnet.com.," [Online].

[7] F. Payri and J. M. Desantes, "Motores de combustión interna alternativos", *Reverté*, 2011.

[8] A. García, P. Piqueras, J. Monsalve-Serrano and R. Lago, "Sizing a Conventinoal Diesel Oxidation Catalyst to be used for RCCI Combustion under real driving conditions", *Applied Thermal Engineering*, vol. 140, pp. 62-72, 2018.

[9] J. B. Heywood, "Internal Combustion Engine Fundamentals", *McGraw-Hill*, Inc, 1988.

[10] Q. Xu, M. Xu, D. Hung and S. Wu, "Diesel Spray Characterization at Ultra-High Injection pressure of DENSO 250 MPa Common Rail Fuel Injection System", *SAE Technical Paper*, 2017.

[11] A. Lefebvre, “Atomization and Sprays”, *Hemisphere Publishing Corporation*, 1989.

[12] J. Arrègle, “Análisis de la estructura y dinámica interna de chorros Diesel”, *Doctoral Thesis*, Universitat Politècnica de València, 1997.

[13] H. Hiroyasu and T. Kadota, "Fuel droplet distribution in diesel combustion chamber", *SAE Technical Paper*, no. 740715, 1974.

[14] D. Siebers, "Liquid-phase fuel penetration in diesel sprays", *SAE Technica Paper*, no. 980809, 1998.

[15] J. Hodges, T. Baritaud and T. Heinze, "Planar liquid and gas fuel and droplet size visualization in a DI diesel engine", *SAE Technical Paper*, no. 910726, 1991.

[16] J. Julía, “Análisis de chorros Diesel mediante fluorescencia inducida por láser”, Barcelona: *Editorial Reverté*, S.A., 2006.

[17] K. R. Browne, I. M. Partrifge and G. Greeves, "Fuel property effects on fuel/air mixing in an experimental Diesel engine", *SAE Paper*, no. 860223, 1986.

[18] B. Higgins, C. Mueller and D. Siebers, "Measurements of fuel effects on liquid-phase penetration in DI sprays", *SAE Paper*, no. 1999-01-0519, 1999.

[19] C. Espey and J. Dec, "The effect of TDC temperature and density on the liquid-phase fuel penetration in a DI Diesel engine", *SAE Papers*, vol. 104, no. 952456, pp. 1400-1414, 1995.

[20] J. García, “El proceso de combustión turbulenta de chorros diésel de inyección directa”, *Doctoral Thesis*, Universitat Politècnica de València, 2004.

[21] J. Dec and C. Espey, "Ignition and early soot formation in a DI diesel engine using multiple 2-D imaging diagnostics", *SAE Paper*, no. 950456, 1995.

[22] J. Dec and C. Espey, "Chemiluminescence imaging of autoignition in a DI diesel engine", *SAE Paper*, no. 982685, 1998.

[23] B. Higgins, D. Siebers and A. Aradi, "Diesel-spray ignition and premixed-burn behaviour", *SAE Paper*, no. 2000-01-0940, 2000.

[24] H. Kosaka, V. Drewes, L. Catalfamo, A. Araldi, N. Iida and T. Kamimoto, "Two-dimensional imaging of formaldehyde formed during the ignition process of a diesel fuel spray", *SAE Paper*, no. 2000-01-0236, 2000.

[25] J. Dec, "A Conceptual Model of DI Diesel Combustion Based on Laser-Sheet Imaging", *SAE Technical Papers*, 1997.

[26] G. Bruneaux, "Combustion structure of free and wall-impinging diesel jets by simultaneous laser-induced fluorescence of formaldehyde, poly-aromatic hydrocarbons, and hydroxides", *International Journal of Engine Research*, vol. 9, no. 3, pp. 249-265, 2008.

[27] H. A. T. K. T. Kosaka, "Two-dimensional imaging of ignition and soot formation processes in a diesel flame", *International Journal of Engine Research*, vol. 6, no. 1, pp. 21-42, 2005.

[28] P. Flynn, R. Durrett, G. Hunter, A. Zur Loye, O. Akinyemi, J. Dec and C. Westbrook, "Diesel combustion: An integrated view combining laser diagnostics, chemical kinetics, and empirical validation", *SAE Technical Papers*, no. 1999-01-0509, 1999.

[29] J. Dec and R. Canaan, "PLIF imaging of NO formation in a DI diesel engine", *SAE Paper*, no. 980147, 1998.

[30] A. García, “Estudios de los efectos de la post inyección sobre el proceso de combustión y la formación de hollín en motores diésel”, *Doctoral Thesis*, Universitat Politècnica de València, 2011.

[31] L. Pickett and D. Siebers, "Soot formation in diesel jets near the lift-off length", *International Journal of Engine Research*, vol. 7, no. 2, pp. 103-130, 2006.

[32] P. Ronney, "Laser versus conventional ignition of flames", *Optical Engineering*, no. 33(2), p. 510, 1994.

[33] M. Chou and T. Zukowski, "Ignition of H2/O2/NH3, H2/AIR/NH3 and CH4/O2/NH3 mixtures by excimer-laser photolysis of NH3", *Combustion and Flame*, no. 87, p. 191–202, 1991.

[34] M. Lavid and J. Stevens, "Photochemical ignition of premixed hydrogen/oxidizer mixtures with excimer lasers", *Combustion and Flame*, no. 60, p. 195–202, 1985.

[35] M. Morsy and S. Chung, "Numerical simulation of front lobe formation in laser-induced spark ignition of CH4/air mixtures", in *29th Symposium (International) on combustion*, 2002.

[36] T. Phuoc, "Laser-induced spark ignition fundamental and applications", *Optics and Lasers in Engineering*, no. 44, pp. 97-351, 2006.

[37] B. Forch and A. Miziolek, "Oxygen-atom two-photon resonance effects in multiphoton photochemical ignition of premixed H2/O2 flows", *Optics Letters*, no. 11, p. 129–31, 1986.

[38] B. Forch and A. Miziolek, "Laser-based ignition of H2/O2 and D2/O2 premixed gases through resonant multiphoton excitation of H and D atoms near 243 nm", *Combustion and Flame*, no. 85, p. 254–62, 1991.

[39] M. Weinrotter, H. Kopecek, E. Wintner, M. Lackner and F. Winter, "Application of laser ignition to hydrogen–air mixtures at high pressures", *International Journal of Hydrogen Energy*, vol. 30, p. 319–26, 2005.

[40] G. Weyl, L. Radziemsky and D. Cremers ," Physics of laser-induced breakdown: an update, in Laser-inducted plasma applications", *M. Dekker*, Ed., New York, 1989, p. 1.

[41] T. Phuoc, C. White and D. McNeill, "Laser spark ignition of a jet diffusion flame", *Optics and Lasers in Engeneering*, no. 38, p. 217–232, 2002.

[42] J. Syage, E. Fournier and R. Rianda, "Dynamics of flame propagation using laser-induced spark initiation: Ignition Energy measurements", *Journal of Applied Phisics*, no. 64, p. 1499, 1988.

[43] B. Lewis and G. von Elbe, "Combustion: Flames Explosions of Gases", *New York: Academic Press*, 1951.

[44] Y. Chen, J. Lewis and C. Parigger, "Spatial and temporal profiles of pulsed laser-induced air plasma emissions", *J. Quant. Spectrosc. Radiat. Transfer*, no. 67, pp. 91-103, 2000.

[45] E. Lim, A. McLLroy, P. Ronney and J. Syage, "Transport Phenomena in Combustion", *London: Taylor & Francis*, 1996, p. 176.

[46] T. Phuoc and F. White, "Laser induced spark ignition of CH4/air mixtures", *Combustion and Flame*, no. 119, pp. 203-216, 1999.

[47] R. Kingdon and F. Weinberg, "The Effect of plasma constitution on laser ignition energies", *in 16th Symposuim (international) on Combustion*, Pittsburgh, 1977.

[48] D. Bradley, C. Sheppard, I. Suardjaja and R. Woolley, "Fundamentals of high-energy spark ignition with lasers", *Combustion and Flame*, no. 138, pp. 55-77, 11 May 2004.

[49] B. Yusoff, "Fundamentals of turbulent combustion related to gasoline engines", *The University of Leeds*, 1995.

[50] T. Spliganin, A. MCliroy, E. Fournier and R. Cohen, "Time-resolved imaging of flame kernels: laser spark ignition of H2/O2/Air mixtures", *Combustion and Flame*, no. 102, pp. 310-28, 1995.

[51] R. Abdel-Gayed, D. Bradley and M. McMahon, "Turbulent flame propagation in premixed gases: Theory and experiment", *in Symposium (International) on Combustion*, 1979.

[52] M. Lawes, "Effects of turbulence on combustion in engines", *Leeds: University of Leeds*, 1987.

[53] J. Dale, M. Checkel and P. Smy, "Application of High Energy Ignition Systems to Engines", *Prog. Energy Combust. Sci.*, no. 23, pp. 379-398, 1997.

[54] J. Ma, D. Alexander and D. Poulain, "Laser Spark Ignition and Combustion Characteristics of Methane-Air Mixtures", *Combustion and Flame*, no. 112, pp. 492-506, 1998.

[55] P. Chylek, A. Maurice, A. Jarzembsky, V. Srivastavam and R. G.Pinnick, *Appl. Opt.*, no. 15, 1990.

[56] R. Hickling and W. Smith, *SAE Trans*, vol. 84, no. 555, 1974.

[57] T.-W. Lee, V. Jain and S. Kozola, "Measurements of minimum ignition energy by using laser sparks for hydrocarbon fuels in air: propane, dodecane, and jet-A fuel", *Combustion and Flame*, vol. 125, no. 4, p. 1320–1328, 2001.

[58] V. Bermúdez, J. García, E. Juliá and S. Martínez, "Engine with optically accessible cylinder head: A research tool for injection and combustion processes", *SAE Technical Papers*, 2003.

[59] J.-G. Nerva, “An assessment of fuel physical and chemical properties in the combustion of a Diesel spray”, *Doctoral Thesis*, Universitat Politècnica de València, 2013.

[60] O. Armas, J. Rodríguez, F. Payri, J. Martín and J. Agudelo, "Effect of the trapped mass and its composition on the heat transfer in the compression cycle of a reciprocating engine", *Applied Thermal Engineering*, vol. 26, pp. 2842-53, 2005.

[61] M. Ikegami and T. Kamimoto, “Flow and Combustion in Reciprocating Engines”, *Springer-Verlag*, 2009.

[62] P. Holland and R. Welsch, "Robust Regression Using Iteratively Reweighted Least-Squares", *Commun. Statis.-Theor. Method*, vol. A6, 1977, pp. 813-827.

[63] W. DuMouchel and F. O'Brien, "Integrating a Robust Option into a Multiple Regression Computing Environment", *Computer Science and*

Statistics: Proceedings of the 21st Symposium on the Interface, Alexandria, VA, 1989.

[64] F. Payri, J. Pastor, N. J.-G. and J. García-Oliver, "Lift-Off Length and KL Extinction Measurements of Biodiesel and Fischer-Tropsch Fuels under Quasi-Steady Diesel Engine Conditions", *SAE International Journal of Engines*, vol. 4, no. 2, pp. 2278-2297, 2011.

[65] R. Payri, J. García-Oliver, M. Bardi and J. Manin, "Fuel temperature influence on diesel sprays in inert and reacting conditions", *Applied Thermal Engineering*, vol. 35, no. 1, pp. 185-195, 2012.

[66] F. Payri, J. Pastor, J. García-Oliver and J. Pastor, "Contribution to the application of two-colour imaging to diesel combustion", *Measurement Science and Technology*, vol. 18, no. 8, pp. 2579-2598, 2007.

[67] C. Micó Reche, "Development of Measurement and Visualization Techniques for Characterization of Mixing and Combustion Process with Surrogate Fuels", *Doctoral Thesis*, Universitat Politecnica de Valencia, 2015.

[68] H. Zhao, "Laser Diagnostics and Optical Measurement Techniques (in Internal Combustion Engines)", Warrendale, PA 15096-0001: *SAE International*, 2012, pp. 13-21.

[69] A. C. Eckbreth, "Laser Diagnostics for Combustion Temperature and Species", A. G. a. D. Lilley, Ed., *Cambridge*, Mass 02139: Abacus Press, 1988.

[70] G. Settles, "Schlieren and Shadowgraph Techniques: Visualizing Phenomena in Transparent Media", Berlin: *Springer-Verlag*, 2001.

[71] L. Pickett, S. Kook and T. Williams, "Visualization of diesel spray penetration, cool-flame, ignition, high-temperature combustion, and soot formation using high-speed imaging", *SAE International Journal of Engines*, vol. 2, no. 2009-01-0658, pp. 439-459, 2009.

[72] J. Naber and D. Siebers, "Effects of gas density and vaporization on penetration and dispersion of diesel sprays", *SAE Technical Paper*, no. 960034, 1996.

[73] J. V. Pastor, R. Payri, J. M. Garcia-Oliver and F. J. Briceño, "Schlieren Methodology for the Analysis of Transient Diesel Flame Evolution", *SAE Technical Paper*, pp. 1167-1676, 8 September 2013.

[74] J. Benajes, R. Payri, M. Bardi and P. Martí-Aldaraví, "Experimental characterization of diesel ignition and lift-off length using a single-hole ECN injector", *Applied Thermal Engineering*, no. 58, pp. 554-563, 2013.

[75] R. Payri, J. M. García-Oliver, T. Xuan and M. Bardi, "A study on diesel spray tip penetration and radial expansion under reacting conditions", *Applied Thermal Engineering*, no. 90, pp. 619-629, 2015.

[76] R. Payri, J. S. Giraldo, S. Ayyapureddi and Z. Versey, "Experimental and analytical study on vapor phase and liquid penetration for a high pressure diesel injector", *Applied Thermal Engineering*, no. 137, pp. 721-728, 2018.

[77] J. V. Pastor, J. J. Lopez, J. M. Garcia and J. M. Pastor, "A 1D model for the description of mixing-controlled inert diesel sprays", *Fuel*, vol. 87, no. 13-14, p. 2871–2885, October 2008.

[78] F. Payri, R. Payri, M. Bardi and M. Carreres, "Engine combustion network: Influence of the gas properties on the spray penetration and spreading angle", *Experimental Thermal and Fluid Science*, vol. 53, pp. 236-243, 2014.

[79] J. Borée, N. Atassi and G. Charnay, "Measurements and image analysis of the turbulent field in an axisymmetric jet subject to a sudden velocity decrease", *Experimental Thermal and Fluid Science*, vol. 14, pp. 45-51, 1997.

[80] J. Pastor, J. García-Oliver, J. Pastor and W. Vera-Tudela, "One-dimensional diesel spray modelling for multicomponent fuels", *Atomization and Sprays*, vol. 25, no. 2, pp. 485-517, 2015.

[81] J. L. Beduneau, B. Kim, L. Zimmer and Y. Ikeda, "Measurements of minimum ignition energy in premixed laminar methane/air flow by using laser induced spark", *Combustion and Flame*, vol. 132, no. 4, pp. 653-665, 2003.

[82] L. M. Pickett, A. A. Hoops and J. M. Headrick, "Laser Ignition of multi-injection gasoline sprays", *SAE Technical Paper*, no. 2011-01-0659, pp. 1-26, 2011.

[83] T. X. Phuoc and F. P. White, "An Optical and Spectroscopic Study of Laser-Induced Sparks to Determine Avaible Ignition Energy", vol. 29, pp. 1621-1628, 2002.

[84] L. M. Pickett and M. P. Musculus, "Diagnostic considerations for optical laser-extinction measurements of soot in high-pressure transient combustion environments", *Combustion and Flame*, no. 141, p. 371–391, March 2005.

[85] J. Pastor, J. García-Oliver, J.-G. Nerva and B. Gimenez, "Fuel effect on the liquid-phase penetration of an evaporating spray under transient diesel-like conditions", *Fuel*, no. 90, pp. 3369-3381, 2011.

[86] J. M. Desantes, J. V. Pastor, J. M. García-Oliver and F. J. Briceño, "An experimental analysis on the evolution of the transient tip penetration in reacting Diesel sprays", *Combustion and Flame*, vol. 161, no. 8, p. 2137–2150, August 2014.

[87] J. V. Pastor, J. M. Garcia-Oliver, J. Pastor and W. Vera-Tudela, "One-Dimensional Diesel Spray Modelling of Multicomponent Fuels", *Atomization and Sprays*, vol. 25, no. 6, pp. 485-517, January 2015.